AD NUMBER

AD866460

LIMITATION CHANGES

TO:

Approved for public release; distribution is unlimited.

FROM:

Distribution authorized to U.S. Gov't. agencies and their contractors; Critical Technology; MAR 1970. Other requests shall be referred to Air Force Arnold Engineering Development Center, Attn: AETS, Arnold AFB, TN 37389. This document contains export-controlled technical data.

AUTHORITY

aedc, usaf ltr, 8 jan 1973

AEDC-TR-70-86

cy 1

CURRENT DISTRIBUTION IN CROSSED-FIELD ACCELERATORS (PART III, ELECTRICAL AND GASDYNAMIC PERFORMANCE OF J X B ACCELERATORS)

G. S. Argyropoulos, M. A. Casteel, and S. T. Demetriades
STD Research Corporation
Pasadena, California

March 1970

ARNOLD ENGINEERING DEVELOPMENT CENTER
AIR FORCE SYSTEMS COMMAND
ARNOLD AIR FORCE STATION, TENNESSEE

NOTICES

When U. S. Government drawings specifications, or other data are used for any purpose other than a definitely related Government procurement operation, the Government thereby incurs no responsibility nor any obligation whatsoever, and the fact that the Government may have formulated, furnished, or in any way supplied the said drawings, specifications, or other data, is not to be regarded by implication or otherwise, or in any manner licensing the holder or any other person or corporation, or conveying any rights or permission to manufacture, use, or sell any patented invention that may in any way be related thereto.

Qualified users may obtain copies of this report from the Defense Documentation Center.

References to named commercial products in this report are not to be considered in any sense as an endorsement of the product by the United States Air Force or the Government.

CURRENT DISTRIBUTION IN CROSSED-FIELD ACCELERATORS (PART III, ELECTRICAL AND GASDYNAMICS PERFORMANCE OF J X B ACCELERATORS)

G. S. Argyropoulos, M. A. Casteel, and S. T. Demetriades
STD Research Corporation
Pasadena, California

FOREWORD

The work reported herein was sponsored by Arnold Engineering Development Center (AEDC), Air Force Systems Command (AFSC), Arnold Air Force Station, Tennessee, under Program Element 62405334, Project 8950, Task 895001.

The research was performed by STD Research Corporation, Box 4127, Catalina Station, Pasadena, California, under Contract AF 40(600)-1166. The work reported herein was performed from 1 January 1968 to 31 October 1969. Technical monitor was Captain E. E. Goins, Jr. (AELT).

The reproducibles used in the reproduction of this report were supplied by the authors.

This technical report has been reviewed and is approved.

Thomas G. Horn
2nd Lieutenant, USAF
Technical Facilities
Development Division
Directorate of Plans
and Technology

Harry L. Maynard
Colonel, USAF
Director of Plans
and Technology

ABSTRACT

Realistic analytical description of the local behavior and of the overall performance of crossed-field accelerators is obtained by computing the coupled two-dimensional distributions of current density, plasma properties, and fluid velocity, temperature and pressure, over the whole length of the channel. The analysis includes consideration of electron nonequilibrium, thermal and concentration diffusion, compressible turbulent boundary layers, finite reaction rates, and electron energy relaxation, and the effect of each of these mechanisms is investigated. The development of compressible, turbulent, magnetohydrodynamic boundary layers on the electrode walls is obtained through a novel formulation, that includes a transport equation for the Reynold's stress, and a fast numerical method of solution. Analytical results obtained in this study gave consistently good agreement with experimental measurements. Applications to seeded-nitrogen and seeded-air accelerators indicate limited current fringing in the entrance and exit regions and rapid approach to periodical current density, electric field, and plasma property distributions in the main part of the channel. Solution of the complete coupled problem for the Hirho experiment gave correct prediction and interpretation of the Hall field and showed the substantial effect of local axial current density even when there is no net axial current leakage; it also showed that the electrical performance could be improved substantially through optimization of the electrode configuration. This work has demonstrated the importance of realistic computations in the design of efficient magnetohydrodynamic channels.

TABLE OF CONTENTS

ILLUSTRATIONS

$\dot{m}$	Mass flow through the flow channel
$\dot{m}_E$	Mass entrainment rate at outer edge of boundary layer
$\dot{m}_I$	Mass flux through the inner edge of the boundary layer
n	Particle number density
p	Gas pressure
Pr	Prandtl number
q	y-component of turbulent heat flux
q_L	y-component of molecular heat flux
R	Hydraulic radius of flow channel (Section II only)
R	Gas constant (Section III only)
$\dot{R}$	Radiation loss term (Eq. 4)
Re_θ	Reynolds number, $U_\infty \theta/\nu$
Re_∞	Reynolds number, $U_\infty x/\nu$
S	Mass flow streamfunction
S_t	Stanton number
Sc	Schmidt number
s_a	Particle source term (Eq. 1')
s_E	Energy source term (Eq. 3")
s_M	Momentum source term (Eq. 2')
T	Gas temperature
T_n	Excitation temperature of gas (Eq. 4)
$\vec{U}$	Mass-average velocity vector
U_∞	Velocity outside the boundary layer
u	x-component of $\vec{U}$
V_{el}	Total electrode voltage drop, $V_s + V_{bl}$
V_{bl}	Electrode boundary layer voltage drop
V_s	Electrode sheath voltage drop
v	y-component of $\vec{U}$
x	Streamwise coordinate
y	Coordinate normal to x and z
z	Coordinate parallel to $\vec{B}$
β	Ohm's Law coefficient (Eq. 5)
γ	Ratio of specific heats, c_p/c_v
δ	Thickness of boundary layer
δ_{995}	Value of y where $u(y) = 0.995\ U_\infty$

δ_{eff}	Effective energy loss factor for electrons in collisions with heavy particles (Eq. 4)
δ^*	Displacement thickness, $\int_o^\delta [(U_\infty - u)/U_\infty]\, dy$
ϵ	Ohms Law coefficient (Eq. 5)
ϵ_i	Ionization potential
θ	Momentum thickness, $\int_o (u/U_\infty)(1 - \frac{u}{U_\infty})\, dy$
μ_L	Molecular viscosity
μ_T	Effective viscosity, due to turbulence
ν	Kinematic viscosity, μ_L/ρ
ν_t	Total collision frequency for electrons with heavy particles (Eq. 4)
ρ	Mass density
σ	Scalar electrical conductivity
τ	Reynolds shear stress, $-\rho \langle u'v' \rangle$
τ_L	Molecular shear stress
$\vec{\Phi}$	Vector function whose 5 components are the dependent variables in the boundary layer, (u, τ, T, c_a, T_e)
Φ	Any component of $\vec{\Phi}$
$\vec{\phi}$	Vector function whose 4 components are (u, T, c_a, T_e)
φ	Angle between current vector and y-axis
Ψ	Electric current streamfunction
ω	Dimensionless cross-stream coordinate (Eq. 37)
$\langle\ \rangle$	Denotes time-averaged value

Subscript Notation

E	Evaluated at the outer edge of the boundary layer
e	Pertaining to electrons
I	Evaluated at the inner edge of the boundary layer
L	Denotes molecular, or laminar, contribution
T	Denotes turbulent contribution
w	Evaluated at the wall
a	Pertaining to one component
∞	Pertaining to conditions outside the boundary layer

Superscript Notation

*	Dimensionless quantity (Section III)
'	Denotes fluctuation about the mean value of a quantity in turbulent flow (where appropriate)

I. INTRODUCTION

This report presents the results of the third phase of a study aimed at providing realistic performance analysis of crossed-field accelerators.

The basic thesis that gave motivation to, and was a posteriori justified by, this work is that realistic description of the overall performance characteristics of magnetohydrodynamic channels can be obtained only by accurate knowledge of the local behavior at every point in the channel and rigorous analytical account of the physical mechanisms that influence the flowing plasma.

The first two phases of this work were devoted to obtaining rigorous solution of the electrical problem (i.e., the current density, electric field, and plasma property distributions) in the main, periodic part of a multielectrode channel. This was successfully accomplished (Refs. 1 and 2): A realistic two-dimensional model for the current density field and for the distributions of electron temperature and plasma composition was formulated, and a numerical method and a computer program were developed to compute these interdependent field distributions. The results have been reported in Refs. 1-5 and include analysis of the effects of thermal and concentration diffusion, electrode-wall boundary layers, finite reaction rates, and electron energy convection.

The third phase, the results of which are described in this report, had the twofold objective to (1) extend the two-dimensional solution of the electrical problem to cover the entire length of a magnetohydrodynamic channel, including the entrance and exit regions, and (2) to obtain solutions of the gasdynamic problem (i.e., the fluid velocity, temperature, and pressure distributions), including velocity and temperature profile developments in the electrode-wall boundary layers, over any prescribed accelerator length.

Fig. 1 is a schematic diagram of the analytical problem that has been solved in this study. Two independent variables are considered: x in the direction of the overall plasma flow and y in the direction of the

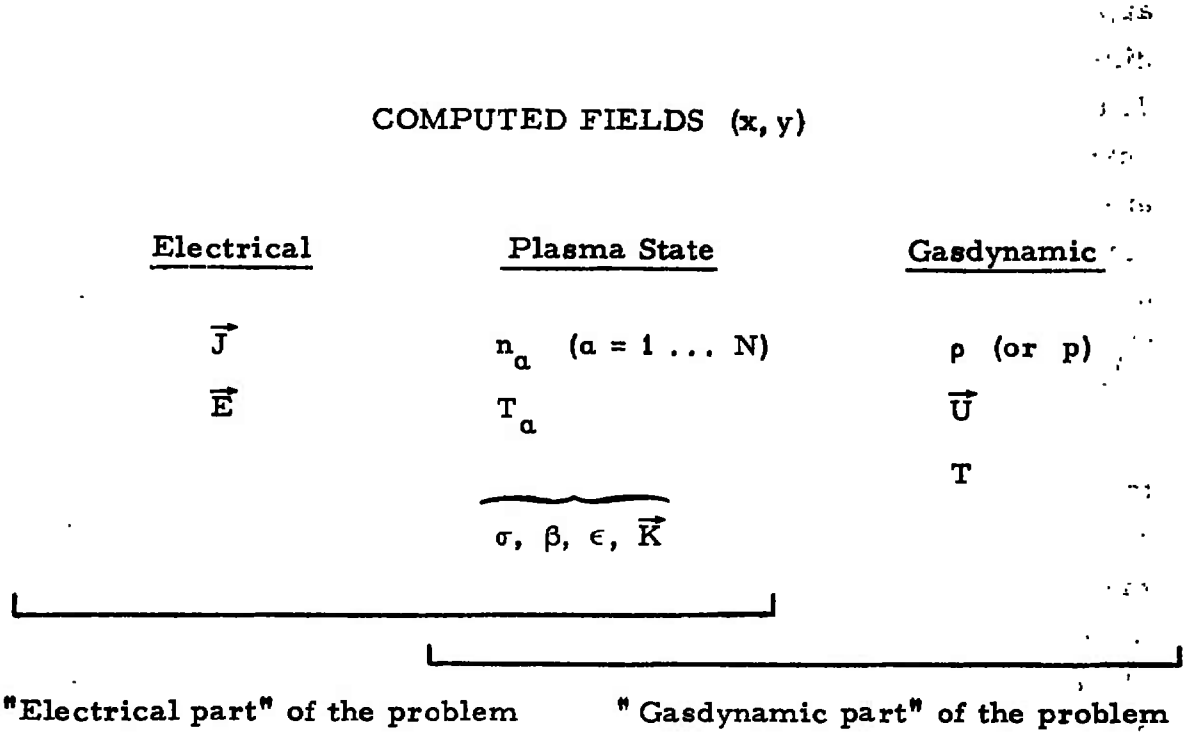

Fig. 1. Schematic diagram of the analytical problem solved in this study.

applied electric field. The magnetic induction $\vec{B}$ is assumed to be directed in the positive z-direction and to be a known function of x. Three classes of computed fields are distinguished. First, the electrical unknowns, namely the current density field $\vec{J}$ and the electric field $\vec{E}$ at every point in the gas. Second, the unknowns that characterize the state of the plasma, namely the number density n_a of each component a that is needed for this purpose, and its characteristic temperature T_a. (Plasma transport properties are then calculable by the methods of Ref. 6.) Finally, the gasdynamic fields, namely the gas density ρ or pressure p, gas velocity $\vec{U}$ and static gas temperature T. If values for the gasdynamic distributions are assumed and the first two classes of unknowns (which are coupled), are solved for, it is called solution of the (still nonlinear) "electrical part" of the problem (see Fig. 1). This is what was done in Phases I and II. If values for the current density or the electric field distribution as assumed and the last two classes of unknowns are solved for, this is called solution of the "gasdynamic part" of the problem (see Fig. 1). In the work reported herein (Phase III) all three classes of unknowns are solved for, over any prescribed channel length, by iteration between the electrical and gasdynamic parts of the problem.

To obtain the solution to the coupled "electrical + gasdynamic" problem over the whole channel, five subproblems had to be considered: (1) solution of electrical part of the problem in the entrance region of the channel, (2) solution of the electrical part of the problem in the periodic part of the channel, (3) solution of the electrical part of the problem in the exit region, (4) solution of the gasdynamic part of the problem in the core of the flow, and (5) solution of the gasdynamic part of the problem in the turbulent boundary layers over the electrode walls. Subproblem (2) had been solved in Phases I and II of the project (see Refs. 1 and 2). Thus, this report will describe the solution of the other four subproblems. Their formulation will be presented in Section II, the methods of solution in Section III, while Section IV will present results for various test cases. The discussion will be more detailed in the case of the more complex of the four subproblems, namely the computation of the compressible turbu-

lent magnetohydrodynamic boundary-layer development over the electrode walls, for which a novel formulation (Ref. 7) has been used.

With the completion of Phase III, this work can make the claim that it can "model" the electrical and gasdynamic performance of magnetohydrodynamic channels realistically. Applications have shown that, unlike previous idealized or oversimplified theories, it can predict experimental results with accuracy, and can provide the experimentalist and development engineer with truly rigorous and practical assistance. Towards this aim, every effort has been made to maintain maximum flexibility, and the analysis can treat (1) different channel, electrode, and insulator geometries, including "staggered" electrodes, (2) different operating modes and magnetic field distributions, (3) different current leakage rates, (4) different combinations of boundary layer and core flow initial conditions, (5) different operating fluids (monatomic, diatomic, or mixtures of gases), (6) different seed materials and seed ratios, (7) different electrode and wall temperatures and cooling rates, (8) different wall ablation rates, and (9) different load conditions.

II. FORMULATION

1. THE ELECTRICAL PROBLEM

The formulation of the electrical problem has been described in detail in Refs. 1 and 2. Unknowns of the problem are (1) the current streamfunction Ψ, (2) the electron temperature T_e, and (3) the number densities n_α ($\alpha = 1 \ldots N$) of all the components that are needed to characterize the state of the plasma. The equations of the problem (equal in number to the above unknowns) are (1) the streamfunction equation, (2) the electron energy equation, and (3) the continuity equations for each plasma component (Refs. 1 and 2). These equations are uniformly valid over the whole length of a multielectrode channel.

To solve the electrical problem over the whole channel, it is convenient to divide the channel into three separate regions:

(1) The entrance region
(2) The main (periodic) part
(3) The exit region

In the main part of the channel, the geometrical periodicity imposed by electrode segmentation, together with the fact that gasdynamic properties change very little over a streamwise distance of the order of one electrode period L (Ref. 1), leads to a "quasiperiodic" distribution of all the unknowns of the electrical problem. The term "quasi-periodic" is used to indicate that, although periodicity is a sufficiently good approximation to the actual situation to allow the use of periodic boundary conditions for each electrode segment in the mathematical formulation, it does not describe a physical fact, and that actually the plasma properties do change slowly from one electrode to the other, as do the gasdynamic variables and possibly the external loading conditions and magnetic induction.

The "quasiperiodic" condition is obviously approached asymptotically away from the entrance and exit regions of the channel. In the case of the first and last electrode pairs, there is not even geometrical periodicity, and this geometric disturbance will of course affect the

solution of the problem for several electrode pairs downstream and upstream, respectively. In addition, even if geometrical periodicity exists, it takes a certain distance before periodicity of the plasma properties can be realized, owing to the finite rates of ionization and of electron energy relaxation.

1.1. Main (Periodic) Part of Channel

As mentioned above, this part of the channel is called periodic only because periodic boundary conditions can be used for the purpose of obtaining the solution. This part covers most of the length of a powered magnetohydrodynamic channel. The solution of the electrical problem in this part of the device has been obtained in Phases I and II.

1.2. Entrance and Exit Regions

The treatment of the boundary conditions for the entrance and exit regions does not differ, since the situation for these two regions is analogous (they are mirror images of each other), and therefore the formulation discussed in this section will be valid for both.

For these two regions, periodic conditions cannot be employed. In addition, owing to the elliptic nature of the streamfunction equation, the whole entrance (and respectively the whole exit) region will have to be treated as the geometry of the problem, and they may have to include several electrode pairs in order to account for the transition region, i.e., before periodicity is realized. Experience with the solution has shown that the axial extent of these transition regions does not exceed 5-8 electrode pairs.

The geometry appropriate to the entrance problem, shown in Fig. 2, starts well upstream of the first powered electrode pair and extends downstream until the condition of quasiperiodicity is satisfied. Thus the entrance region actually consists of two parts, a powered section and an unpowered one. The unpowered section is bounded in the y-direction by insulating walls of length L_o and/or K_o unpowered electrode pairs. The powered section is bounded by K-K_o electrode pairs. The con-

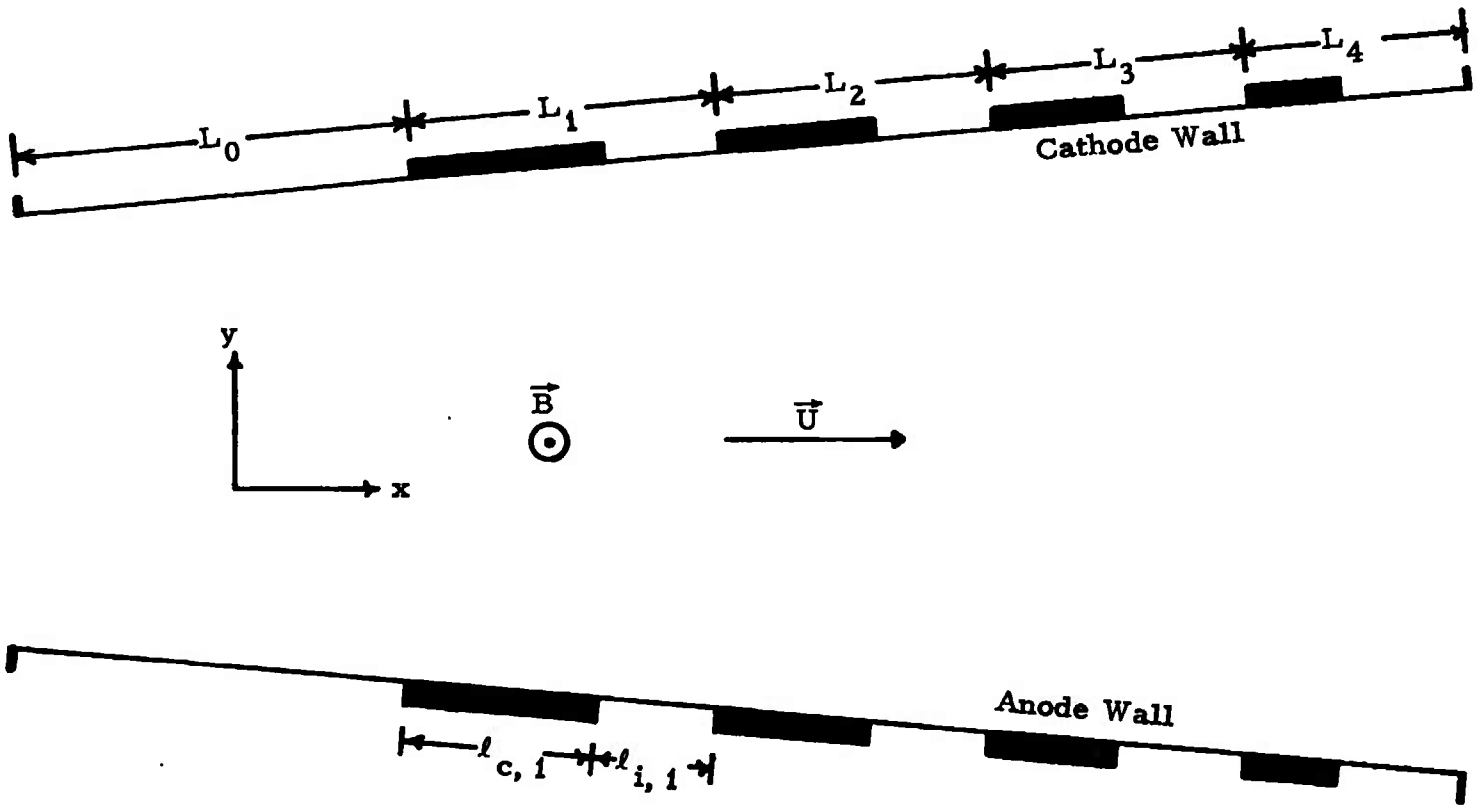

Fig. 2. Geometry of entrance region of J × B accelerator.

ductor and insulator segments of each electrode pair k (k = 1, 2, . . . , K) have lengths $\ell_{c,k}$ and $\ell_{i,k}$ respectively, so that the total length of each electrode pair is $L_k = \ell_{c,k} + \ell_{i,k}$. In obtaining the solution, the number K of electrode pairs is varied until the actual extent of the entrance region (as defined above) is ascertained.

The boundary conditions on the y-walls reflect the alternation of successive conductor and insulator segments. The form of these conditions is identical to those used in Phases I and II (Refs. 1 and 2), namely Ψ = const along the surface of insulator segments and $E_x = 0$ along the surface of conductor segments. The total current $I_{y,k}$ passed in the positive y-direction per unit width of each conductor k will be equal to the difference between the value of the streamfunction Ψ on the insulator segments k and k-1. Thus, in the case of an unpowered electrode k, the value of the streamfunction on the k and k-1 insulator segments will be the same.

The boundary conditions at the upstream plane $x_u = 0$ of the entrance region will be of the Dirichlet type, i.e., the values of the streamfunction for all y will be known. They will be defined by the assumed distribution of net axial current leakage I_x through the channel. For example, vanishing leakage would correspond to constant $\Psi(0, y)$, while uniform current leakage density would be represented by linear variation of $\Psi(0, y)$ from a value Ψ_a on the anode wall to a value Ψ_c on the cathode wall ($\Psi_a - \Psi_c = I_x$). At the downstream (periodic) end $x_d = L_o + \sum_k L_k$ of the entrance region, one of two kinds of boundary conditions can be used: (1) Dirichlet type conditions obtained by previous solution of the one-electrode problem at that station or (2) the condition of periodic fields at the stations x_d and $x_d - L_K$. Both kinds of conditions have alternatively been used for solutions obtained in this study with very little difference in the overall results.

Finally, note that this formulation can treat the case of an MHD generator (rather than a crossed-field accelerator) simply by using negative values for $I_{y,k}$ and I_x, i.e., by reversing the position of the anode and cathode walls.

2. THE GASDYNAMIC PROBLEM

The gasdynamic problem is solved in two parts. In the core of the flow a quasi-one-dimensional solution is used (a two-dimensional inviscid solution for the core has also been coded), while a two-dimensional numerical solution is carried out for the compressible magnetohydrodynamic boundary layer development on the electrode walls.

2.1. Quasi-one-dimensional Solution for Core Flow

This formulation assumes that all quantities represent an average over the cross sectional area A of the core at each point x, so that only their x-variation is of importance. For example, the gas velocity u(x) is defined by $u(x) = \frac{1}{A} \int_A u(x, y)\, dA$.

The term quasi-one-dimensional is used to indicate that, although one-dimensional equations cannot by definition describe fluxes in the y-direction, such as viscous friction and heat conduction, nevertheless empirical terms describing these fluxes have been included in the momentum and energy equations.

It is assumed that the area variation A(x) of the channel, the magnetic induction variation B(x), and the loading variation $J_y(x)$ are given over the entire channel. Note that $J_y > 0$ in an accelerator.

Under these assumptions, (see also Ref. 8) the following "channel flow" equations are obtained for the $N + 3$ unknowns, which are the N number densities n_a of the plasma components, the axial velocity u, the gas temperature T and the electron temperature T_e.

(1) Continuity equations for each component a

$$\rho u \frac{d}{dx} (n_a/\rho) = s_a \tag{1}$$

where s_a is the source term (i.e., the rate of production of particles of component a) owing to the reactions that take place in the plasma. Appropriate expressions for these source terms are given in Ref. 2; for example, the important 3-body recombination-ionization reaction of a

species contributes to the rate of production of electrons the amount

$$s_r = k_r' n_e n_a - k_r n_e^2 n_i \tag{1'}$$

where k_r' and k_r are the ionization and recombination rate coefficients for this reaction r (they are functions of the electron temperature – see Ref. 2) and n_i, n_a are the number densities of ions and neutrals, respectively, of the species in question.

(2) Overall momentum equation

$$\rho u \frac{du}{dx} = - \frac{dp}{dx} + J_y B - s_M \tag{2}$$

where s_M is loss of momentum due to friction and is given by

$$s_M = c_f \rho u^2 / R \tag{2'}$$

where c_f is the friction coefficient and R is the hydraulic radius of the channel. In the case of a channel with rectangular cross section, R is defined as $R \equiv aD/(a+D)$, where D is the channel height (in the y-direction) and a the channel width (in the z-direction). The friction coefficient c_f is computed as a function of the local plasma conditions.

(3) Overall energy equation

$$\rho u \frac{d}{dx} \left[h + \frac{1}{2} u^2 + \frac{1}{\rho} \sum_i \epsilon_i n_i \right] = \vec{E} \cdot \vec{J} - s_E \tag{3}$$

This equation describes the transport of the total energy

$$h_t = h + \frac{1}{2} u^2 + \frac{1}{\rho} \sum_{i=\text{ions}} \epsilon_i n_i \tag{3'}$$

where ϵ_i is the ionization potential for each ion i and h the enthalpy of the gas corresponding to the temperature T. The loss of energy due to heat transfer to the walls, s_E, consists of two terms, i.e.,

$$s_E = 2\rho u S_t \frac{h_{ad} - h_w}{R} + \left| \frac{V_s}{D} J_y \right| \tag{3''}$$

where S_t is the Stanton number computed for the local plasma conditions, $h_{ad} \equiv h + \frac{r}{2} u^2$ where r is the recovery factor, h_w the enthalpy corresponding to the wall temperature T_w, and V_s is the sheath drop in volts. Note that the sheath drop V_s constitutes only a part of the total electrode drop V_{el}, the latter including also the voltage drop due to the boundary layers.

(4) Electron energy equation

$$\rho u \left[\frac{d}{dx} \frac{3}{2} \frac{p_e}{\rho} + p_e \frac{d}{dx} \frac{1}{\rho} \right] =$$

$$= \vec{E}' \cdot \vec{J}_e - \frac{3}{2} k n_e \nu_t \delta_{eff} (T_e - T_n) - \sum_i \epsilon_i s_i - \dot{R} \qquad (4)$$

where p_e is the electron partial pressure $p_e \equiv n_e k T_e$ (k Boltzmann's constant), $\vec{E}' \equiv \vec{E} + \vec{U} \times \vec{B}$, $\vec{J}_e$ the electron current, ν_t the total collision frequency for electrons (as defined in Ref. 6), δ_{eff} the effective energy loss factor for electrons (see Refs. 1 and 2, and also Ref. 9), T_n the excitation temperature of the gas (see Ref. 10), and $\dot{R}$ the radiation loss from the gas. Detailed descriptions of each term on the right-hand side of Eq. (4) have been given in previous work (Refs. 1-6 and 9-10). Therefore it is necessary only to note here that the first term expresses the Ohmic heating of the electrons, the second term the collisional energy transfer from electrons to heavy particles by all elastic and inelastic collisional processes other than ionization or electronic excitation, and the third term expresses the energy needed for ionization or released by recombination.

Equations (1), (2), (3), and (4) are the $N + 3$ differential equations used for the solution of the quasi-one-dimensional problem. Note that from Eqs. (1)

$$\rho u \frac{d}{dx} \frac{1}{\rho} \sum_i \epsilon_i n_i = \sum_i \epsilon_i s_i \qquad (1'')$$

and consequently the overall energy equation (3) can be written in the form

$$\rho u \frac{d}{dx} \left[h + \frac{1}{2} u^2 \right] = \vec{E} \cdot \vec{J} - \sum_i \epsilon_i s_i - s_E \qquad (3a)$$

The relation (1‴) was used in deriving Eq. (4).

In addition to the above differential equations, two constitutive relations, Ohm's law and an equation of state, are used to express the electric field $\vec{E}$ and the gas pressure p, respectively. Ohm's law has the following form (Refs. 1, 2, and 6), in which the contribution of thermal diffusion has been omitted for the purpose of treating the core of the flow:

$$\vec{E'} = \frac{\epsilon}{\sigma}\vec{J} + \frac{\beta}{\sigma}\vec{J} \times \vec{k} \tag{5}$$

where $\vec{k}$ is the unit vector in the z-direction, and the coefficients σ, β, ϵ are computed to the second approximation following the methods of Ref. 6. On the other hand, the equation of state has the general form

$$p = p(n_a, T_a) \tag{6}$$

where n_a and T_a are the number density and characteristic temperature, respectively, of each component a. In the present solution, the equation of state is used in its simplest form

$$p = k\left[n_e T_e + \left(\sum_{\kappa \neq e} n_\kappa\right) T\right] \tag{6a}$$

Finally, note that use of the complete set of Eqs. (1) implies that the overall conservation of mass

$$\rho u A = \dot{m} = \text{constant} \tag{1‴}$$

is also satisfied, where $\dot{m}$ is the mass flow rate in the channel.

The quasi-one-dimensional formulation of the gasdynamic problem in the core of the flow is completed by specifying initial conditions for the unknowns at a given station x_o of the channel.

2.2. Compressible Turbulent Boundary Layer Development

Boundary layer development on the electrode walls of magnetohydrodynamic channels is a major factor in determining their performance The serious problem of channel choking by boundary layer growth has often occurred and been reported in the past (Refs. 11 and 12). Also, Phases I and II of this study have demonstrated that gasdynamic boundary layers have a decisive influence on the electrical performance.

A realistic analytical treatment of these boundary layers must account for the fact that they are compressible and turbulent, and that in addition to the presence of both mean and fluctuating electromagnetic forces and heat sources, the very structure of turbulence is affected by the presence of strong electromagnetic fields in these devices.

Such a treatment has been carried out by this study, employing a novel formulation developed previously (Ref. 7). This formulation is based on the close relation that is found to exist between the turbulent shear stress τ and the turbulence kinetic energy. Using experimental data to derive universal turbulence structure parameters a_1, a_2, and a_3 that correlate the turbulent shear stress with the intensity, dissipation, and diffusion of turbulence energy (see Ref. 7), the turbulence energy equation (which is an equation for the rate of change of turbulence kinetic energy along a streamline of the mean flow) is converted into a transport equation for the rate of change of turbulent shear stress. Then this equation, together with the mean momentum equation, the mean continuity equation and, for the compressible case, the mean energy equation form a closed system (provided the turbulent heat conduction q can also be related to the other variables) that can be solved numerically. Thus, this formulation avoids the use of phenomenological "mixing length" expressions, and can treat the influence of electromagnetic fields on the turbulence structure quite naturally: turbulence suppression by the magnetic field is accounted for by an additional term in the turbulence kinetic energy equation.

This novel formulation has been used in this study in parallel with the traditional "eddy viscosity" approach so as to provide a comparison of the two, and continuous check of the novel method. The method of solution for the two formulations is basically the same (see Section III).

The unknowns of the two-dimensional compressible turbulent magnetohydrodynamic boundary-layer problem, as formulated in this study, are

(1) the mean velocity $\vec{U} = (u, v)$,
(2) the turbulent shear stress $\tau \equiv -\rho \langle u'v' \rangle$,
(3) the gas enthalpy $h = e + p/\rho$,
(4) the number densities n_a (or partial mass densities ρ_a, or concentrations $c_a \equiv \rho_a/\rho$) of each component a, and
(5) the characteristic temperatures T_a (or enthalpies h_a) of each component a.

Primed symbols denote the fluctuating part of each quantity; the reader is referred to Ref. 7 for detailed definitions.

The formulation described in Ref. 7 presents a closed system of equations for the first four* of the above unknowns plus the turbulent energy flux $q \equiv \rho \langle e'v' \rangle$ and the mass diffusion fluxes $d_a \equiv \langle \rho_a' v' \rangle$, with the requirement that the values of nine universal structure parameters a_1 to a_9 be known as functions of the normalized cross-coordinate y/δ. However, sufficient experimental data are available only for a_1, a_2, and a_3; only very scarce measurements exist for the turbulence correlations necessary for defining the other six structure parameters. Consequently, in this study the use of turbulent structure functions has been limited to a_1, a_2, and a_3, and for the moment, the conventional concepts of turbulent diffusivity and turbulent heat conductivity have been relied upon, through the use of a turbulent Schmidt

*The characteristic temperatures T_a were not considered as additional unknowns in Ref. 7 because thermal equilibrium ($T_a = T$) was assumed therein. Also, the energy e rather than the enthalpy h was used in Ref. 7 to characterize the thermal state of the gas; the enthalpy h was chosen here because of the availability of a convenient thermal equation of state for air (Ref. 13) in the form $h = h(p, T)$.

number and turbulent Prandtl number, to replace a_4 to a_9. In addition, only one characteristic temperature other than the static gas temperature T has been distinguished, namely the electron temperature T_e.

The system of equations corresponding to these unknowns in the body-oriented coordinate system (x, y) are the following (see Ref. 7):

(1) Overall mass conservation equation

$$\frac{\partial}{\partial x} \rho u + \frac{\partial}{\partial y} \rho v + \frac{\partial}{\partial y} \langle \rho' v' \rangle = 0 \tag{7}$$

The last term, denoting mass diffusion due to fluctuations in density and transverse velocity component, is negligible compared to the other two terms for free-stream Mach number up to about 5 (because the local Mach number, based on the fluctuating velocity, will then be small). Thus the overall conservation equation will be used in this study in the form

$$\frac{\partial}{\partial x} \rho u + \frac{\partial}{\partial y} \rho v = 0 \tag{7a}$$

(2) Overall momentum equation

$$\rho \left\{ u \frac{\partial}{\partial x} + v \frac{\partial}{\partial y} \right\} u + \langle \rho' v' \rangle \frac{\partial u}{\partial y} - \frac{\partial}{\partial y} (\tau_L + \tau) =$$

$$= - \frac{dp}{dx} + J_y B \tag{8}$$

where τ is the turbulent shear stress and τ_L the laminar stress due to molecular viscosity μ_L ($\tau_L = \mu_L \partial u/\partial y$). Note that $\tau >> \tau_L$ in the main part of the turbulent boundary layer; however, since τ_L is of significance in the wall region it will be retained in the momentum equation. On the other hand, the term $\langle \rho' v' \rangle \frac{\partial u}{\partial y}$ is negligible compared to the other terms of Eq. (8), for free-stream Mach number up to 5, and will be omitted. Thus the overall momentum equation will be used in this study in the form

$$\rho \left\{ u \frac{\partial}{\partial x} + v \frac{\partial}{\partial y} \right\} u = \frac{\partial}{\partial y} \left[\tau + \mu_L \frac{\partial u}{\partial y} \right] - \frac{dp}{dx} + J_y B \tag{8a}$$

(3) Turbulent shear transport equation

$$\rho\left\{u\frac{\partial}{\partial x}+v\frac{\partial}{\partial y}\right\}\frac{\tau}{2a_1\rho}+\frac{(\tau/\rho)_{max}}{U_\infty}\frac{\partial}{\partial y}a_3\tau=$$

$$=\tau\frac{\partial u}{\partial y}-\frac{\rho}{a_2\delta}\left(\frac{\tau}{\rho}\right)^{3/2}-\frac{1}{3}\frac{\epsilon\sigma B^2}{\epsilon^2+\beta^2}\frac{\tau}{a_1\rho} \qquad (9)$$

As discussed in Ref. 7, the first two terms on the right-hand side of Eq. (9) describe the production and dissipation, respectively, of turbulence kinetic energy due to fluctuations, while the third term accounts for turbulence suppression by magnetic fields, which is due to the interaction between the flow field and the electromagnetic interactions. The conductivity σ, the Hall coefficient β and the ion-slip parameter ϵ are defined in Refs. 1, 2, and 6, while the turbulence structure parameters a_1, a_2, and a_3 are defined in Ref. 7. Their values across the boundary layer are given in Section III.

(4) Overall energy equation

$$\rho\left\{u\frac{\partial}{\partial x}+v\frac{\partial}{\partial y}\right\}h+\langle\rho'v'\rangle\frac{\partial h}{\partial y}+\frac{\partial}{\partial y}\left\{\rho\langle h'v'\rangle+q_L\right\}=$$

$$=u\frac{dp}{dx}+\tau_L\frac{\partial u}{\partial y}+\frac{\rho}{a_2\delta}\left(\frac{\tau}{\rho}\right)^{3/2}+\vec{J}\cdot(\vec{E}+\vec{U}\times\vec{B})+\frac{1}{3}\frac{\epsilon\sigma B^2}{\epsilon^2+\beta^2}\frac{\tau}{a_1\rho} \qquad (10)$$

where q_L is the thermal conduction due to molecular heat conductivity and species diffusion. The terms $\partial q_L/\partial y$ and $\tau_L(\partial u/\partial y)$ are generally small compared to the other terms of Eq. (10), but will be retained because of their significance close to the wall. On the other hand, the term $\langle\rho'v'\rangle(\partial h/\partial y)$ is negligible for free-stream Mach number up to 5 and will be omitted. Note that

$$\tau_L\frac{\partial u}{\partial y}=\mu_L\left(\frac{\partial u}{\partial y}\right)^2 \qquad (11)$$

and

$$q_L=-\frac{k_L}{c_p}\sum_a c_a\frac{\partial h_a}{\partial y}-\rho D_L\sum_a h_a\frac{\partial c_a}{\partial y}$$

where μ_L, k_L, and D_L are the molecular viscosity, heat conductivity,

and binary diffusion coefficient, respectively. Using the definition

$$h = \sum_a c_a h_a \tag{12}$$

it is possible to express

$$\sum_a c_a \frac{\partial h_a}{\partial y} = \frac{\partial h}{\partial y} - \sum_a h_a \frac{\partial c_a}{\partial y} \tag{13}$$

The concepts of the laminar Prandtl and Schmidt numbers Pr_L and Sc_L, respectively, can be introduced so that

$$\begin{aligned} k_L &= \frac{c_p \mu_L}{Pr_L} \\ \rho D_L &= \frac{\mu_L}{Sc_L} \end{aligned} \tag{14}$$

Eqs. (13) and (14) can then be used to express

$$q_L = -\mu_L \left[\frac{1}{Pr_L} \frac{\partial h}{\partial y} + \left(\frac{1}{Sc_L} - \frac{1}{Pr_L} \right) \sum_a h_a \frac{\partial c_a}{\partial y} \right] \tag{15}$$

The turbulent heat flux $\rho\langle h'v'\rangle$ is also expressed by using the definition (12), which leads to the result

$$\begin{aligned} \rho\langle h'v'\rangle &= \rho \left\{ \sum_a c_a \langle h_a' v' \rangle + \sum_a h_a \langle c_a' v' \rangle \right\} \\ &= -\frac{\tau}{\partial u/\partial y} \left[\frac{1}{Pr_T} \frac{\partial h}{\partial y} + \left(\frac{1}{Sc_T} - \frac{1}{Pr_T} \right) \sum_a h_a \frac{\partial c_a}{\partial y} \right] \end{aligned} \tag{16}$$

where the concepts of the turbulent Prandtl and Schmidt numbers Pr_T and Sc_T, respectively, have been introduced to relate the turbulent fluxes $\rho\langle h_a' v'\rangle$ and $\rho\langle c_a' v'\rangle$ to the gradients $\partial h_a/\partial y$ and $\partial c_a/\partial y$ as follows:

$$\begin{aligned} \rho\langle h_a' v'\rangle &= -\frac{\tau}{Pr_T \, \partial u/\partial y} \frac{\partial h_a}{\partial y} \\ \rho\langle c_a' v'\rangle &= -\frac{\tau}{Sc_T \, \partial u/\partial y} \frac{\partial c_a}{\partial y} \end{aligned} \tag{17}$$

The turbulent Prandtl number has generally been found to have values close to 0.9 (Refs. 14 and 15).

Using the expressions for q_L and $\rho\langle h'v'\rangle$ given by Eqs. (15) and (16), respectively, Eq. (10) can be written in the form

$$\rho\left\{u\frac{\partial}{\partial x}+v\frac{\partial}{\partial y}\right\}h=\frac{\partial}{\partial y}\left[\left(\frac{\mu_L}{Pr_L}+\frac{\tau}{Pr_T\,\partial u/\partial y}\right)\frac{\partial h}{\partial y}+\right.$$

$$+\left\{\mu_L\left(\frac{1}{Sc_L}-\frac{1}{Pr_L}\right)+\frac{\tau}{\partial u/\partial y}\left(\frac{1}{Sc_T}-\frac{1}{Pr_T}\right)\right\}\sum_a h_a\frac{\partial c_a}{\partial y}\left.\right]+$$

$$+u\frac{dp}{dx}+\mu_L\left(\frac{\partial u}{\partial y}\right)^2+\frac{\rho}{a_2\delta}\left(\frac{\tau}{\rho}\right)^{3/2}+\vec{J}\cdot(\vec{E}+\vec{U}\times\vec{B})+$$

$$+\frac{1}{3}\frac{\epsilon\sigma B^2}{\epsilon^2+\beta^2}\frac{\tau}{a_1\rho} \tag{10a}$$

Note: An alternative form of the overall energy equation, that can be convenient to use, is the transport equation for the total enthalpy $H = h + \frac{u^2}{2}$. It has the form

$$\rho\left\{u\frac{\partial}{\partial x}+v\frac{\partial}{\partial y}\right\}H+\langle\rho'v'\rangle\frac{\partial H}{\partial y}+\frac{\partial}{\partial y}\left\{\rho\langle H'v'\rangle+q_L\right\}=$$

$$=\frac{\partial}{\partial y}\tau_L u+\vec{E}\cdot\vec{J} \tag{18}$$

The turbulent flux $\rho\langle H'v'\rangle$ can be written

$$\rho\langle H'v'\rangle\approx\rho\langle h'v'\rangle+\rho u\langle u'v'\rangle$$

$$=\rho\langle h'v'\rangle-u\tau \tag{19}$$

and again the term $\langle\rho'v'\rangle\,\partial H/\partial y$ can be omitted. Consequently, Eq. (18) can be written in the form

$$\rho\left\{u\frac{\partial}{\partial x}+v\frac{\partial}{\partial y}\right\}H=\frac{\partial}{\partial y}\left[\left(\frac{\mu_L}{Pr_L}+\frac{\tau}{Pr_T\,\partial u/\partial y}\right)\frac{\partial H}{\partial y}+\right.$$

$$\left.+u\left\{\left(1-\frac{1}{Pr_L}\right)\mu_L\frac{\partial u}{\partial y}+\left(1-\frac{1}{Pr_T}\right)\tau\right\}+\right.$$

$$+\left\{\mu_L\left(\frac{1}{Sc_L}-\frac{1}{Pr_L}\right)+\frac{\tau}{\partial u/\partial y}\left(\frac{1}{Sc_T}-\frac{1}{Pr_T}\right)\right\}\sum_a h_a\frac{\partial c_a}{\partial y}\Bigg]+\vec{J}\cdot\vec{E} \quad (18a)$$

(4) Species conservation equation

$$\frac{\partial}{\partial x}\rho_a u+\frac{\partial}{\partial y}\rho_a v+\frac{\partial}{\partial y}\left\{\langle\rho_a' v'\rangle+d_{a,L}\right\}=m_a\langle s_a\rangle$$

or, equivalently,

$$\rho\left\{u\frac{\partial}{\partial x}+v\frac{\partial}{\partial y}\right\}c_a+\langle\rho' v'\rangle\frac{\partial c_a}{\partial y}+\frac{\partial}{\partial y}\left\{\rho\langle c_a' v'\rangle+d_{a,L}\right\}=$$

$$=m_a\langle s_a\rangle \quad (20)$$

where $\langle s_a\rangle$ is the mean source of particles of component a due to chemical reactions. The molecular diffusion term $\partial d_{a,L}/\partial y$ is generally small compared to the other terms of Eq. (20) in the main part of the turbulent boundary layer, but will be retained because of its significance close to the wall. It will be expressed in terms of the laminar Schmidt number Sc_L as usual:

$$d_{a,L}=-\rho D_L\frac{\partial c_a}{\partial y}=-\frac{\mu_L}{Sc_L}\frac{\partial c_a}{\partial y} \quad (21)$$

On the other hand, the term $\langle\rho' v'\rangle\,\partial c_a/\partial y$ that appears in the second version of Eq. (20) is negligible for the same reasons mentioned in the derivation of the continuity, momentum, and energy equations, and will be omitted.

The turbulent diffusion flux $\rho\langle c_a' v'\rangle$ can be written in terms of the turbulent Schmidt number Sc_T as indicated by the second of Eqs. (17).

Consequently, the second of Eqs. (20) can be given in the following form, which will be used in this study:

$$\rho\left\{u\frac{\partial}{\partial x}+v\frac{\partial}{\partial y}\right\}c_a=\frac{\partial}{\partial y}\left(\frac{\mu_L}{Sc_L}+\frac{1}{Sc_T}\frac{\tau}{\partial u/\partial y}\right)\frac{\partial c_a}{\partial y}+m_a\langle s_a\rangle \quad (20a)$$

(5) Electron energy equation

$$\rho\left\{u\frac{\partial}{\partial x}+v\frac{\partial}{\partial y}\right\}c_e h_e+\langle\rho' v'\rangle\frac{\partial}{\partial y}c_e h_e+$$

$$+\frac{\partial}{\partial y}\left\{\rho\langle(c_e h_e)' v'\rangle+q_{e,L}\right\}-\left\{u\frac{\partial}{\partial x}+v\frac{\partial}{\partial y}\right\}p_e=$$

$$=\vec{J}_e\cdot(\vec{E}+\vec{U}\times\vec{B})+\langle\vec{J}_e'\cdot(\vec{E}'+\vec{U}'\times\vec{B})\rangle-$$

$$-\frac{3}{2}kn_e\nu_t\delta_{eff}(T_e-T_n)-\sum_{ions}\epsilon_i\langle s_i\rangle-\dot{R} \qquad (22)$$

where $c_e \equiv \rho_e/\rho$ is the electron concentration, $h_e \equiv (5k/2m_e)T_e$ the electron enthalpy ($c_{p,e} \equiv 5k/2m_e$), $p_e \equiv n_e kT_e$ the electron pressure, T_e the electron temperature, T_n the excitation temperature of the gas (Ref. 10), ϵ_i the ionization potential for each ionizing species, and $q_{e,L}$ the heat flux due to conduction and diffusion of electrons, expressed as

$$q_{e,L}=-k_e\frac{\partial T_e}{\partial y}-\rho D_L h_e\frac{\partial c_e}{\partial y}$$

$$=-\mu_L\left\{\frac{c_e}{Pr_L}\frac{\partial h_e}{\partial y}+\frac{1}{Sc_L}h_e\frac{\partial c_e}{\partial y}\right\} \qquad (23)$$

where k_e is the thermal conductivity for electrons. Note that Eq. (23) is consistent with the multicomponent expression for q_L given by Eq. (11). Again, for free-stream Mach number up to 5, the term $\langle\rho' v'\rangle\frac{\partial}{\partial y}c_e h_e$ is negligible compared to the other terms of Eq. (22) and will be omitted.

The turbulence flux $\rho\langle(c_e h_e)' v'\rangle$ can be expressed as follows

$$\rho\langle(c\ h_e)' v'\rangle=\rho c_e\langle h_e' v'\rangle+\rho h_e\langle c_e' v'\rangle$$

$$=-\frac{\tau}{\partial u/\partial y}\left[\frac{c_e}{Pr_T}\frac{\partial h_e}{\partial y}+\frac{h_e}{Sc_T}\frac{\partial c_e}{\partial y}\right] \qquad (24)$$

where use has been made of Eqs. (17).

Finally, the total current density $\vec{J}$ in a magnetohydrodynamic channel is very closely approximated by the electronic current $\vec{J}_e$ alone, so that the results of Ref. 7 can be used to express

$$\langle \vec{J}'_e \cdot (\vec{E}' + \vec{U}' \times \vec{B}) \rangle \approx \langle \vec{J}' \cdot (\vec{E}' + \vec{U}' \times \vec{B}) \rangle =$$

$$= \frac{1}{3} \frac{\epsilon \sigma B^2}{\epsilon^2 + \beta^2} \frac{\tau}{a_1 \rho} \tag{25}$$

Using the expressions given by Eqs. (23) - (25), Eq. (22) can be written in the form

$$\rho \left\{ u \frac{\partial}{\partial x} + v \frac{\partial}{\partial y} \right\} c_e h_e =$$

$$= \frac{\partial}{\partial y} \left[\left(\frac{\mu_L}{Pr_L} + \frac{\tau}{\partial u / \partial y} \frac{1}{Pr_T} \right) c_e \frac{\partial h_e}{\partial y} + \left(\frac{\mu_L}{Sc_L} + \frac{\tau}{\partial u / \partial y} \frac{1}{Sc_T} \right) h_e \frac{\partial c_e}{\partial y} \right] +$$

$$+ \left\{ u \frac{\partial}{\partial x} + v \frac{\partial}{\partial y} \right\} p_e + \vec{J}_e \cdot (\vec{E} + \vec{U} \times \vec{B}) + \frac{1}{3} \frac{\epsilon \sigma B^2}{\epsilon^2 + \beta^2} \frac{\tau}{a_1 \rho} -$$

$$- \frac{3}{2} k n_e \nu_t \delta_{eff} (T_e - T_n) - \sum_{\text{ions}} \epsilon_i \langle s_i \rangle - \dot{R} \tag{22a}$$

Equations (7a), (8a), (9), (10a) or (18a), (20a) and (22a) constitute a system of $N + 5$ partial differential equations for the $N + 5$ unknown quantities u, v, τ, T, c_a and T_e of the gasdynamic problem in the compressible turbulent boundary layers.

The use of a transport equation for τ to replace the conventional algebraic "eddy-viscosity" relation is discussed in detail in Ref. 7. It results in a momentum equation [Eq. (8a)] in which the diffusion term $\partial \tau / \partial y$ is not of gradient diffusion type. It is worthy of note that the diffusion term in the turbulent shear stress equation (9) is not of gradient-diffusion type either (Ref. 7). As a consequence of these two facts, the

system of governing equations is hyperbolic.

Note that, when convection, diffusion, and magnetic suppression terms are negligible, Eq. (9) reduces to an algebraic expression of the form of the mixing length relation, namely

$$(\tau/\rho)^{1/2} = a_2\delta \frac{\partial u}{\partial y} \tag{9a}$$

with the dissipation length $a_2\delta$ appearing in place of Prandtl's mixing length ℓ. This situation prevails close to the wall. On the other hand, near the outer edge of the boundary layer the diffusion and convection terms are dominant in Eq. (9), which therefore assumes the form

$$\rho\left\{u \frac{\partial}{\partial x} + v \frac{\partial}{\partial y}\right\}\frac{\tau}{2a_1\rho} + \frac{(\tau/\rho)_{max}}{U_\infty} \frac{\partial}{\partial y} a_3\tau = 0 \tag{9b}$$

This form of Eq. (9) is utilized to relate the entrainment rate $\dot{m}_E$ through the outer boundary to the turbulence structure parameters a_1 and a_3. Let the outer edge of the boundary layer be defined as the line $y_E(x)$ on which the streamwise velocity u equals 99.5% of the free-stream value; in other words, $y_E(x) = \delta_{995}(x)$, where $u(x, \delta_{995}) = 0.995\ U_\infty$ at every x. Accordingly, Eq. (9b) yields

$$\dot{m}_E = -2a_1a_3\rho_\infty U_\infty^{-1}\left(\frac{\tau}{\rho}\right)_{max} \tag{26}$$

Eq. (26) has been used to obtain the structure parameter $a_3(y)$ experimentally through measurements of the entrainment rate (Ref. 14).

III. METHODS OF SOLUTION

1. ELECTRICAL PROBLEM

The solution of the electrical problem in the entrance and exit regions follows closely the methods used in Phases I and II for the single electrode problem. In fact, the solution of the streamfunction equation employs exactly the same method, with different boundary conditions, while the simultaneous solution of the continuity and electron energy equations on each streamline (see Ref. 2) is simplified by the fact that initial, rather than boundary-type, conditions are now used for n_a and T_e. (This fact eliminates the need for carrying out the "initial condition iteration" described in Ref. 2.)

The rectangular variable-mesh grid of points used for the numerical solution consists, as in the single electrode problem, of m rows and n columns, where row 1 coincides with the anode surface $y = 0$ and row m coincides with the cathode surface $y = D$. However, columns 1 and n now define the upstream and downstream boundaries of the whole entrance (or exit) region. Care is taken that each of the points on the y-walls that separate conductor from insulator segments (i.e., each of the singular points of the geometry) lies on a grid column; this is always possible owing to the variable spacing of the grid.

As mentioned above, the finite-difference solution of the streamfunction equation in the entrance and exit regions is accomplished by the same direct method that was employed in Phases I and II (refs. 1 and 2). The number of "fundamental unknowns" (see Ref. 1) is now $n - 2$.

Finally, concerning the simultaneous solution of the continuity and electron energy equations, it is well to elaborate on the important point mentioned above: When solving the electrical problem in the periodic part of the channel without any prior knowledge of the plasma properties at the initial plane of one electrode-pair region (as was done in Phases I and II), boundary-type (i.e., periodicity) conditions with with respect to x must be used, both for the current streamfunction and

for the plasma properties. But in solving the electrical problem for the entrance and exit regions, initial type conditions for n_a and T_e, and for the plasma properties can be used. Furthermore, since after solution of the entrance problem the values of n_a and T_e will have been obtained at the beginning of the periodic part of the channel, initial type conditions for n_a and T_e can be used throughout the downstream solution of the electrical problem for subsequent electrode pairs. This leads to a significant reduction in computation time.

Appendix A describes the computer program INLET, which has been coded in FORTRAN for the solution of the electrical problem in the entrance or exit regions. It includes a list of routines and important variables, specification of required input data and formats, and a description of available output.

2. GASDYNAMIC PROBLEM

In solving the two-dimensional gasdynamic problem the flow region has been separated, as mentioned in Section II, into the core and the boundary layers, at least up to the point where the latter may meet to result in fully developed viscous flow. The gasdynamic problems of the core flow and the boundary layers are coupled (in addition to their being coupled to the results of the electrical problem): the boundary layer growth determines the shape of the effective channel area A(x) to be used in the core flow solution, while the impressed free stream conditions determine the boundary layer structure and growth rate.

2.1. Core Flow Solution

The solution of the quasi-one-dimensional problem for the core flow, which was formulated in Section II, is accomplished by a straightforward 4th order Runge-Kutta-Gill integration method. In this formulation the magnetic induction B in the z-direction, the component J_y of the current density in the y-direction, and the effective channel area A are specified functions of the streamwise coordinate x.

For the purposes of this solution, the ordinary differential equations of the problem, given in Section II, are put in canonical form, namely

$$\vec{y}' = \vec{f}(x, \vec{y}) \tag{27}$$

where the vector $\vec{y}(x)$ has as components the $N + 3$ unknowns of the problem at each station x, while $\vec{y}'$ is the vector $\frac{d}{dx}\vec{y}$, and $\vec{f}$ the appropriate vector function. The vector function $\vec{f}$ is readily found by transformation of Eqs. (1) - (4) of Section II. Employing also the overall continuity equation (1^m)

$$\rho u A = \dot{m} = \text{constant},$$

the components of $\vec{f}$ are then given by the following expressions

(1) Continuity equations for each component a

$$\frac{d}{dx} n_a = \frac{s_a}{u} - n_a\left(\frac{1}{A}\frac{dA}{dx} + \frac{1}{u}\frac{du}{dx}\right) \tag{28}$$

(2) Overall momentum equation

$$\frac{du}{dx} = -\frac{\gamma R M^2}{u(M^2-1)}(\Sigma_1 + \Sigma_2) \tag{29}$$

(3) Overall energy equation

$$\frac{dT}{dx} = \frac{(\gamma M^2 - 1)\Sigma_1 + (\gamma - 1)M^2\Sigma_2}{M^2 - 1} \tag{30}$$

(4) Electron energy equation

$$\frac{d}{dx} T_e = \frac{(2/3k)(\vec{E}' \cdot \vec{J}_e - \sum \epsilon_i s_i) - T_e s_e}{n_e u} - \frac{\nu_t \delta_{eff}(T_e - T_n)}{u} + \frac{2}{3} T_e \left(\frac{1}{A}\frac{dA}{dx} + \frac{1}{u}\frac{du}{dx}\right) \tag{31}$$

where

$$\Sigma_1 \equiv \frac{\vec{E} \cdot \vec{J} - s_E + (V_{bl}/D)J_y - \sum_i \epsilon_i s_i}{c_p \rho u} \tag{32}$$

$$\Sigma_2 \equiv \frac{s_M - J_y B}{\rho R} - \frac{T}{A}\frac{dA}{dx} \tag{33}$$

and R is the gas constant, $\gamma \equiv c_p/c_v$ the ratio of specific heats, $M \equiv u/(\gamma RT)^{1/2}$ the Mach number, and V_{bl} the part of the electrode voltage drop V_{el} that is due to the boundary layers. All other quantities have been defined in Section II.

The Runge-Kutta-Gill integration formula, giving the value of $\vec{y}$ at the point x_{n+1} when its value at the point x_n has been found, reads

$$\vec{y}_{n+1} = \vec{y}_n + \frac{1}{6}\left[\vec{k}_1 + 2(1 - \sqrt{1/2})\vec{k}_2 + 2(1 + \sqrt{1/2})\vec{k}_3 + \vec{k}_4\right] \tag{34}$$

where $\vec{y}_{n+1} = \vec{y}(x_{n+1})$, $\vec{y}_n = \vec{y}(x_n)$, $x_{n+1} = x_n + h$ (h the integration step) and

$$\begin{aligned}
\vec{k}_1 &= h\,\vec{f}\,(x_n, \vec{y}_n) \\
\vec{k}_2 &= h\,\vec{f}\,(x_n + \tfrac{1}{2}h,\ \vec{y}_n + \tfrac{1}{2}\vec{k}_1) \\
\vec{k}_3 &= h\,\vec{f}\,(x_n + \tfrac{1}{2}h,\ \vec{y}_n + (-\tfrac{1}{2} + \sqrt{1/2})\vec{k}_1 + (1 - \sqrt{1/2})\vec{k}_2) \\
\vec{k}_4 &= h\,\vec{f}\,(x_n + h,\ \vec{y}_n - \sqrt{1/2}\,\vec{k}_2 + (1 + \sqrt{1/2})\vec{k}_3)
\end{aligned} \tag{34a}$$

The error in this integration formula is of order $O(h^5)$. In practice, accuracy is controlled by varying h so as to limit the relative changes of all unknown quantities over each integration step to given maximum values.

The above system of differential equations is a "stiff" set of equations, for the low mass of the electrons results in a comparatively small time constant for Eq. (31). Because of this disparity in time

constants, it is often desirable to treat the electron energy equation separately, by replacing the x-derivative with a two-point difference expression and reformulating Eq. (31) into an implicit algebraic equation, which may be solved by iteration (see Ref. 2). The resulting equation is

$$T_e(x) = \left\{ \frac{\vec{E}' \cdot \vec{J}_e - \sum_i \epsilon_i s_i}{n_e k} + \frac{3}{2}\left(\nu_t \delta_{eff} T + \frac{u}{x - x_o} T_{e,o}\right) \right\} \Bigg/ \left\{ \frac{3}{2}\left(\nu_t \delta_{eff} + \frac{u}{x - x_o} + \frac{s_e}{n_e}\right) + \frac{du}{dx} + \frac{u}{A}\frac{dA}{dx} \right\} \tag{31a}$$

where x_o is the value of x at the beginning of the current integration step, and $T_{e,o} = T_e(x_o)$.

Appendix B describes the computer program CHANNEL, which has been coded in FORTRAN for the solution of the gasdynamic problem in the core region. It includes a list of routines and important variables, specification of required input data and formats, and a description of available output.

2.2. Boundary Layer Solution

For the solution of the compressible turbulent magnetohydrodynamic boundary layer problem, which was formulated in Section II, a finite-difference method has been developed incorporating some of the desirable features of the method originally suggested by Patankar (Ref. 15) for the treatment of the incompressible eddy-viscosity model.

As developed in this work, the method of solution is applicable to compressible or incompressible, two-dimensional or axi-symmetric flows over straight or slightly curved surfaces, with or without magnetohydrodynamic effects, and with or without mass injection or suction at the walls. The most attractive characteristics of this method are:

(1) The use of the normalized streamfunction as the cross-

coordinate. This results in a coordinate system that adjusts automatically to the thickness of the boundary layer, while the number of calculation steps in the transverse direction remains constant as the boundary layer grows. In other words, the step size in the mathematical coordinate system remains constant, although the physical distance corresponding to this step size varies as the boundary layer grows in the streamwise direction. This is in marked contrast with the complicated artificial devices that are usually employed to satisfy the conflicting requirements of covering the entire boundary layer without allowing the number of transverse calculation steps to grow excessively with growing boundary layer thickness (Ref. 18).

(2) The use of an implicit difference scheme for the numerical solution of the boundary layer equations. Use of this scheme assures stability of the numerical method irrespective of step size. In other words, step size can be chosen so as to satisfy a given requirement of numerical accuracy without concern about the stability of the method.

(3) The use of universal, Couette-type, solutions for the thin laminar sublayer (adjacent to the wall). In this region of extremely steep transverse gradients, use of a finite-difference computation would necessitate extremely small step sizes and thus excessive computer time. Fortunately, in this region one can take advantage of the fact that inertia forces are very small compared to viscous stresses and pressure forces, so that the boundary layer equations can be given the form of total differential equations with derivatives only in the cross-stream directions. This feature is used in the present method and leads to significant reduction in computer time compared to previous methods.

2.2.1. Coordinate system

The coordinate system used is shown on Fig. 3. It can be seen that both axi-symmetric and plane flows are allowed for, with x in the approximately streamwise direction and y in the transverse direction. The transverse geometrical coordinate y is measured from the I-boundary of the layer. The direction of the I-streamlines (i.e., the direction of the inner wall) is allowed to vary with x; however, this variation is assumed

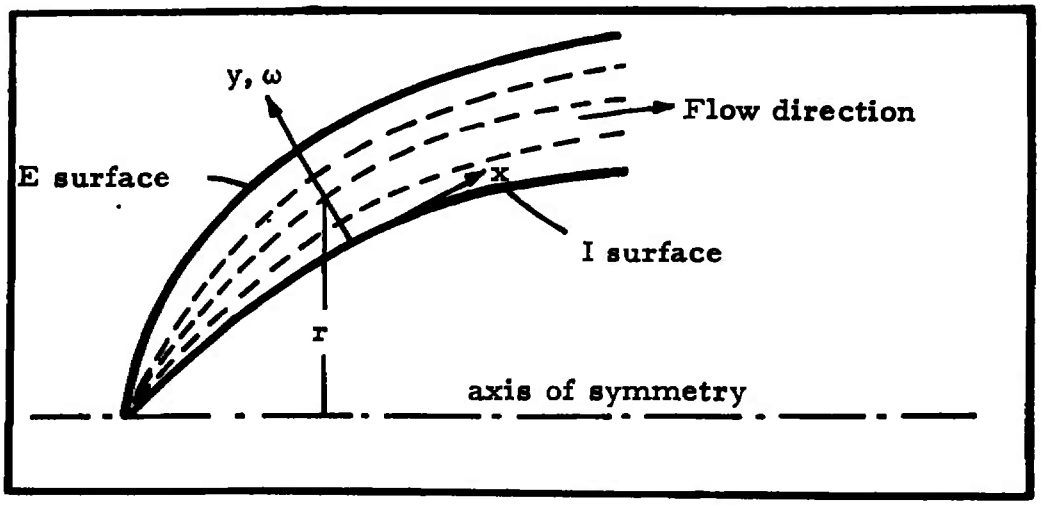

Fig. 3. The coordinate system.

to be sufficiently slow so as not to give rise to any additional (centrifugal, or Coriolis) forces.

The flow is assumed to be bounded by the I and the E boundaries. The discussion here will concentrate on the case where the I-boundary is a flat material wall, and the E-boundary the edge of the boundary layer, i.e. a free boundary. The method can easily be adapted to other flow situations (e.g. mixing layers).

The coordinate system is transformed by using the von Mises transformation (Ref. 19). This is done by introducing the streamfunction S, defined by

$$\rho \vec{U} \equiv \nabla \times (S\vec{k}) \tag{35}$$

where again $\vec{k}$ is the unit vector in the z-direction. Eq. (35) of course implies that

$$\frac{\partial S}{\partial x} = -\rho v$$
$$\frac{\partial S}{\partial y} = +\rho u \tag{35a}$$

so that the continuity equation (7a) is satisfied automatically. All equations can now be transformed from the system (x, y) to the system (x, S) by using the relations

$$\left(\frac{\partial}{\partial x}\right)_y = \left(\frac{\partial}{\partial x}\right)_S - \rho v \left(\frac{\partial}{\partial S}\right)_x$$
$$\left(\frac{\partial}{\partial y}\right)_x = \rho u \left(\frac{\partial}{\partial S}\right)_x \tag{36}$$

Under this transformation, the convective operator $\rho\vec{U}\cdot\nabla$ which in the (x, y) coordinate system has the form $\rho\left\{u\left(\frac{\partial}{\partial x}\right)_y + v\left(\frac{\partial}{\partial y}\right)_x\right\}$ now becomes simply $\rho u\left(\frac{\partial}{\partial x}\right)_S$, which is of course a direct result of the definition of the streamfunction.

Following the von Mises transformation, the coordinate S is

normalized by again transforming the coordinate system from (x, S) to (x,ω) where

$$\omega = \frac{S - S_I}{S_E - S_I} \tag{37}$$

and $S_I(x)$ and $S_E(x)$ are the values of the streamfunction at the two boundaries of the flow for a given x. As long as the possibility of mean flow reversal is excluded (which is actually the condition for the streamfunction to be single-valued), the boundary layer flow region is always imbedded in the constant interval $0 \leq \omega \leq 1$.

It is clear from the definition of S_I and S_E that

$$\frac{d}{dx} S_I = - \dot{m}_I$$
$$\frac{d}{dx} S_E = - \dot{m}_E \tag{38}$$

where $\dot{m}_I$ and $\dot{m}_E$ are the mass transfer rates across the two boundaries. Consequently, the transformation from the system (x, y) to the system (x, ω) will proceed according to the relations

$$\left(\frac{\partial}{\partial x}\right)_y = \left(\frac{\partial}{\partial x}\right)_\omega + \frac{-\rho v + \dot{m}_I + \omega(\dot{m}_E - \dot{m}_I)}{S_E - S_I} \left(\frac{\partial}{\partial \omega}\right)_x$$
$$\left(\frac{\partial}{\partial y}\right)_x = \frac{\rho u}{S_E - S_I} \left(\frac{\partial}{\partial \omega}\right)_x \tag{39}$$

Accordingly, the convective operator now becomes

$$\rho \vec{U} \cdot \nabla = \rho u \left[\left(\frac{\partial}{\partial x}\right)_\omega + R \left(\frac{\partial}{\partial \omega}\right)_x \right] \tag{40}$$

where

$$R(x, \omega) \equiv \frac{\dot{m}_I + \omega (\dot{m}_E - \dot{m}_I)}{S_E - S_I} \tag{40a}$$

2.2.2. The transformed equations

In the "modified" von Mises coordinate system (x, ω) the governing equations of the problem (see Section II) read as follows:

(1) Overall momentum equation

$$\left\{\frac{\partial}{\partial x} + R\,\frac{\partial}{\partial \omega}\right\}u - \frac{\partial \tau/\partial \omega}{S_E - S_I} - \frac{1}{(S_E - S_I)^2}\,\frac{\partial}{\partial \omega}\,\mu_L \rho u\,\frac{\partial u}{\partial \omega} =$$

$$= \frac{1}{\rho u}\left\{-\frac{dp}{dx} + J_y B\right\} \tag{41}$$

(2) Turbulent shear transport equation

$$\left\{\frac{\partial}{\partial x} + R\,\frac{\partial}{\partial \omega}\right\}\frac{\tau}{2a_1\rho} + \frac{(\tau/\rho)_{max}}{U_\infty (S_E - S_I)}\,\frac{\partial}{\partial \omega}\,a_3\tau =$$

$$= \frac{\tau}{S_E - S_I}\,\frac{\partial u}{\partial \omega} - \frac{1}{\rho u}\left[\frac{\rho}{a_2\delta}\left(\frac{\tau}{\rho}\right)^{3/2} + \frac{1}{3}\,\frac{\epsilon\sigma B^2}{\epsilon^2+\beta^2}\,\frac{\tau}{a_1\rho}\right] \tag{42}$$

(3) Overall energy equation

$$\left\{\frac{\partial}{\partial x} + R\,\frac{\partial}{\partial \omega}\right\}h = \frac{1}{(S_E - S_I)^2}\,\frac{\partial}{\partial \omega}\,\rho u\left[\left(\frac{\mu_L}{Pr_L} + \frac{\tau}{Pr_T\,\partial u/\partial y}\right)\frac{\partial h}{\partial \omega} + \right.$$

$$+\left\{\mu_L\left(\frac{1}{Sc_L} - \frac{1}{Pr_L}\right) + \frac{\tau}{\partial u/\partial y}\left(\frac{1}{Sc_T} - \frac{1}{Pr_T}\right)\right\}\sum_a h_a\,\frac{\partial c_a}{\partial \omega}\left.\right] +$$

$$+\frac{1}{\rho}\,\frac{dp}{dx} + \frac{\mu_L \rho u}{(S_E - S_I)^2}\left(\frac{\partial u}{\partial \omega}\right)^2 + \frac{1}{\rho u}\left[\frac{\rho}{a_2\delta}\left(\frac{\tau}{\rho}\right)^{3/2} + \right.$$

$$\left. + \vec{J}\cdot(\vec{E} + \vec{U}\times\vec{B}) + \frac{1}{3}\,\frac{\epsilon\sigma B^2}{\epsilon^2+\beta^2}\,\frac{\tau}{a_1\rho}\right] \tag{43}$$

or, for the total enthalpy H,

$$\left\{\frac{\partial}{\partial x} + R\,\frac{\partial}{\partial \omega}\right\}H = \frac{1}{(S_E - S_I)^2}\,\frac{\partial}{\partial \omega}\,\rho u\left[\left(\frac{\mu_L}{Pr_L} + \frac{\tau}{Pr_T\,\partial u/\partial y}\right)\frac{\partial H}{\partial \omega} + \right.$$

$$\left. + \left\{\mu_L\left(\frac{1}{Sc_L} - \frac{1}{Pr_L}\right) + \frac{\tau}{\partial u/\partial y}\left(\frac{1}{Sc_T} - \frac{1}{Pr_T}\right)\right\}\sum_a h_a\,\frac{\partial c_a}{\partial \omega}\right] +$$

$$+ \frac{1}{(S_E - S_I)}\,\frac{\partial}{\partial \omega}\left[u\left\{\left(1 - \frac{1}{Pr_T}\right)\tau + \left(1 - \frac{1}{Pr_L}\right)\frac{\mu_L \rho u}{S_E - S_I}\,\frac{\partial u}{\partial \omega}\right\}\right] + \frac{\vec{E}\cdot\vec{J}}{\rho u} \qquad (44)$$

(4) Species conservation equation

$$\left\{\frac{\partial}{\partial x} + R\,\frac{\partial}{\partial \omega}\right\}c_a = \frac{1}{(S_E - S_I)^2}\,\frac{\partial}{\partial \omega}\left[\rho u\left(\frac{\mu_L}{Sc_L} + \frac{1}{Sc_T}\,\frac{\tau}{\partial u/\partial y}\right)\frac{\partial c_a}{\partial \omega}\right]$$

$$+ \frac{1}{\rho u}\,m_a\langle s_a\rangle \qquad (45)$$

(5) Electron energy equation

$$\left\{\frac{\partial}{\partial x} + R\,\frac{\partial}{\partial \omega}\right\}c_e h_e = \frac{1}{(S_E - S_I)^2}\,\frac{\partial}{\partial \omega}\,\rho u\left[\left(\frac{\mu_L}{Pr_L} + \frac{\tau}{\partial u/\partial y}\,\frac{1}{Pr_T}\right)c_e\,\frac{\partial h_e}{\partial \omega} + \right.$$

$$\left. + \left(\frac{\mu_L}{Sc_L} + \frac{\tau}{\partial u/\partial y}\,\frac{1}{Sc_T}\right)h_e\,\frac{\partial c_e}{\partial \omega}\right] + \frac{1}{\rho}\left\{\frac{\partial}{\partial x} + R\,\frac{\partial}{\partial \omega}\right\}p_e +$$

$$+ \frac{1}{\rho u}\left[\vec{J}_e\cdot(\vec{E} + \vec{U}\times\vec{B}) + \frac{1}{3}\,\frac{\epsilon B^2}{\epsilon^2 + \beta^2}\,\frac{\tau}{a_1 \rho} - \right.$$

$$\left. - \frac{3}{2}\,k n_e \nu_t \delta_{eff}(T_e - T_n) - \sum_{ions}\epsilon_i\langle s_i\rangle - \dot{R}\right] \qquad (46)$$

Equations (41), (42), (43) or (44), (45), and (46) constitute the system of partial differential equations that are solved numerically for the unknowns u, τ, T, c_a, and T_e. Note that the density ρ is not a true additional variable, since it is related to the temperature and pressure, the latter being a given function of x determined by the free-stream conditions.

2.2.3. Finite difference formulation

An important step in the numerical method is the discretization procedure, i.e. the transformation of the differential equations of the problem into a suitable system of algebraic, finite-difference equations.

To derive these finite-difference expressions an implicit scheme suggested by Pakankar has been utilized (Ref. 17). The notation appropriate to this derivation is shown on Fig. 4. A rectangular grid of points is used in the x-ω plane with variable spacing in both the x- and ω-directions, to provide for desirable requirements of accuracy in regions of special interest, e.g. near separation, or near an electrode spot. This grid requires no adjustment in the ω-direction in succeeding x-stations. It is assumed that the values of all dependent variables are known at the grid points U^-, U, and U^+, which belong to the upstream station $x = x_u$. Their values at the points D^-, D and D^+, which belong to the downstream station $x = x_d$ are to be found. The finite difference equations are derived by integrating each of the differential equations of the problem over a control volume bounded by the points UU^+, UU^-, DD^+ and DD^- under the assumption of a simple variation of all dependent variables between grid points. Specifically, in the ω-direction the dependent variables are assumed to vary linearly (or quadratically) between grid points, while in the x direction a step-wise (or linear) variation is assumed. When a step-wise x-variation is utilized, then the values of the dependent variables in the interval between x_u and x_d (except at x_u) are assumed uniform and equal to those at x_d. The use of this procedure guarantees that the conservation equations will be satisfied uniformly throughout the boundary layer. Note also the use of a step-wise x-variation implies that the derivatives in the ω-direction are evaluated at $x = x_d$. This implicit difference scheme is known to be unconditionally stable for linear systems of differential equations (Ref. 20). Of course, the system of equations governing this problem is not a linear one. Nevertheless, the employed implicit difference scheme has shown good stability.

The important question that arises when attempting to solve the

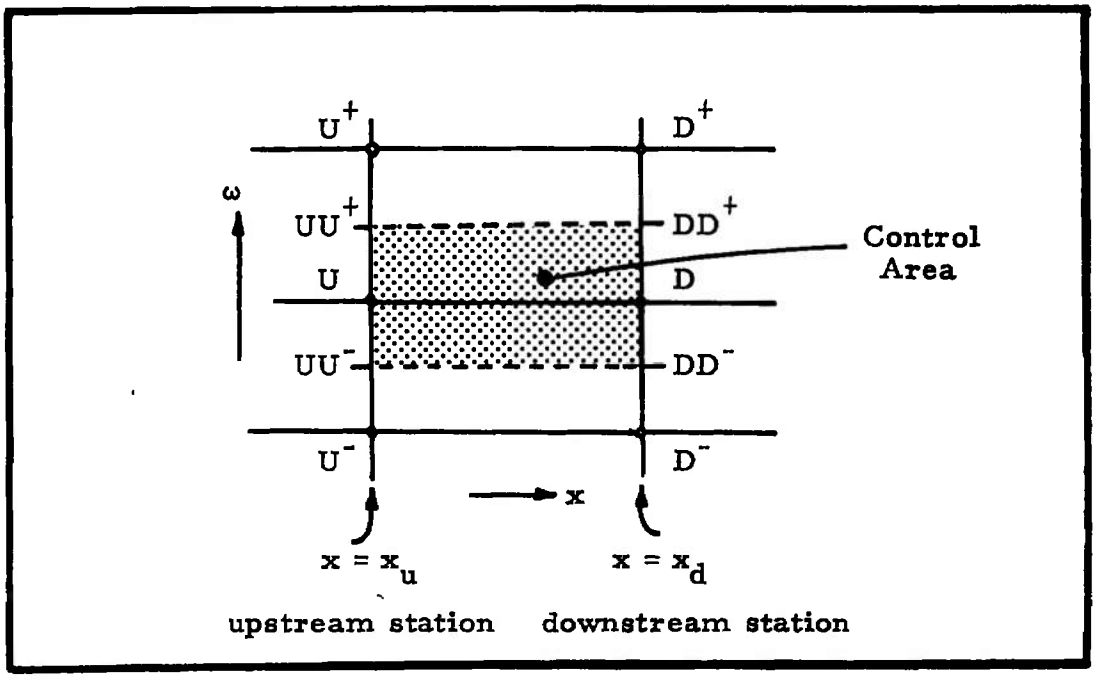

Fig. 4. Control area for the implicit finite-difference scheme.

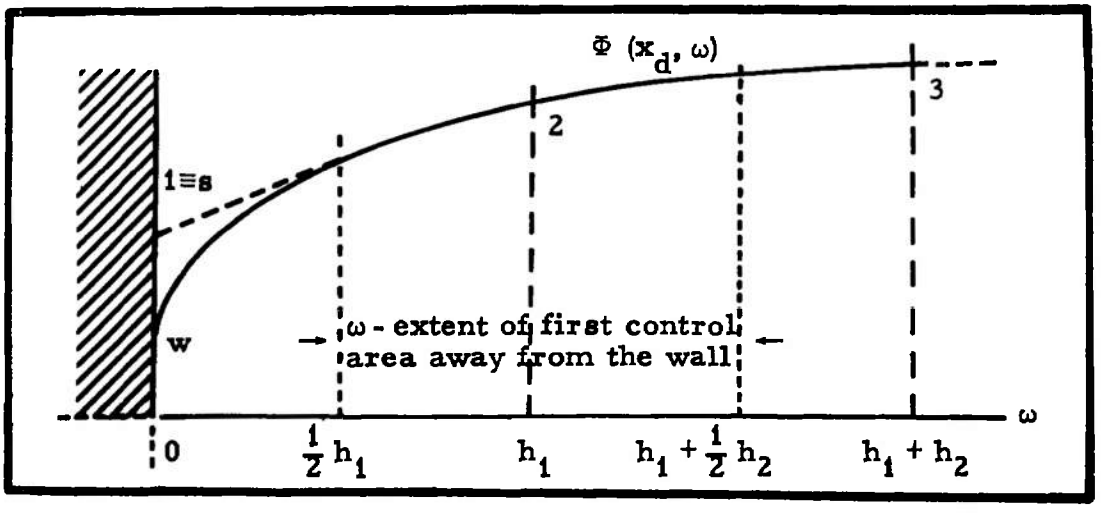

Fig. 5. Definition of "slip values" for each dependent variable Φ.

system of derived finite-difference equations is how to maintain a linear system (which is readily solvable) without loss of accuracy. This is accomplished in this method of solution by combined application of the techniques of quasi-linearization and iteration; in other words, the known upstream values of the dependent variables are utilized to evaluate selected coefficients in the system of equations so as to linearize it, and then the results are enriched by iteration.

The governing differential equations, except Eq. (42) where the diffusion term is not of gradient-diffusion type, have the general form

$$\frac{\partial \Phi}{\partial x} + (a + b\omega) \frac{\partial \Phi}{\partial \omega} = \frac{\partial}{\partial \omega} c \frac{\partial \Phi}{\partial \omega} + d \tag{47}$$

where the left-hand side expresses the convection term and the right-hand side contains the diffusion term and a general source term d. It is clear that the convection term is linear, involving linear first order differential operators, and therefore results in linear finite-difference expressions for each unknown Φ. On the other hand, the diffusion term is not always linear with respect to the dependent variables because c can be a function of some of them. Similarly, the source term d, involving general production and dissipation terms, is generally nonlinear with respect to the dependent variables. The treatment of the source terms in the solution procedure is extremely critical because of the importance of production and dissipation terms in the boundary layer equations. A method of quasi-linearization has been successfully adopted, which entails expressing the downstream value d_d of each source term in terms of its known upstream value d_u as follows:

$$d_d = d_u + (\vec{\Phi}_d - \vec{\Phi}_u) \cdot (\nabla_\Phi d)_u \tag{48}$$

where $\vec{\Phi}$ is the vector of the unknowns (u, τ, T, c_a, T_e).

When all terms in the differential equations of the problem are transformed by the quasi-linearization procedure described above, then to each control volume across the boundary layer at a station x there

corresponds a system of linear finite difference equations of the form

$$\vec{\Phi}_D = A \cdot \vec{\Phi}_{D^+} + B \cdot \vec{\Phi}_{D^-} + \vec{C} \tag{49}$$

where A and B are matrices and $\vec{C}$ a vector of coefficients. There are n-2 such control volumes across the boundary layer, where n is the number of grid points in the ω-direction. On the other hand, there are n unknowns $\vec{\Phi}$. The additional 2 equations needed for the solution will be the boundary conditions at the two edges of the boundary layer. At the outer edge $\omega = 1$, the boundary condition may be applied simply by setting the values of the dependent variables at that point equal to their free-stream values. At the inner edge $\omega = 0$, on the other hand, the boundary condition will be expressed by utilizing Couette-type solutions, which will account for the strong gradients of the dependent variables in the wall region.

2.2.4. The wall-region Couette-type solutions

It has already been mentioned that an important feature of this method, leading to significant savings in computer time, is the treatment of the wall-region of the boundary layer, i.e. the thin "sublayer" adjacent to the wall.

There are two main reasons for a special treatment of this "sublayer":

(1) Since the scale and the intensity of turbulence tend to zero close to a solid wall, the laminar contributions to the fluxes become significant, and, very close to the wall (in the so-called "laminar sublayer"), they become dominant. This applies both to momentum transport and to heat conduction.

(2) The transverse gradients of the dependent variables become very steep in this region, so that a finite-difference solution in this region would require an excessively fine grid in the ω-direction.

This method takes advantage of the fact that in the wall region, where u is small, streamwise convective effects (and thus stream-

wise derivatives) can be neglected in the governing equations. In other words, there exists a one-dimensional boundary layer near the wall; this is what is also known as "Couette flow." Then the flow problem in this region reduces to solving ordinary rather than partial differential equations, and, once these solutions are obtained, they will be uniformly valid (i.e. independently of x). This means that these "inner solutions" can then be used as asymptotic forms, or boundary conditions, for the solution of the partial differential equations in the main part of the boundary layer.

In obtaining the Couette-type solutions in the wall-region, the turbulent shear stress τ is expressed by Eq. (9a), which is valid in this region where diffusion and convection of turbulence energy are indeed negligible. Thus, the concept of the "eddy-viscosity" μ_T can be applied in this region without contradicting the transport formulation for the turbulent shear, and Eq. (42) can be replaced by the algebraic relation

$$\mu_T = \rho(a_2\delta)^2 \left|\frac{\partial u}{\partial y}\right| = \frac{\tau}{\partial u/\partial y} \tag{50}$$

Under these assumptions, the following Couette-type first integrals of the remaining governing equations can be obtained:

(1) Overall momentum

$$(\mu_L + \mu_T)\frac{du}{dy} = \tau_w + \dot{m}_w u + \frac{dp}{dx}y - \int_o^y J_y B\, dy \tag{51}$$

where $\dot{m}_w$ is the mass flux through the well due to injection or suction, τ_w the shear stress at the wall, and the subscript w generally denotes conditions at the solid wall.

(2) Overall energy equation

$$\left(\frac{\mu_L}{Pr_L} + \frac{\mu_T}{Pr_T}\right)\frac{dh}{dy} = q_w + \dot{m}_w(h - h_w) + \left\{\mu_L\left(\frac{1}{Pr_L} - \frac{1}{Sc_L}\right) + \mu_T\left(\frac{1}{Pr_T} - \frac{1}{Sc_T}\right)\right\}\sum_a h_a \frac{dc_a}{dy} -$$

$$- \left\{ \mu_L \left(\frac{1}{Pr_L} - \frac{1}{Sc_L} \right) \sum_a h_a \frac{dc_a}{dy} \right\}_w - \int_o^y \left[u \frac{dp}{dx} + \mu_L \left(\frac{\partial u}{\partial y} \right)^2 + \right.$$

$$\left. + \frac{\rho}{a_2 \delta} \left(\frac{\tau}{\rho} \right)^{3/2} + \vec{J} \cdot (\vec{E} + \vec{U} \times \vec{B}) + \frac{1}{3} \frac{\epsilon \sigma B^2}{\epsilon^2 + \beta^2} \frac{\tau}{a_1 \rho} \right] dy \qquad (52)$$

or

$$\left(\frac{\mu_L}{Pr_L} + \frac{\mu_T}{Pr_T} \right) \frac{\partial H}{\partial y} + u \left\{ \left(1 - \frac{1}{Pr_L} \right) \mu_L + \left(1 - \frac{1}{Pr_T} \right) \mu_T \right\} \frac{du}{dy} =$$

$$= q_w + \dot{m}_w (H - H_w) +$$

$$+ \left\{ \mu_L \left(\frac{1}{Pr_L} - \frac{1}{Sc_L} \right) + \mu_T \left(\frac{1}{Pr_T} - \frac{1}{Sc_T} \right) \right\} \sum_a h_a \frac{dc_a}{dy} -$$

$$- \left\{ \mu_L \left(\frac{1}{Pr_L} - \frac{1}{Sc_L} \right) \sum_a h_a \frac{dc_a}{dy} \right\}_w - \int_o^y \vec{E} \cdot \vec{J} \, dy \qquad (53)$$

(3) Species continuity equation

$$\left(\frac{\mu_L}{Sc_L} + \frac{\mu_T}{Sc_T} \right) \frac{dc_a}{dy} = d_{a,w} + \dot{m}_w (c_a - c_{a,w}) - m_a \int_o^y \langle s_a \rangle \, dy \qquad (54)$$

(4) Electron energy equation

$$\left(\frac{\mu_L}{Pr_L} + \frac{\mu_T}{Pr_T} \right) c_e \frac{dh_e}{dy} = q_{e,w} + (\dot{m}_w c_{e,w} - d_{e,w}) \cdot (h_e - h_{e,w}) -$$

$$- \int_o^y \left[v \frac{dp_e}{dy} + \vec{J}_e \cdot (\vec{E} + \vec{U} \times \vec{B}) + \frac{1}{3} \frac{\epsilon \sigma B^2}{\epsilon^2 + \beta^2} \frac{\tau}{a_1 \rho} - \right.$$

$$\left. - \frac{3}{2} k n_e \nu_t \delta_{eff} (T_e - T_n) - \sum_{ions} \left\{ (\epsilon_i - m_e h_e) \langle s_i \rangle \right\} - \dot{R} \right] dy \qquad (55)$$

where the species continuity equation (54) for electrons ($a \equiv e$) has been used.

In order to solve these first integrals, to obtain the Couette-

type solutions for the unknown vector $\vec{\phi} \equiv (u, T, c_a, T_e)$, an analytical expression for μ_T or $a_2\delta$ is necessary, that will be valid and accurate very close to the wall. For this purpose von Karman's expression Ky (K = 0.4 is von Karman's constant), multiplied by an exponential damping factor, is used for the dissipation length $a_2\delta$ in the wall region, as suggested by Van Driest (Refs. 14 and 21):

$$a_2\delta = Ky\left[1 - \exp\left\{-\frac{y}{A_t\mu_L}\sqrt{\rho(\tau_w + \frac{dp}{dx}y)}\right\}\right] \tag{56}$$

The values 0.4 and 26.0 have been employed for the dimensionless constants K and A_t, respectively (Ref. 21). The presence of the exponential factor in Eq. (56) allows its use arbitrarily close to the wall, i.e., even in a purely laminar region.

It is then possible to integrate Eqs. (51)-(55) once more to obtain the Couette flow solutions for the dependent variables $\vec{\phi}$. In general, this second integration will have to be carried out numerically to yield

$$\vec{\phi} = \vec{\phi}(\omega, \vec{\phi}_w, \vec{F}_w; \frac{dp}{dx}, \dot{m}_w, \vec{J}, \vec{E}, \vec{B}) \tag{57}$$

where the vector $\vec{F}_w \equiv (\tau_w, q_w, d_{a,w}, q_{e,w})$ contains the wall fluxes corresponding to $\vec{\phi} \equiv (u, T, c_a, T_e)$. At a given station x, the mass flux through the wall $\dot{m}_w$ and the wall value $\vec{\phi}_w$ of the dependent variables is generally known. In addition the pressure gradient dp/dx and the electrical fields $\vec{J}$, $\vec{E}$ and $\vec{B}$ are prescribed. Thus, the Couette-type "inner" solutions will contain as parameters the wall fluxes $\vec{F}_w$. The values of these parameters will be determined by matching both the magnitude and the derivative of the "inner" to the "outer" solutions at some appropriate points y_F where both solutions remain valid. Fortunately, the choice of y_F is not critical, since both solutions are valid within a fairly broad common domain, the so-called "log" region or "buffer" layer that lies between the thin laminar sublayer and the region where streamwise convection effects start being significant. In fact, due to the extreme thinness of the inner region, it is usually sufficient (Ref. 17)

to locate y_F in the middle of the first grid step in the ω-direction.

It would, of course, be desirable to obtain analytical expressions for the Couette-type solutions. Unfortunately, however, analytical solutions of Eqs. (51) to (55) can be obtained only after imposing severe simplifying assumptions. To give an example, an analytical solution of Eq. (51) can be obtained under the assumptions (1) that the exponential factor in Eq. (56) can be omitted, (2) that ρ = const (this reduces the Couette-type solution for u to a 1-parametric family), (3) that $\dot{m}_w = 0$, (4) that $dp/dx = 0$, and (5) that $\int_o^y J_y B \, dy = 0$. Then, using the dimensionless variables

$$y^* = K \frac{\sqrt{\rho \tau_w}}{\mu_L} y$$

$$u^* = \frac{K}{\sqrt{\tau_w/\rho}} u \tag{58}$$

Eq. (51) can be integrated to obtain

$$u^* = - \frac{2y^*}{1 + \sqrt{1 + 4y^{*2}}} + \ln (2y^* + \sqrt{1 + 4y^{*2}}) \tag{59}$$

Then, this solution can be used to integrate also the remaining Eqs. (52)-(55) under the additional simplifying assumptions that (6) all laminar and turbulent Prandtl and Schmidt numbers are equal to 1, and (7) that the integrals appearing in Eqs. (52)-(55) can be approximated by y times the average value Q of the integrands in the wall region. Using the dimensionless variables

$$\phi^* = K \frac{\sqrt{\rho \tau_w}}{\left(\mu_L \frac{d\phi}{dy}\right)_w} (\phi - \phi_w)$$

$$Q^* = \frac{\mu_L}{K \left(\mu_L \frac{d\phi}{dy}\right)_w \sqrt{\rho \tau_w}} Q \tag{60}$$

Eqs. (52) - (55) can be expressed in the common form

$$\frac{d\phi^*}{dy^*} = \frac{1 + Q^*}{1 + \dfrac{2y^{*2}}{1 + \sqrt{1 + 4y^{*2}}}} \tag{61}$$

which can be integrated to yield

$$\phi^* = u^* + \frac{Q^*}{2}\left\{ \sqrt{1 + 4y^{*2}} - 1 - \ln \frac{1 + \sqrt{1 + 4y^{*2}}}{2} \right\} \tag{62}$$

As mentioned above, the present method has not relied on such analytical solutions, but has carried out and used numerical solutions of Eqs. (51) - (55). Occasionally, it has been possible to fit these numerical solutions to suitable analytical formulas, as suggested in Ref. 17.

2.2.5. Matching of "inner" and "outer" solutions

The first control volume away from the wall utilized for the discretization of the differential equation of the problem starts at the half-way point $\omega = \frac{1}{2} h_1$ of the first grid size in the ω-direction (see Fig. 5). For the discretization the dependent variables have been assumed to vary linearly in the ω-direction between grid points. However, since the first control volume employed for this purpose starts at $\omega = \frac{1}{2} h_1$, only the variation of each unknown between $\omega = h_1$ and $\omega = \frac{1}{2} h_1$ has been actually used. If this linear variation were extrapolated to the wall ($\omega = 0$) there could be found a value for each dependent variable, called a "slip value" $\vec{\phi}_s = (u_s, T_s, c_{a,s}, T_{e,s})$, that could be very different from the actual value $\vec{\phi}_w$ of the dependent variables at the wall (see Fig. 5). This is due to the sharp variation of the variables near the wall, which makes the assumption of linear variation a very poor one in that region. In fact care must be taken that the discretization for the "outer" solution remains valid as close to the wall as $\omega = \frac{1}{2} h_1$. The fictitious "slip values" of the dependent variables are, however, the proper boundary conditions to be used for the "outer"

solution. This means that the two-dimensional calculation can be formally started "at the wall" provided the defined slip-values $\vec{\phi}_s$ (which will have to be found via the matching procedure) are used as boundary conditions instead of the physical wall conditions $\vec{\phi}_w$ of the problem. In other words, the presence of the inner layer is formally equivalent to the introduction of appropriate slip-conditions at the wall.

The matching procedure by which the slip values are determined is shown on Fig. 5: The linear variation of each dependent variable between the slip value at the wall and its value at the point $\omega = h_1$ must be such that both its value and its derivative at $\omega = \frac{1}{2} h_1$ agree with the value and slope of the Couette-type solution at that point. (In a generalization that has been found to improve the accuracy of the solution, the slopes are required to be matched at $\omega = \xi h_1$, where $\frac{1}{2} \leq \xi < 1.$)

Analytically, this matching procedure can be defined as follows, using the expression given by Eq. (57) for the Couette-type solution for the dependent variables:

$$\frac{\vec{\phi}_2 + \vec{\phi}_s}{2} = \vec{\phi}\left(\frac{1}{2} h_1, \vec{\phi}_w, \vec{F}_w\right)$$

$$\frac{\vec{\phi}_2 - \vec{\phi}_s}{h_1} = \frac{d\vec{\phi}}{d\omega}\left(\xi h_1, \vec{\phi}_w, \vec{F}_w\right) \tag{63}$$

Eqs. (63) constitute a system of two equations for expressing the two unknowns $\vec{\phi}_s$ and $\vec{F}_w$ in terms of $\vec{\phi}_w$ and $\vec{\phi}_2$. The first of these results, namely

$$\vec{\phi}_s = \vec{\phi}_s(\vec{\phi}_2, \vec{\phi}_w) \tag{64}$$

will be used as the wall boundary condition for the outer solution, while the second, namely

$$\vec{F}_w = \vec{F}_w(\vec{\phi}_2, \vec{\phi}_w) \tag{65}$$

will provide the values of the wall fluxes $\vec{F}_w$ after the outer solution (and hence $\vec{\phi}_2$) have been determined.

Alternatively, in case $\vec{F}_w$ rather than $\vec{\phi}_w$ have been specified, Eqs. (63) will be solved for $\vec{\phi}_s$ and $\vec{\phi}_w$ in terms of $\vec{F}_w$ and $\vec{\phi}_2$:

$$\vec{\phi}_s = \vec{\phi}_s (\vec{\phi}_2, \vec{F}_w) \tag{66}$$

$$\vec{\phi}_w = \vec{\phi}_w (\vec{\phi}_2, \vec{F}_w) \tag{67}$$

Finally, note that the boundary conditions expressed by Eq. (64), or Eq. (66), refer to the unknowns $\vec{\phi}$, which do not include τ. A boundary condition for the latter is also needed in order to solve the system of equations (49). This conditions is obtained simply by matching the linear variation of τ between τ_s and τ_2 with the value of the Couette-type variation of τ (namely $\tau = \mu_T \frac{\partial u}{\partial y}$) at the point $\omega = \frac{1}{2} h_1$:

$$\frac{\tau_2 + \tau_s}{2} = \left[\mu_T \frac{du}{dy} \right]_{\omega = \frac{1}{2} h_1} \tag{68}$$

Note that the Couette-flow solution for u, and hence for $\tau = \mu_T \frac{du}{dy}$, has already been obtained as the first component of Eq. (64), or Eq. (66).

2.2.5. Solution by elimination

The system of finite-difference equations (49), which can be written in the form

$$\vec{\Phi}_i = A_i \cdot \vec{\Phi}_{i+1} + B_i \vec{\Phi}_{i-1} + \vec{C}_i \tag{69}$$

$$(i = 2, 3, \ldots, n-1)$$

together with the boundary conditions constitute a system of n equations for the n unknowns $\vec{\Phi}_i = (u_i, \tau_i, T_i, c_{a,i}, T_{e,i})$, where the subscript i corresponds to each grid point in the ω-direction. Note that each equation (69) is the result of discretization in the control

volume centered around the point i. As pointed out earlier, the first control volume away from the wall that is used for discretization of the differential equations is the one centered around the point 2, while the last is the one centered around the point n-1. This is reflected by the range of i in Eq. (69). The two boundary conditions have the same general form as Eqs. (69) and can therefore be considered as the finite-difference equations corresponding to points i = 1 and i = n. As already mentioned, the one corresponding to i = 1 is made up of Eqs. (64) – or (66) – together with Eq. (68) and gives the values of $\vec{\Phi}_s \equiv \vec{\Phi}_1$ in terms of the values of $\vec{\Phi}_2$ and $\vec{\Phi}_w$ (or $\vec{F}_w$); the one corresponding to i = n simply fixes the values of $\vec{\Phi}_n$ by equating them to the free-stream values.

Since the value of $\vec{\Phi}_w$ (or $\vec{F}_w$) is given, the inner boundary condition (i = 1) can be written in the form

$$\vec{\Phi}_1 = A_1 \cdot \vec{\Phi}_2 + \vec{C}_1 \tag{70}$$

Then, by substituting $\vec{\Phi}_1$ in Eq. (69) for i = 2, we find

$$\vec{\Phi}_2 = A_2' \cdot \vec{\Phi}_3 + \vec{C}_2' \tag{71}$$

with $A_2' = (1 - B_2 \cdot A_1)^{-1} A_2$ and $\vec{C}_2' = (1 - B_2 \cdot A_1)^{-1}(B_2 \cdot \vec{C}_1 + \vec{C}_2)$. Continuing this process, all 3-term recursion equations (69) can be reduced to 2-point recursion equations of the form

$$\vec{\Phi}_i = A_i' \cdot \vec{\Phi}_{i+1} + \vec{C}_i' \tag{72}$$

$$(i = 2, 3, \ldots, n-1)$$

where the matrix A_i' and the vector $\vec{C}_i'$ are found by substituting $\vec{\Phi}_{i-1}$ as given by Eq. (72) in Eq. (69):

$$\vec{\Phi}_i = A_i \cdot \vec{\Phi}_{i+1} + \vec{B}_i \cdot (A_{i-1}' \cdot \vec{\Phi}_i + \vec{C}_{i-1}') + \vec{C}_i$$

This results, for i = 2, 3, . . . , n-1, in the recursion relations

$$A_i' = (1 - B_i \cdot A_{i-1}')^{-1} A_i$$

$$\vec{C}_i = (1 - B_i \cdot A_{i-1}')^{-1} \cdot (B_i \cdot \vec{C}_{i-1}' + \vec{C}_i)$$

It is clear from Eq. (70) that the coefficients $A_1' = A_1$ and $\vec{C}_1' = \vec{C}_1$ are given by the inner boundary condition. Consequently, starting with $i = 2$, Eqs. (73) can be applied for each subsequent i to yield to actual numerical values for all coefficients A_i' and $\vec{C}_i'$ up to $i = n-1$.

When A_{n-1}' and $\vec{C}_{n-1}'$ are known, then Eq. (72) for $i = n-1$, namely the relation

$$\vec{\Phi}_{n-1} = A_{n-1}' \vec{\Phi}_n + \vec{C}_{n-1}' \tag{74}$$

yields the numerical value of $\vec{\Phi}_{n-1}$, since the value of $\vec{\Phi}_n$ is given as the outer boundary condition.

Then, using Eqs. (72) successively in the order $i = n-2, n-3, \ldots, 2$ together with the computed coefficients A_i' and $\vec{C}_i'$, the numerical values of all unknowns $\vec{\Phi}_i$ inside the boundary layer are found at the station $x = x_d$. Note that the slip value $\vec{\Phi}_1$ is also available through Eq. (70).

The elimination procedure described above is analogous to the more elaborate direct method used for the solution of the streamfunction equation in the electrical problem (see Ref. 1). In fact, the method described above is equivalent to considering the unknown $\vec{\Phi}_{n-1}$ as a "fundamental unknown" in the context of the terminology used in Ref. 1.

2.2.6. Definition of the external boundary and of the entrainment rate

When considering flows where the external boundary is a free boundary, there is considerable freedom in defining the position $y_E(x)$ of this boundary for mathematical convenience. There is of course a one-to-one correspondence between the criterion selected for the definition of the external boundary and the resulting entrainment rate $\dot{m}_E$ through this boundary. Note that the entrainment rate enters in the solution of the boundary layer problem both by appearing explicitly in the differential equations through the quantity R [see Eq. (40a)] and by defining the normalization of the dimensionless cross-stream variable ω.

An advantageous choice of the E-boundary is to define it as the line on which the streamwise velocity u equals a given percentage of the free-stream value U_∞. This choice has already been introduced in the process of formulating this model (see Section II). The definition $y_E(x) = \delta_{995}(x)$ is consistent with the definition used to obtain measurements of the entrainment rate (Refs. 16 and 22). These measurements were used to derive numerical values of the turbulent structure parameter a_3 through Eq. (26).

2.2.7. Turbulence structure parameters a_1, a_2, a_3

Values for the turbulence structure parameters a_1, a_2, a_3 measured and reported by Bradshaw (Ref. 16 and 22) have been used in carrying out the numerical computations reported herein. These measurements were carried out under a variety of boundary layer conditions and constitute limited experimental proof of the universality of these parameters. The parameter a_1 has thus been shown to be constant across the boundary layer, with a numerical value of 0.15; the numerical values of a_2 and a_3 used in the computations are given in Table 1 as functions of the dimensionless boundary layer coordinate y/δ.

TABLE 1

$\frac{y}{\delta}$	$a_2 \times 10^2$	a_3
0.0	0.0	0.0
0.1	4.0	0.2
0.2	7.5	1.0
0.3	8.8	2.0
0.4	9.2	3.0
0.5	9.5	5.0
0.6	9.2	7.7
0.7	8.5	14.0
0.8	7.4	23.5
0.9	6.0	30.0
1.0	4.1	33.0
1.1	2.0	36.0
1.2	0.5	37.3
1.3	0.1	38.5
1.4	0.0	41.5

Appendix C describes the computer program LAYER, which has been coded in FORTRAN for the solution of the gasdynamic problem in the compressible, turbulent magnetohydrodynamic boundary layer. It includes a list of routines and important variables, specification of required input data and formats, and a description of available output.

IV. APPLICATIONS

As the solutions to each of the subproblems described in Section I were obtained, appropriate test cases were analyzed, with the dual intent of checking the solution procedure and developing insight into the physical roles of the mechanisms under study.

Subsequent to the separate development work on each subproblem, the electrical solution over the entrance region and the solution of the gasdynamic problem were coupled together and used to analyze the electrical characteristics of the Hirho accelerator at AEDC.

In this Section the results obtained by solving each subproblem in various geometries and operating conditions will be described.

1. SOLUTIONS OF THE ELECTRICAL PROBLEM

To apply the solution of the electrical problem over the entire channel, it was natural to select cases that had been investigated extensively during the previous two phases of this study. Accordingly, the first test case chosen was that of a $J \times B$ accelerator as analyzed in Refs. 1 and 2 operating with nitrogen seeded with 0.5% (by weight) potassium at $p = 0.5$ atm, with average $J_y = 30$ A/cm^2 and uniform magnetic induction of 2 Wb/m^2. The geometry of each electrode pair was as in Refs. 1 and 2, namely 12 mm for the conductor and 3 mm for the insulator segment, with an interelectrode distance of 20 mm. For the entrance region it was found sufficient to consider six electrode pairs (of identical dimensions $\ell_{c,i} = 12$ mm and $\ell_{i,i} = 3$ mm) preceded by 57 mm of insulating wall. As in Ref. 2, three computations were carried out, differing only in the assumed T and U profiles: the first computation used uniform gas temperature $T = 3000\ ^{o}K$ and uniform gas velocity $U = 3000$ m/s; the second computation used uniform $T = 3000\ ^{o}K$ and uniform gas velocity 300 m/s, one order of magnitude smaller than in the first computation; the third computation accounted for the variation of both T and U in the electrode wall boundary layers, as described in Ref. 2.

Fig. 6 presents the current distribution and Fig. 7 the electric potential distribution corresponding to each of these computations.

These computations illustrate again, as did the computations described in Ref. 2, how the local electrical behavior is influenced by finite reaction rates, electron energy convection and thermal and velocity boundary layers. These effects have been discussed in Ref. 2. In addition, however, the present solutions over the entire entrance region, illustrate the following facts:

(1) The physical extent of current fringing upstream of the first electrode is small in this seeded nitrogen accelerator, not exceeding approximately one electrode period L. This shows that the finite insulator length L_o used upstream of the first electrode is more than sufficient for the mathematical treatment of the entrance region of this accelerator.

(2) The current and electric field distributions (see Figs. 6 and 7), as well as the distributions of n_e, T_e and of all plasma properties, can be considered periodic, to a very good approximation, after the third or fourth electrode pair. This shows, again, that the number of electrode pairs used for the mathematical treatment of the entrance region is more than sufficient for this accelerator. Comparison of the periodic parts of Fig. 6 with the corresponding current distributions computed in Phase II under the imposed assumption of periodicity (Figs. 1, 4, 7 of Ref. 2) show detailed agreement.

The limited current fringing and rapid approach to periodicity exhibited by these computations is, of course, dependent upon the choice of the working fluid. On the other hand, computations performed by this method for monatomic seeded and unseeded gases have indicated similar characteristics: current fringing extended at most a few electrode periods upstream of the first electrode pair, while periodicity was reached by, at most, the eighth electrode pair.

Finally, these computations have illustrated that current fringing in the exit region of $J \times B$ accelerators is not more severe than the

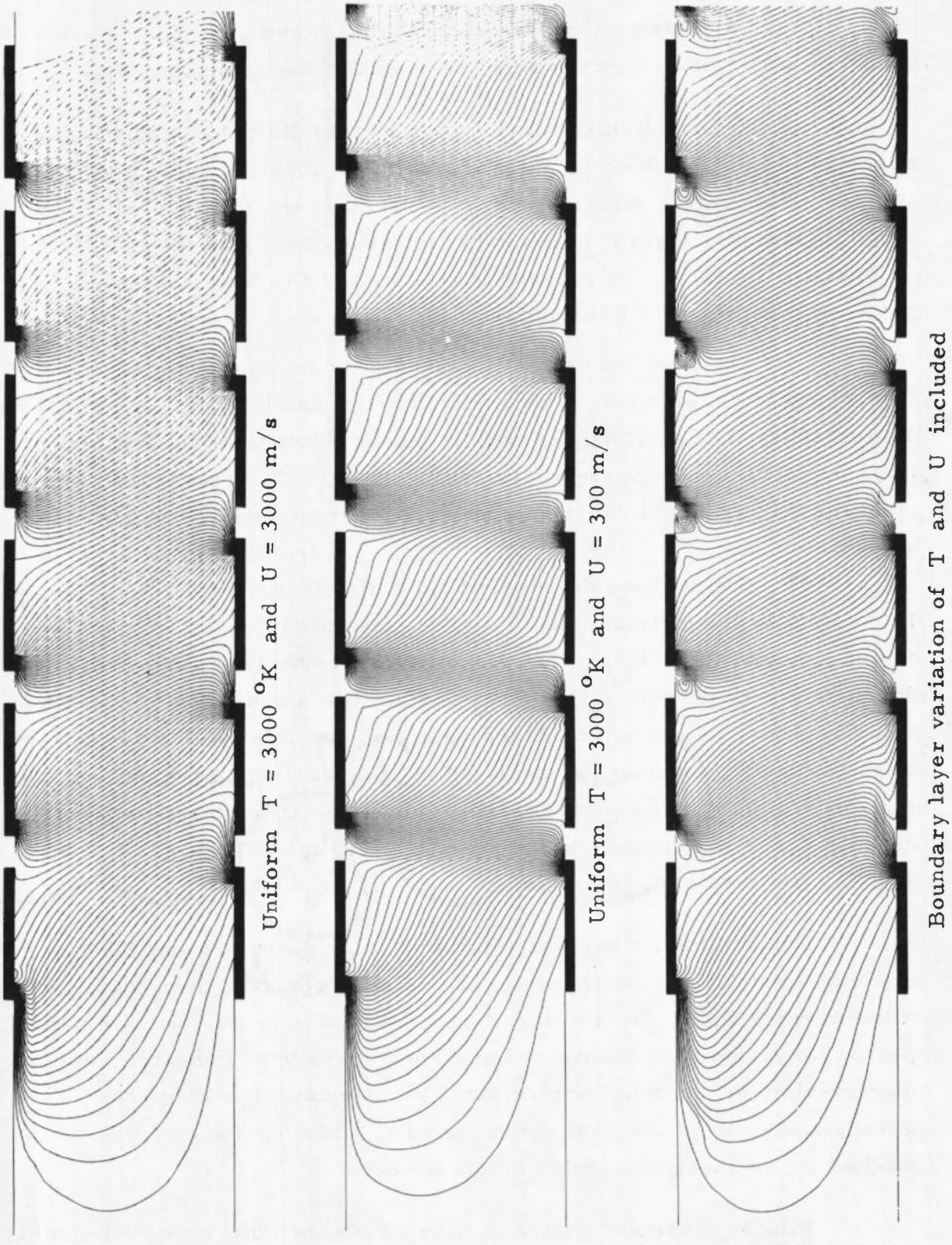

Fig. 6. Current distributions in seeded-nitrogen accelerator

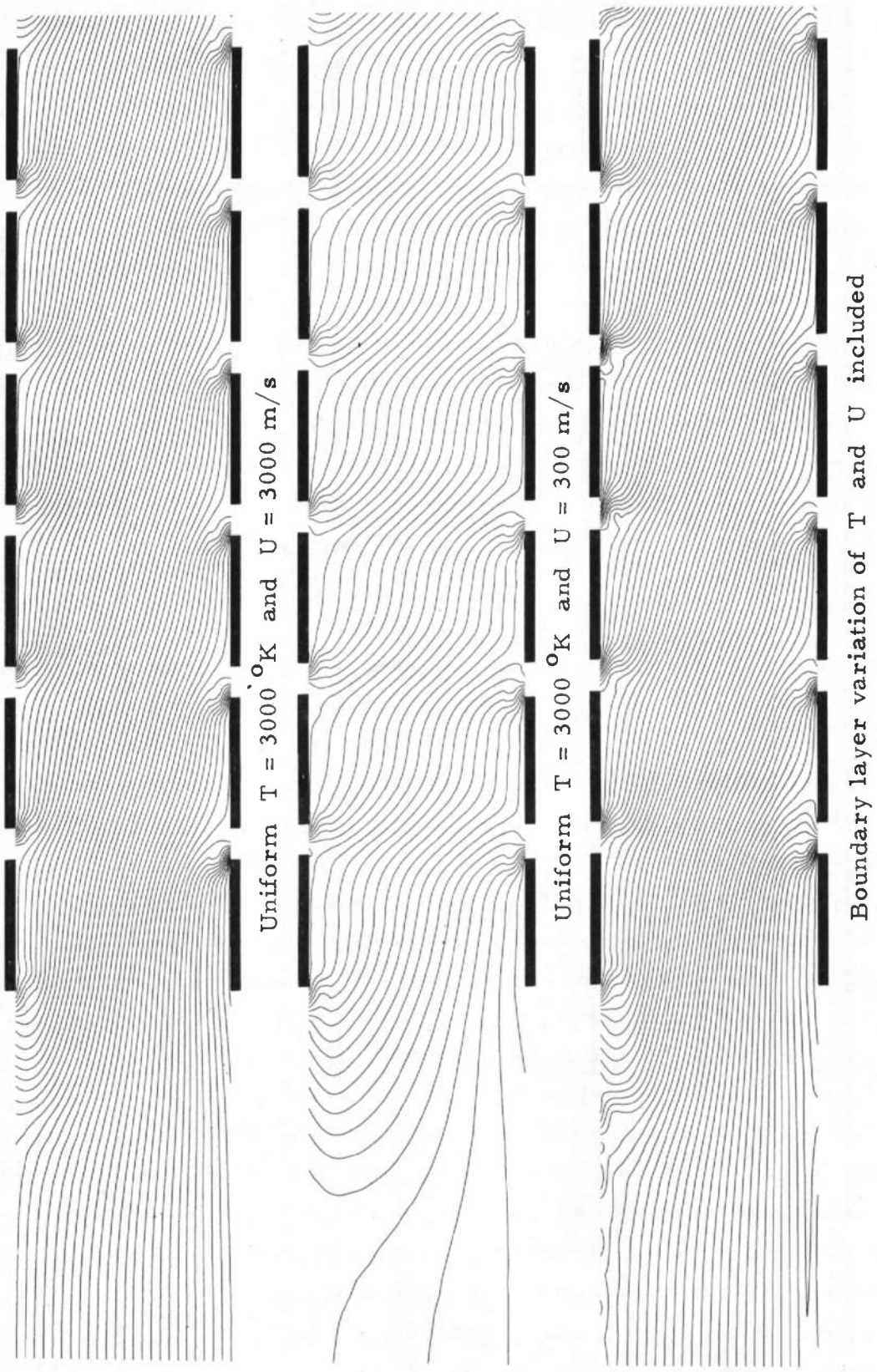

Fig. 7. Electric potential distributions in seeded-nitrogen accelerator

fringing reported above for the entrance region.

2. BOUNDARY LAYER SOLUTIONS

The novel formulation and method of solution used in this study for the boundary layer problem has provided inducement for careful testing of their accuracy and reliability. For this purpose, consistent and well documented cases of turbulent boundary layer flows were sought, for which experimental results were also available. It was natural, therefore, to select test cases from the 33 incompressible turbulent flows documented by D. Coles for the AFOSR-IFP-Stanford 1968 Conference on Turbulent Boundary Layers (Refs. 23 and 24). The experimental results collected for this conference (Ref. 24) and the results of the computations carried out by the participants (Ref. 23) concerned the axial variation of the skin friction coefficient c_f, the shape factor $H \equiv \delta^*/\theta$, and the momentum-thickness-Reynolds number $Re_\theta \equiv U_\infty \theta/\nu$, where δ^* is the displacement thickness, θ the momentum thickness and ν the kinematic viscosity. These particular quantities were selected on the basis that they should provide a more sensitive indication of the accuracy of the prediction method than the overall velocity profile. For the purpose of the conference, values of these quantities were obtained numerically from measured velocity profiles at various axial stations. Specifically, c_f was obtained by fitting the "logarithmic law of the wall" to the experimental velocity profile, and δ^* and θ were calculated using a modified Simpson integration. The predictions reported in Ref. 23 were all started at a specified station in each case, with initial conditions such as to match c_f and Re_θ with the experimental values at that station.

Two of the cases that were selected for testing of the present method, and which will be described here, were those identified in the conference as cases 2100 and 2400. Case 2100 was subject to an initial mildly negative pressure gradient, which then became strongly positive at about $x = 18$ feet, leading to eventual separation. Case 2400 involved a moderately positive pressure gradient, which dropped abruptly to zero near $x = 5$ feet.

The numerical results obtained for these two cases by the various participants in the conference are shown on Figs. 8 and 12 respectively. (These figures are reproduced here from Ref. 23.) The results of the new solution method developed in this study are shown on Figs. 9-11 for Case 2100, and on Figs. 13-15 for Case 2400; note that the latter results were obtained by matching the initial values of c_f and of the kinematic viscosity only.

It is clear from Figs. 8-15 that the new method of solution developed in this study gives quite satisfactory results for these two incompressible test cases, and in fact shows up quite well in comparison to conventional methods. In particular, the results for c_f are in very good agreement with the experimental data.

Results obtained by the new method of solution for the compressible magnetohydrodynamic boundary layer development in the Hirho experiment will be described in the following subsection.

3. COMPUTATIONS PERTAINING TO THE HIRHO EXPERIMENTS

The complete two-dimensional solution of the coupled electrical and gasdynamic problems has been carried out over the entire powered section of the AEDC Hirho channel (Ref. 8) with seeded air as the operating fluid. This was the first application of the complete method; it included two-dimensional solution of the electrical problem, quasi-one-dimensional solution of the gasdynamic problem in the core of the flow, and two-dimensional boundary-layer solution on the electrode walls. This application gave impressive demonstration of how essential it is to avoid oversimplifications when attempting to predict or interpret the behavior of multielectrode $J \times B$ devices. It has already been found for the Hirho channel (Ref. 8), as for many other cases, that as long as one-dimensional analyses are employed there results considerable discrepancy between predicted and observed Hall fields. This work has shown that correct prediction and interpretation of the Hall field, which is an important design parameter for magnetohydrodynamic channels, cannot be attained even by the two-dimensional but linearized,

X Experimental (Ref. 24) ——— Theoretical (Ref. 23)

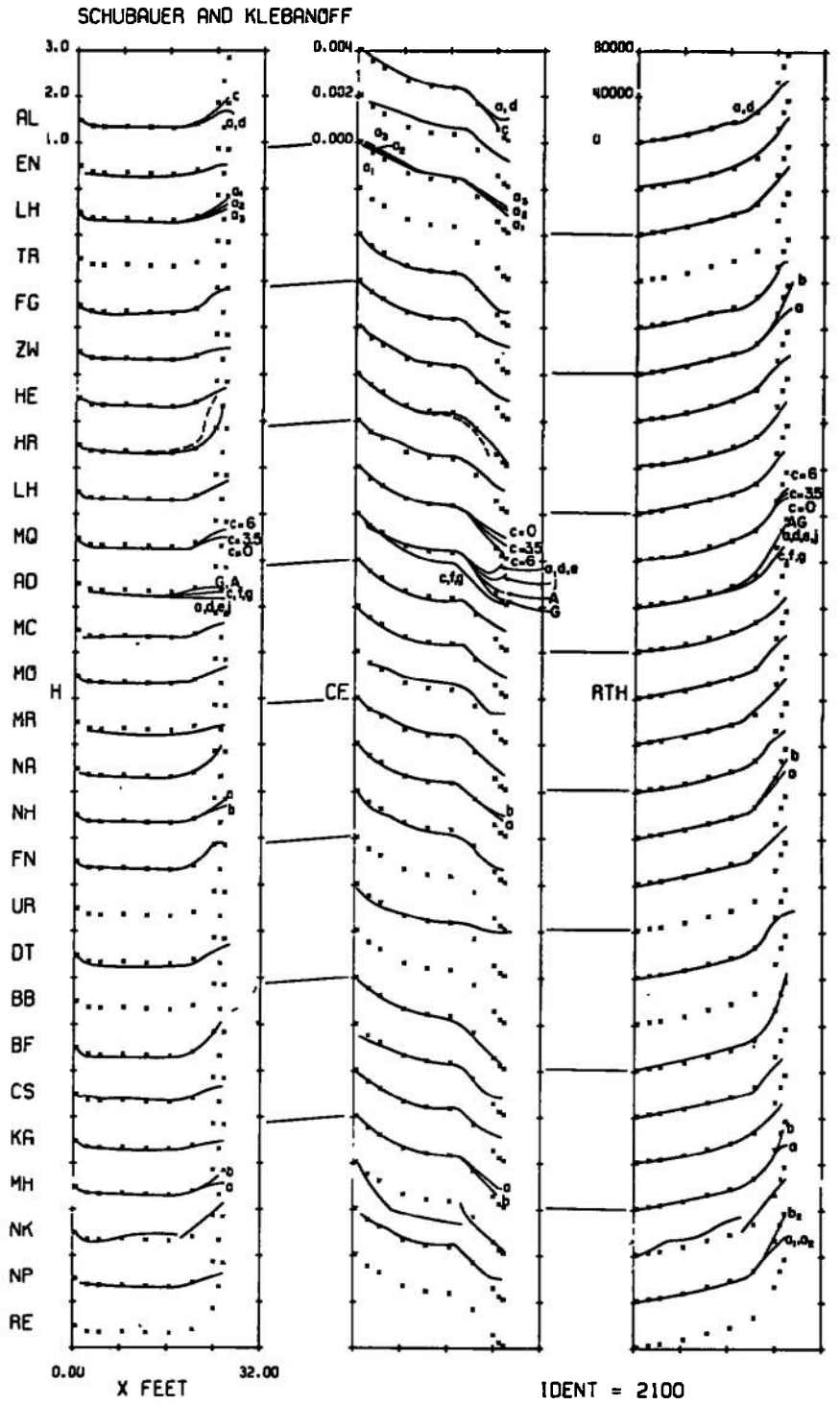

Fig. 8. $H \equiv \delta^*/\theta$, c_f and Re_θ for the conditions of Case 2100

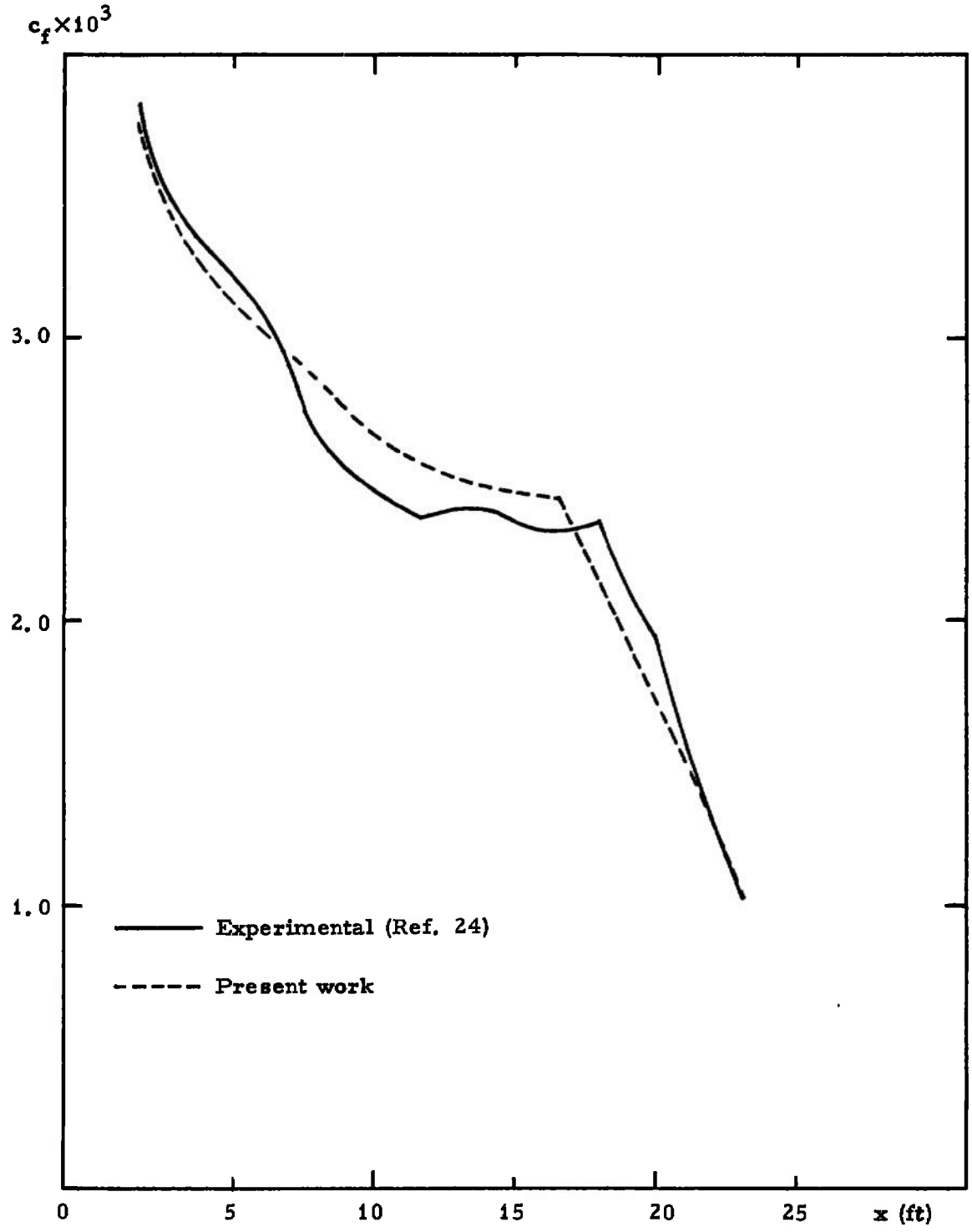

Fig. 9. c_f vs. x for the conditions of Case 2100.

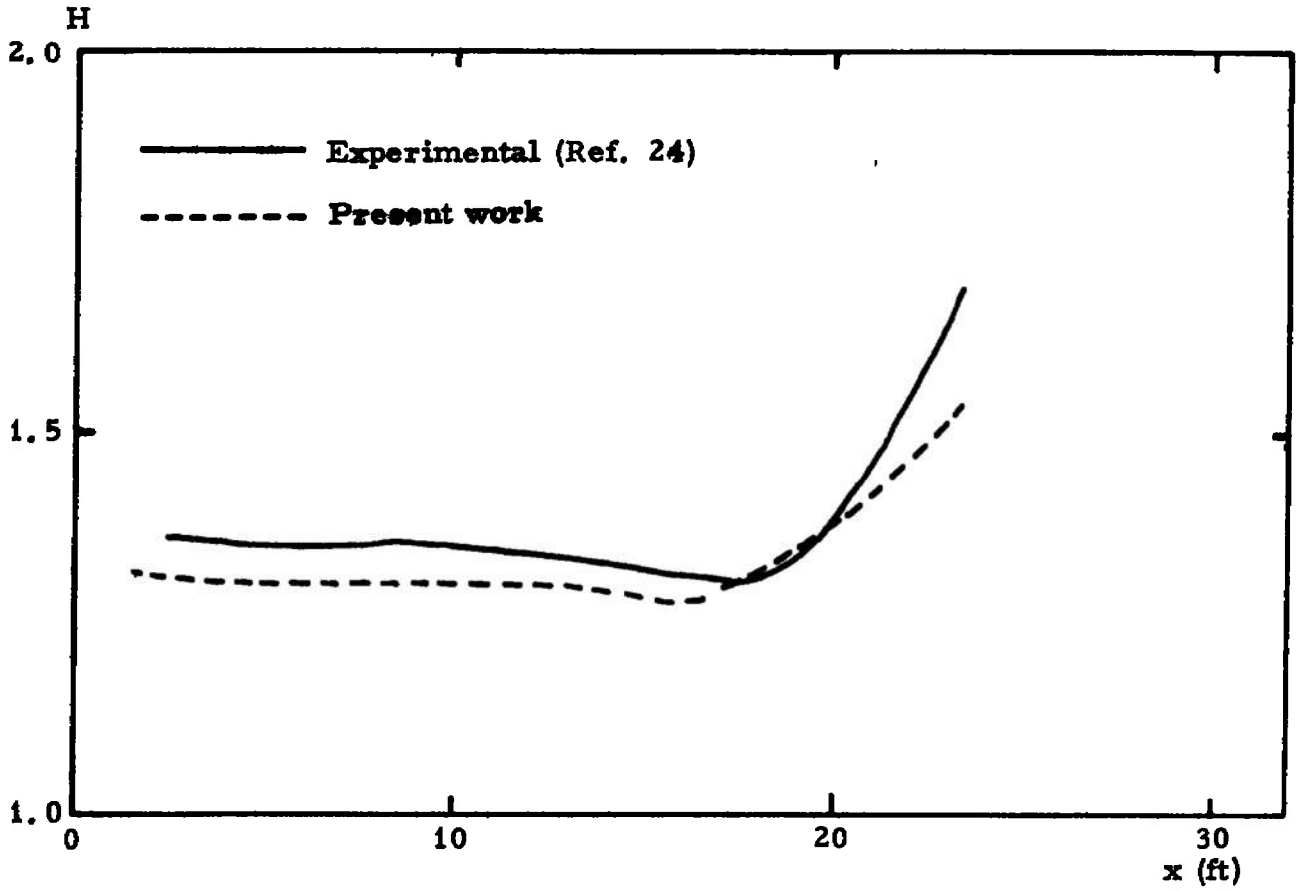

Fig. 10. $H \equiv \delta^*/\theta$ vs. x for the conditions of Case 2100.

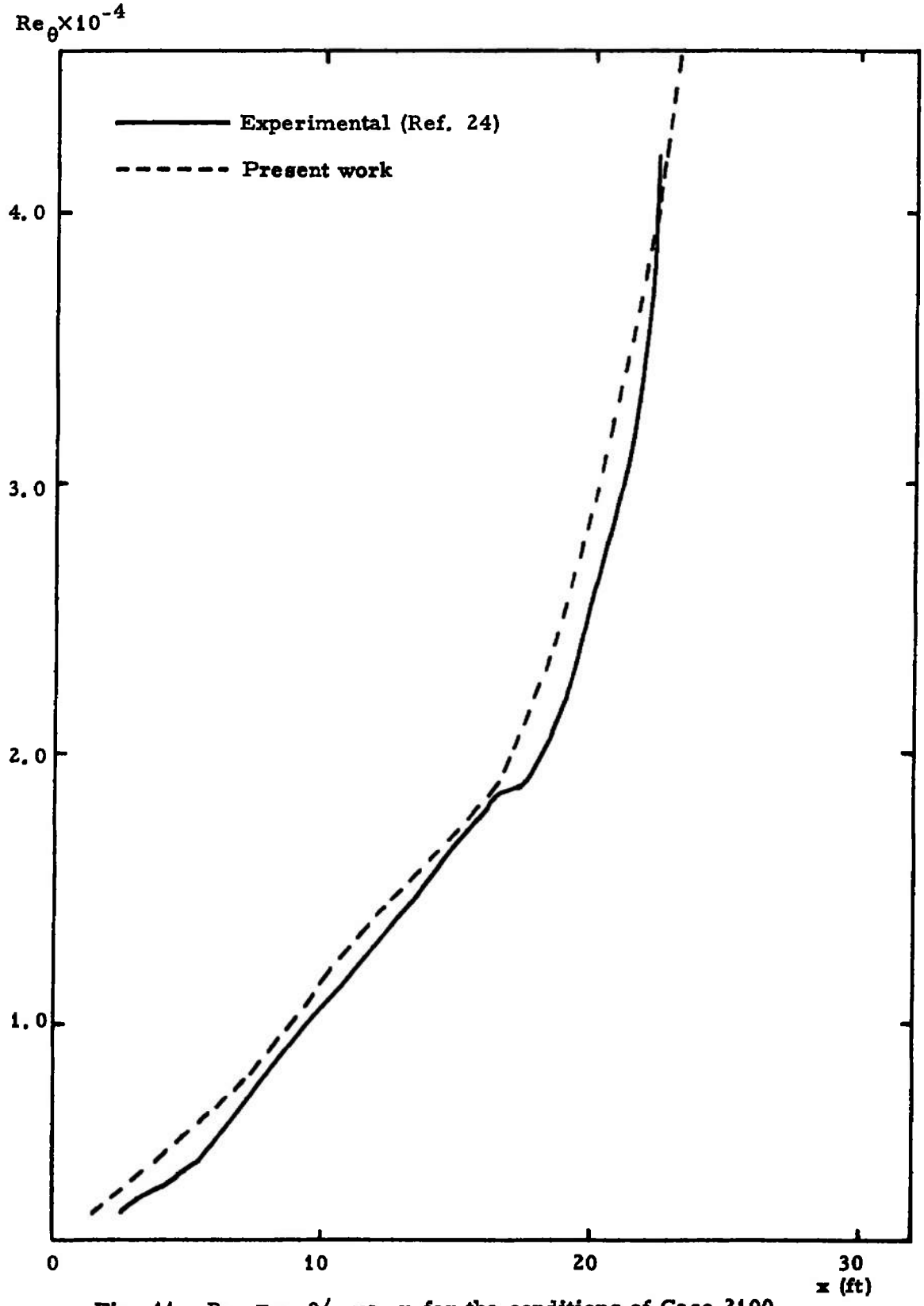

Fig. 11. $Re_\theta \equiv u_\infty \theta/\nu$ vs. x for the conditions of Case 2100.

X Experimental (Ref. 24) ——— Theoretical (Ref. 23)

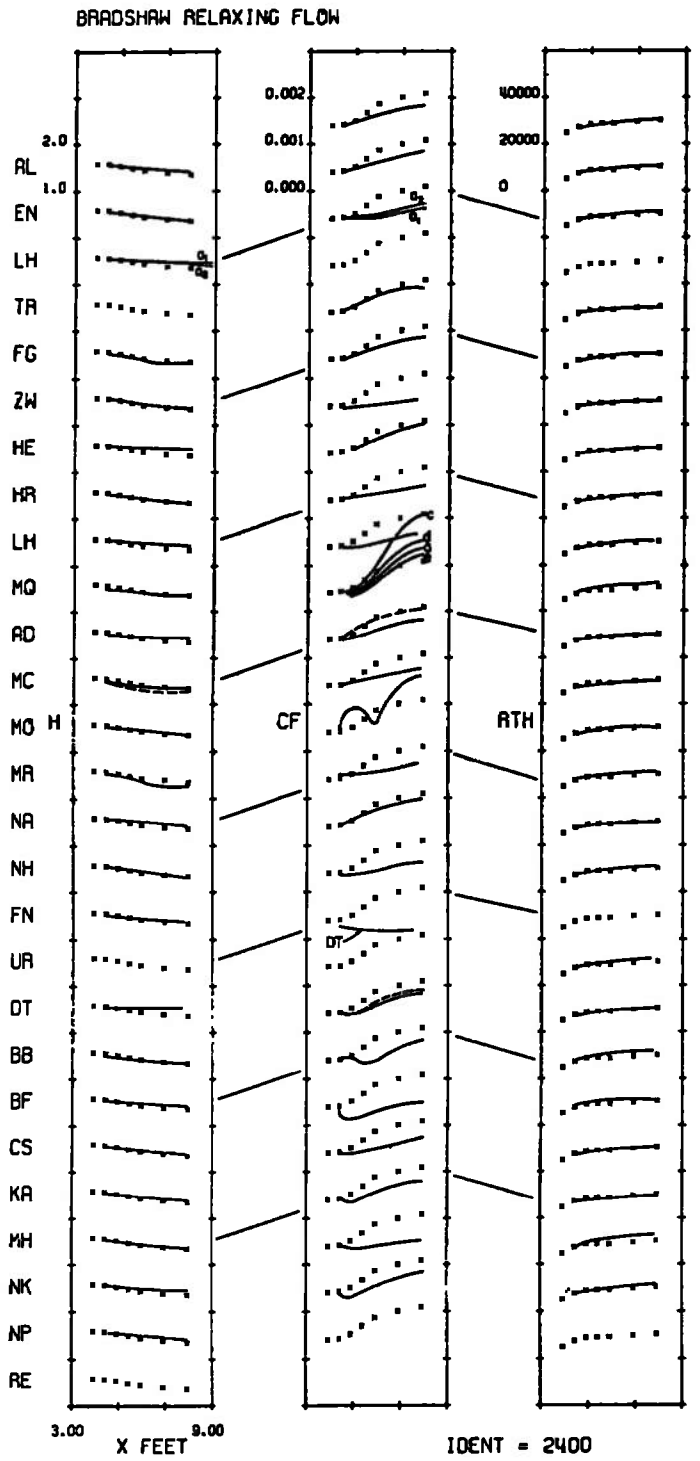

Fig. 12. $H \equiv \delta^*/\theta$, c_f and Re_θ for the conditions of Case 2400

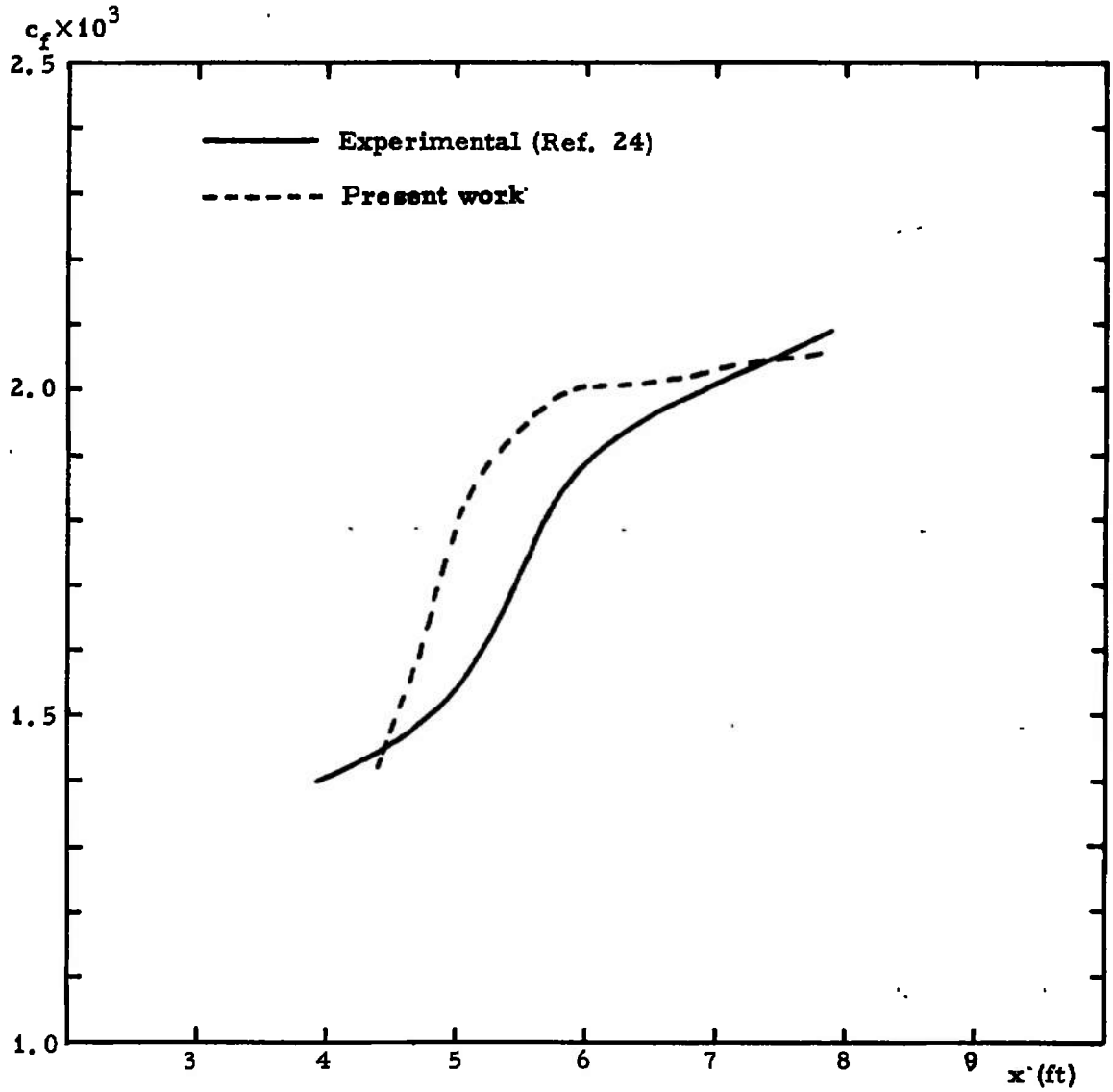

Fig. 13. c_f vs. x for the conditions of Case 2400.

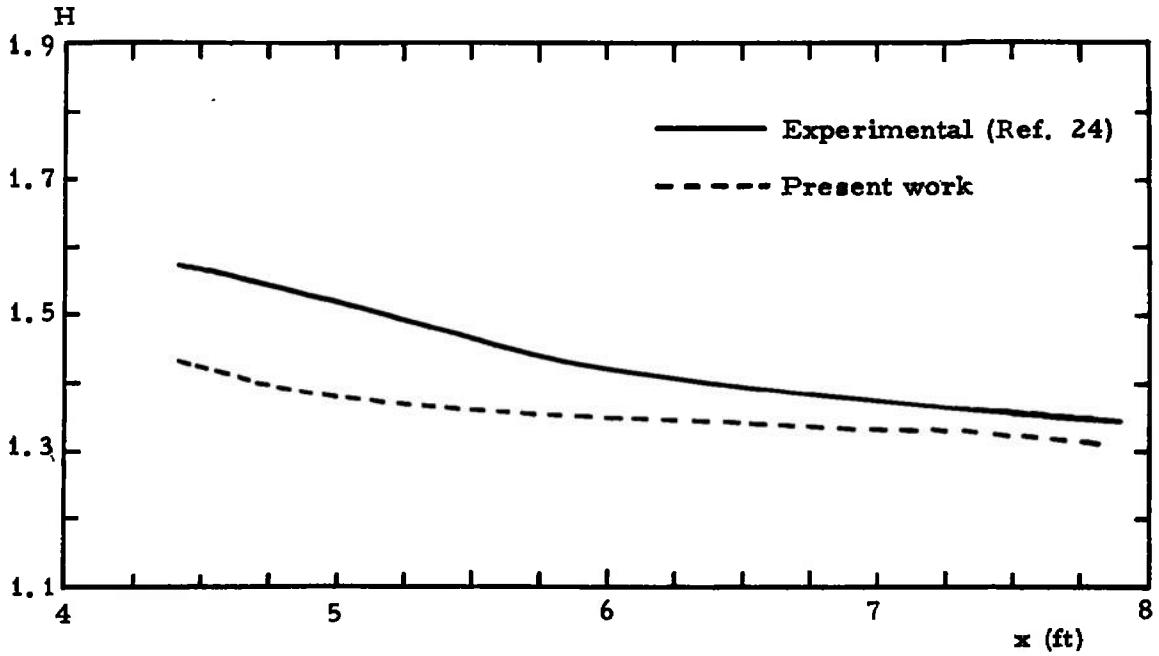

Fig. 14. $H \equiv \delta^*/\theta$ vs. x for the conditions of Case 2400.

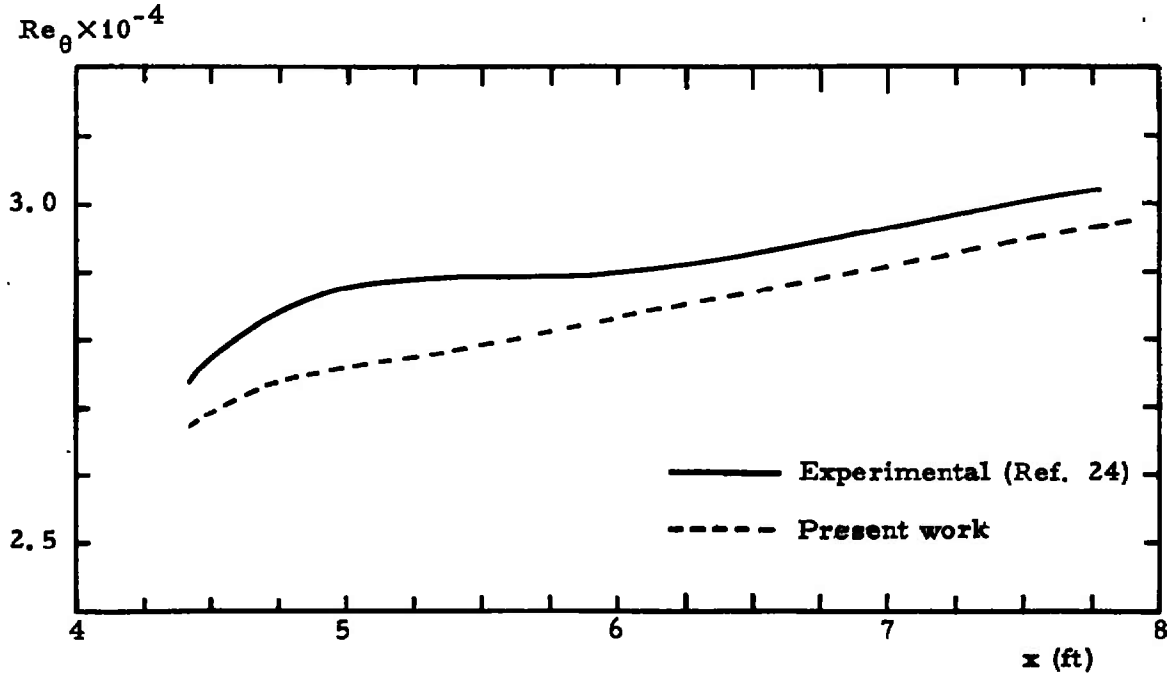

Fig. 15. $Re_\theta \equiv u_\infty \theta/\nu$ vs. x for the conditions of Case 2400.

"constant-property," computation.

The present method has been very successful in predicting and interpreting the experimental results (Ref. 8) that have been obtained in the Hirho channel. In particular, it demonstrated the substantial effect of the local axial current density J_x on the Hall field, especially at relatively low values of the Hall parameter β/ϵ. The presence of finite (and negative) J_x in the core of $J \times B$ accelerators tends to reduce the Hall field E_x, even when there is no net axial current leakage, as can be clearly seen by writing Ohm's law in the x-direction in the form

$$E_x + K_x = \frac{\epsilon}{\sigma} J_y \left[- tg\ \varphi + \frac{\beta}{\epsilon} \right] \tag{75}$$

where $\vec{K}$ the thermal diffusion vector (Refs. 1 and 2) and φ the angle the current density $\vec{J}$ makes with the positive y-axis. First, a finite J_x leads to finite tg φ which diminishes the absolute value of the square bracket in Eq. (75). Secondly, and more importantly, a finite J_x increases the rate of local Ohmic heating and can thus result in substantially higher values of the scalar conductivity σ, which appears in the denominator in Eq. (75).

The cumulative effects of these two mechanisms on the Hall field in the Hirho channel, as investigated by this study, are illustrated on Fig. 16: The quantity chosen for this illustration is the potential of each cathode in the channel relative to cathode No. 1; this choice allows direct comparison with experimental measurements (shown as curve 1 on Fig. 16). The operating conditions were those of Hirho Run No. 1412 (Ref. 8). Curve 4 shows the results of a one-dimensional computation, performed by the authors of Ref. 8, which shall be called computation I. Computation I estimated the average J_y from the given electrode currents, and assumed J_x to be zero (or at most a small fraction of J_y, estimated as in Ref. 25, but without any effect on the local Ohmic heating). Curve 3 shows the results of a two-dimensional solution of the electrical problem by the present method, which however used as inputs the distributions of the gasdynamic unknowns U and T obtained from computation I. Finally, curve 2 was obtained by coupling the electrical

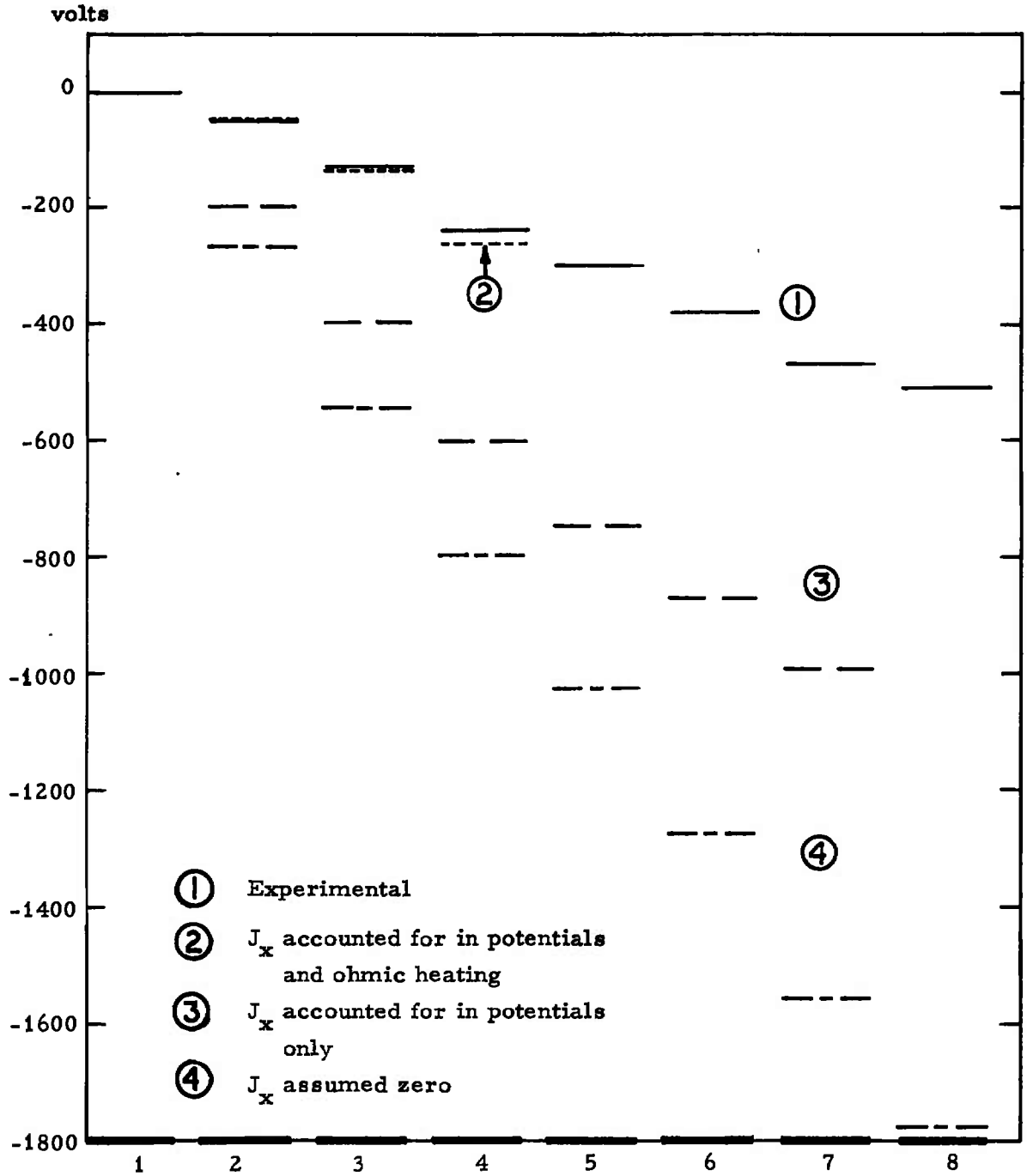

Fig. 16. Cathode potentials relative to cathode #1 for a J × B accelerator. [Operating conditions correspond to Hirho run 1412 (Ref. 8).]

and gasdynamic problems over the first four electrodes, and accounting fully for the increased Ohmic heating due to finite local J_x. Curve 2 demonstrates the ability of this method to predict and interpret the operating characteristics of multielectrode $J \times B$ devices.

After the effect of finite J_x was demonstrated, additional computations were performed to investigate possibilities of improving the performance by diminishing the angle φ through changes in the electrode geometry. Thus a second run treated a "staggered-electrode" geometry, where the cathodes were shifted in the downstream direction by 5/9 of the electrode period (i.e., approximately 1") compared to the position of the corresponding anodes, and a third run treated a geometry with finer electrode segmentation (L/D = 5/9 instead of 9/8). The operating conditions used in all computations were those of Run No. 1412 (Ref. 8). The results are shown on Figs. 17 and 18.

Figure 17(a) shows the current distribution in the actual Hirho geometry as computed by the idealized "constant property" method, to contrast with Fig. 17(b) which shows the current distribution as computed by the present method, including thermal diffusion, finite reaction rates, and electron energy convection. The generally greater angle φ between the current lines and the y-axis (and correspondingly greater J_x for given J_y) is the most noticeable characteristic of Fig. 17(b) as compared to Fig. 17(a). The potential distribution corresponding to the current distribution of Fig. 17(b) is shown on Fig. 17(c), on which the contours are equipotentials for the electric field $\vec{E}$ (unprimed) and the contour interval is 50 volts.

Figure 18(a) shows the current distribution in the "staggered-electrode" geometry, and demonstrates that in this case the angle φ has an average value of the order of 5°, as opposed to 20° in the actual geometry (Fig. 17(b)). Finally, Fig. 18(b) shows the current distribution in the case of finer segmentation and demonstrates that in this case the average value of the angle φ is of the order of 10°.

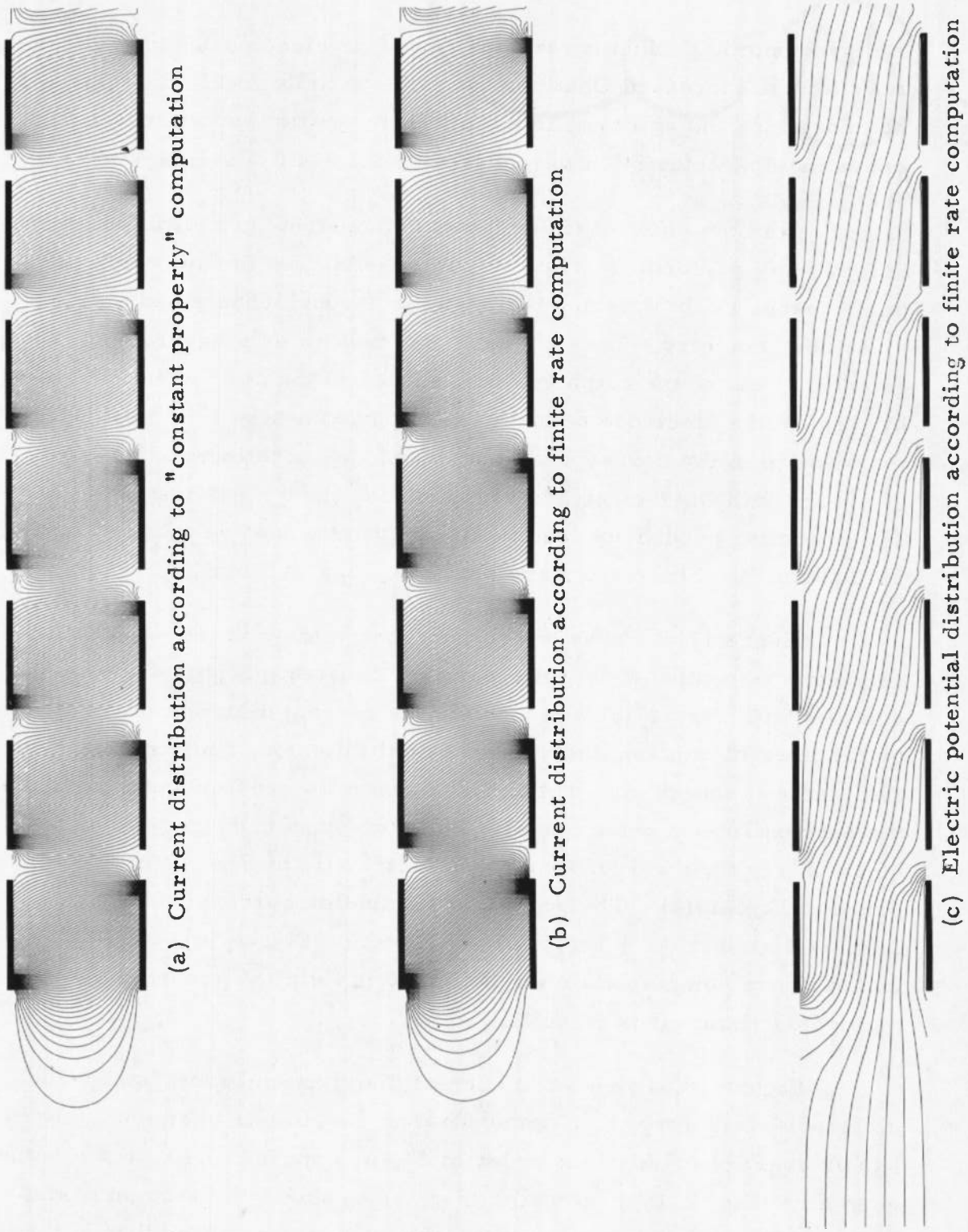

Fig. 17. Current and electric potential distributions for actual Hirho geometry.

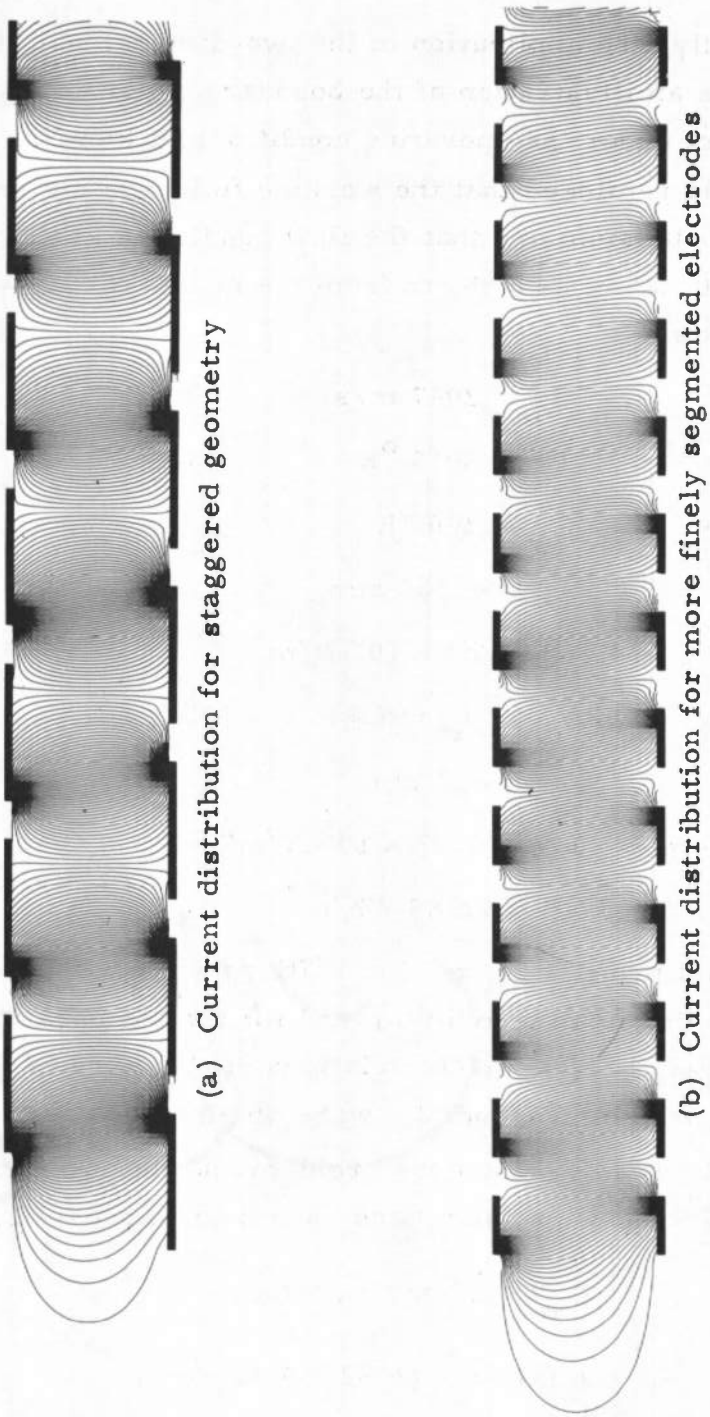

Fig. 18. Current distributions corresponding to modified Hirho geometries.

Finally, the application of the two-dimensional boundary-layer solution gave an illustration of the boundary-layer development in the Hirho channel under the operating conditions of Run No. 1412 (Ref. 8). The reader is reminded that the working fluid was air seeded with 0.2% (by weight) potassium and that the flow conditions at the selected initial station $x = 0$ (at $d = 44.88$ cm from the nozzle throat — see Ref. 8) were as follows:

$$U_\infty = 2947 \text{ m/s}$$

$$T_\infty = 3017 \ ^\circ\text{K}$$

$$T_w = 300 \ ^\circ\text{K}$$

$$p = 4.56 \text{ atm}$$

$$\frac{dp}{dx} = -2 \times 10^6 \text{ N/m}^3$$

$$Re_\infty = U_\infty d/\nu = 8.7 \times 10^6$$

$$\delta = 6.1 \text{ mm}$$

$$\langle J_y \rangle = 4.07 \times 10^5 \text{ A/m}^2$$

$$B = 2.85 \text{ Wb/m}^2$$

For the initial profiles at $x = 0$ a 1/7th power law variation has been assumed for the mean velocity u and for the temperature ratio $(T-T_w)/(T_\infty-T_w)$. The axial variations of U_∞ and of the current density components J_x and J_y were obtained from the quasi-one-dimensional solution of the core problem and the two-dimensional solution of the electrical problem, and have been expressed as follows:

$$U_\infty(x) = 2947 + 2250x \qquad \text{m/s}$$

$$J_x(x) = -(2.52 + 5.96x) \cdot 10^5 \qquad \text{A/m}^2$$

$$J_y(x) = (4.07 + 34.6x) \cdot 10^5 \qquad \text{A/m}^2$$

The solution has provided, in addition to the description of boundary-layer development, the distributions of skin friction and wall heat transfer rate along the channel. The results are shown on

Figs. 19-25. Figures 19, 20, 21, 22, and 23 present the profiles of the unknowns u, τ, T, n_e, and T_e respectively, at various x-stations. Note that Fig. 20 shows the profile of the turbulent shear stress τ alone. If the laminar contribution were added, the total shear stress $\tau_L + \tau$ would have a maximum at the wall due to the effective favorable pressure gradient in the supersonic diverging channel. Fig. 21 shows how the mean gas temperature profile, which was initially assumed to follow a 1/7 power law, is affected by Ohmic heating and dissipation so as to develop a peak close to the wall at downstream stations. It should be pointed out that a more realistic initial profile could be prescribed in terms of the turbulent version of Crocco's relation (Ref. 26)

$$c_p T + \frac{1}{2} u^2 \approx c_p T_\infty^o \left[(1 - \eta) \frac{u}{U_\infty} + \eta \right] \tag{76}$$

where T_∞^o is the freestream stagnation temperature and $\eta = T_w/T_\infty^o$.

The computed results for the variation of the skin friction coefficient c_f and the heat transfer coefficient $c_H \equiv -(k \frac{\partial T}{\partial y})_w / [\rho_\infty U_\infty (H_\infty - H_w)]$ along the channel are shown on Fig. 24. The skin friction results lie between those obtained by the method of Enkenhus and Mahez and by that of Elliot, Bartz, and Silver and reported in Ref. 8. The computed growth of the boundary layer thickness δ and of the displacement thickness δ^* are shown on Fig. 25. The latter, by definition, reduces the effective channel height D for the core flow. Taking into consideration that the channel height D at the initial station x = 0 is 3.28 cm, and the angle of divergence of the channel is $1^o26'$, we see that the ratio δ^*/D varies from approximately 6×10^{-3} at x = 0 to 3×10^{-2} at x = 14 cm.

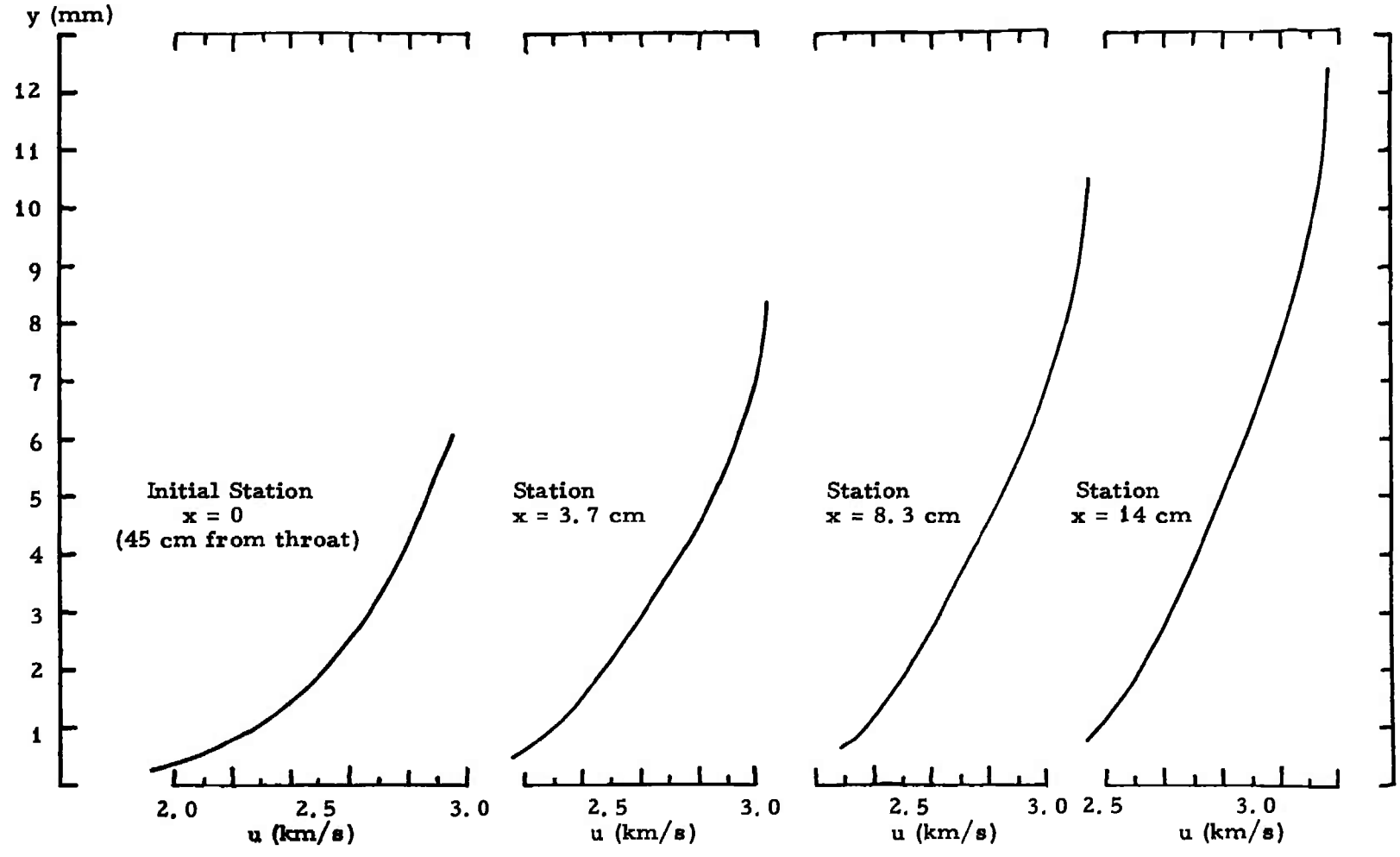

Fig. 19. Development of mean velocity profile in a J × B accelerator [Operating conditions correspond to Hirho run 1412 (Ref. 8).]

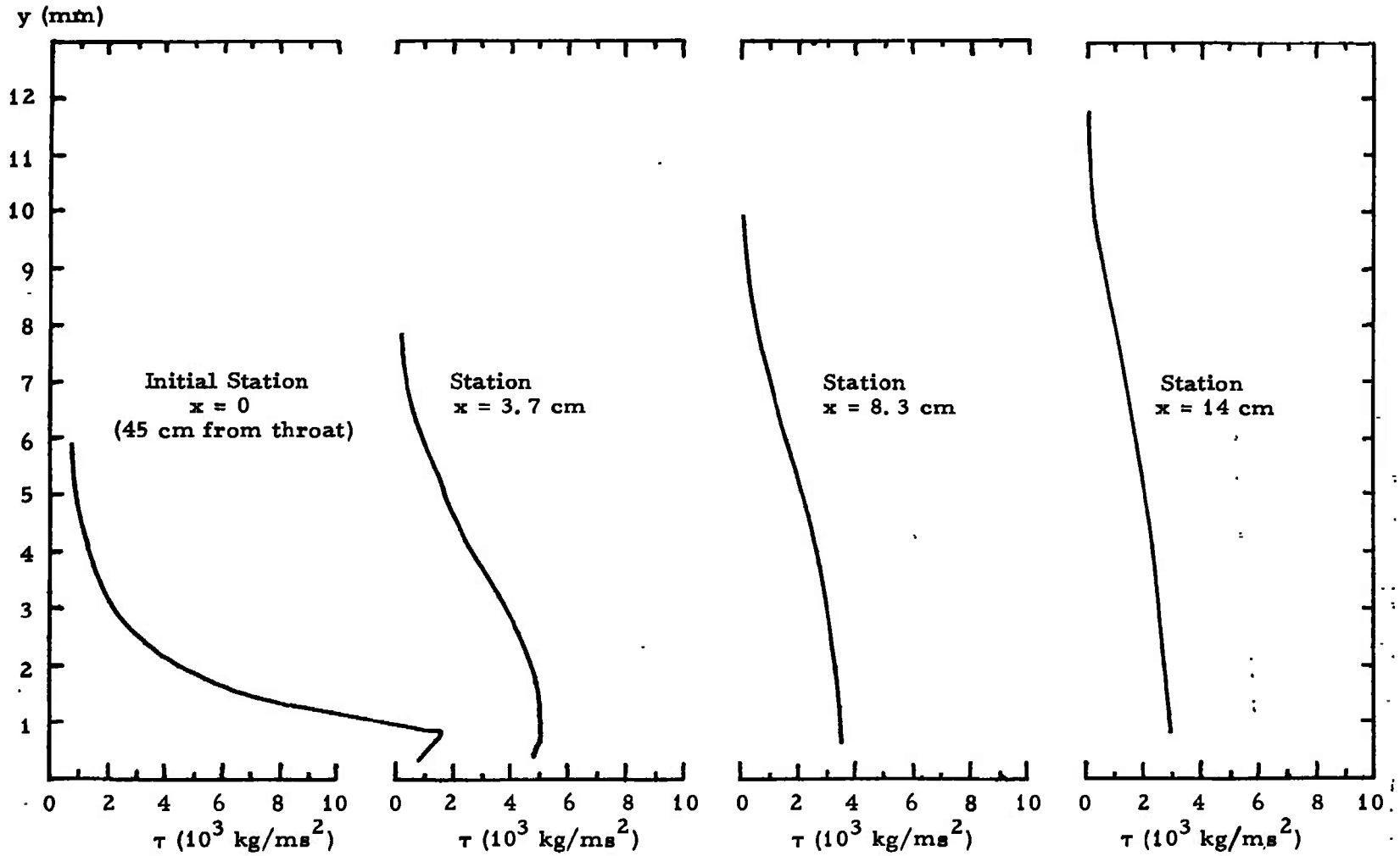

Fig. 20. Development of turbulent shear stress profile in a J × B accelerator [Operating conditions correspond to Hirho run 1412 (Ref. 8).]

AEDC-TR-70-86

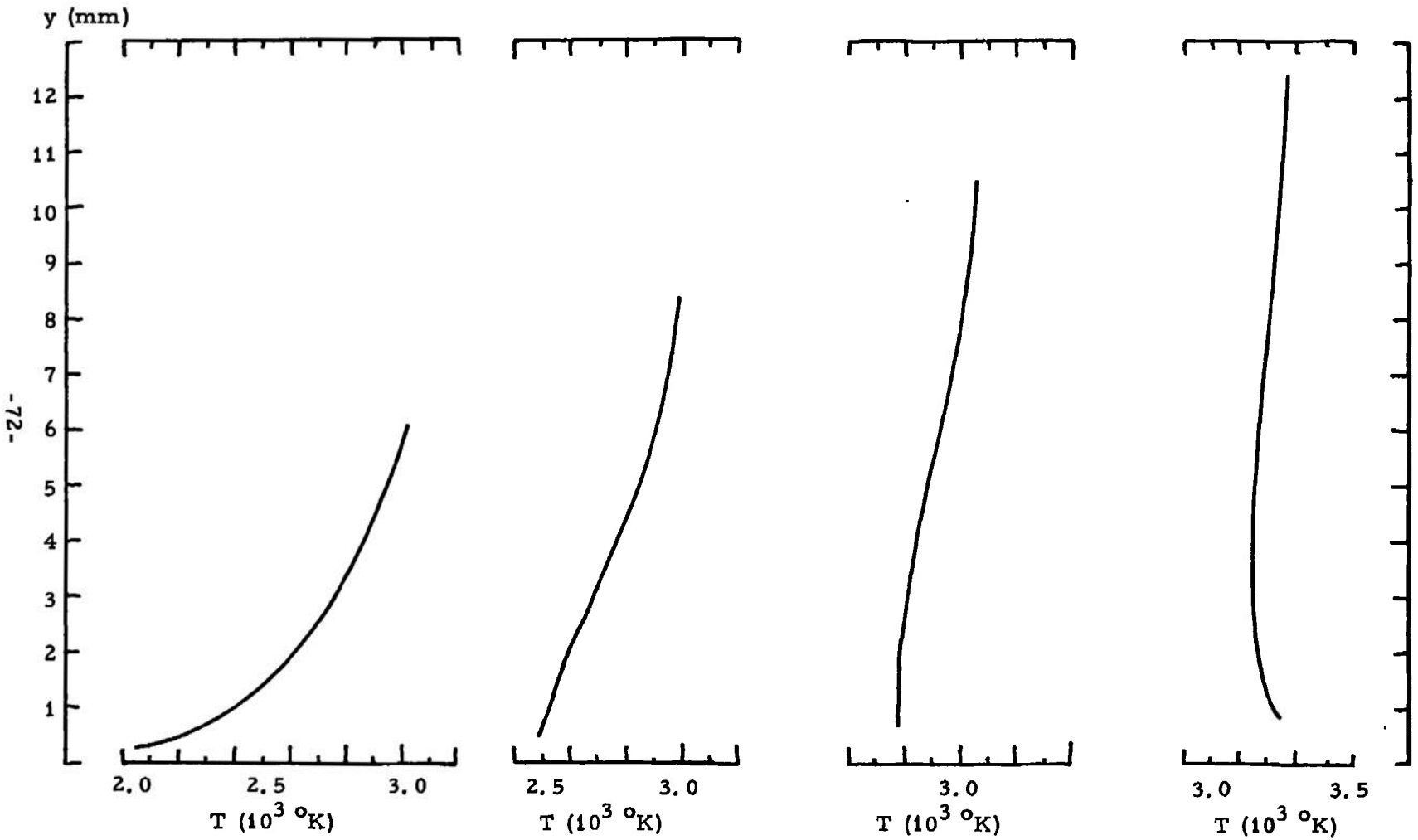

Fig. 21. Development of mean gas temperature profile in a J × B accelerator [Operating conditions correspond to Hirho run 1412 (Ref. 8).]

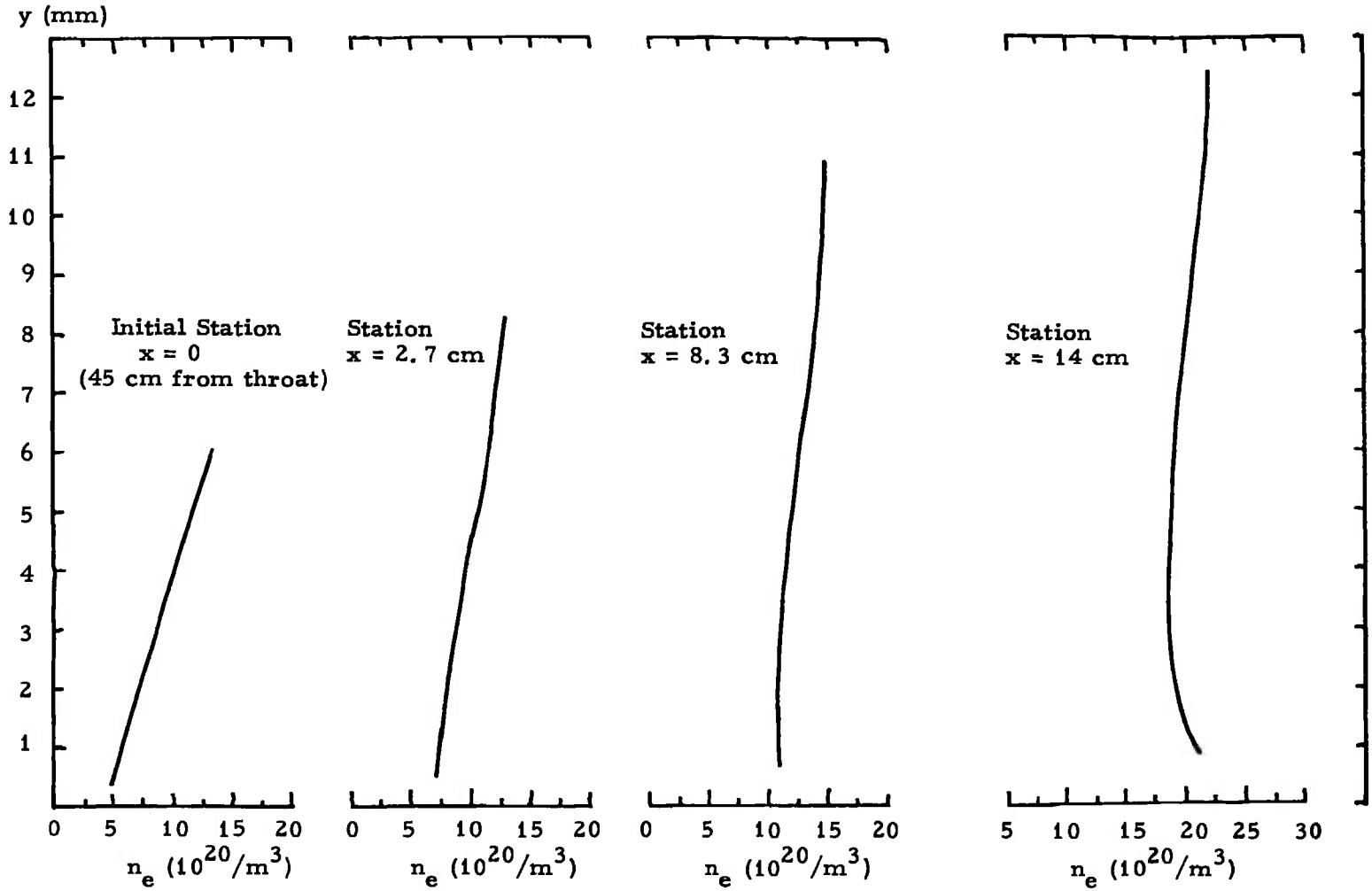

Fig. 22. Development of mean electron number density profile in a J × B accelerator [Operating conditions correspond to Hirho run 1412 (Ref. 8).]

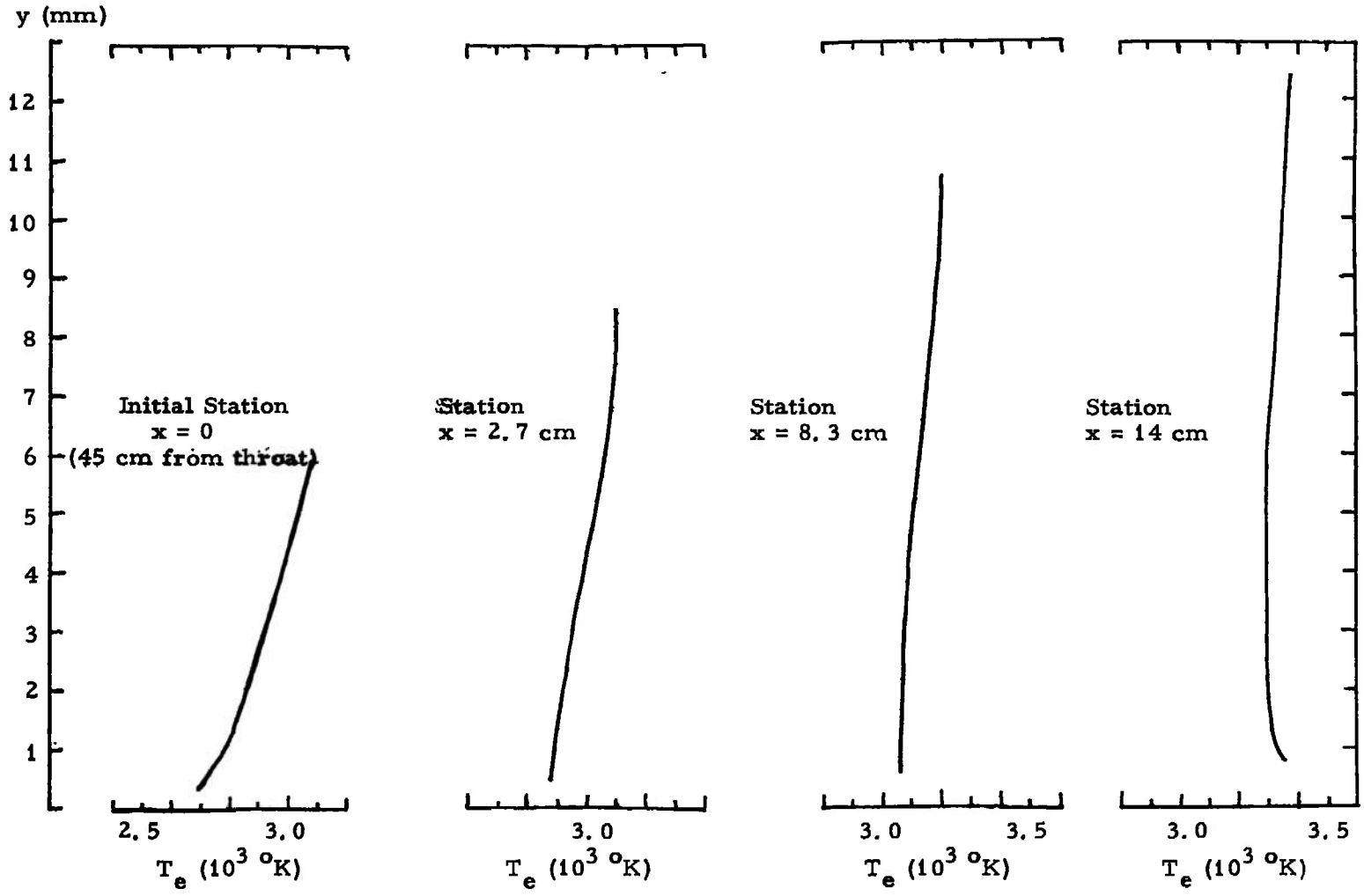

Fig. 23. Development of mean electron temperature profile in a J × B accelerator [Operating conditions correspond to Hirho run 1412 (Ref. 8).]

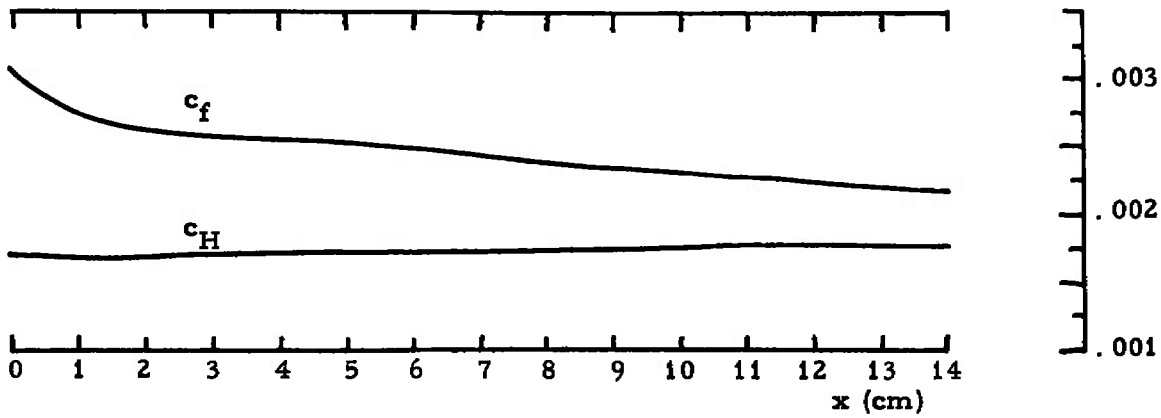

Fig. 24. Streamwise variation of skin friction and wall heat transfer rate coefficients in a J × B accelerator. [Operating conditions correspond to Hirho run 1412 (Ref. 8).]

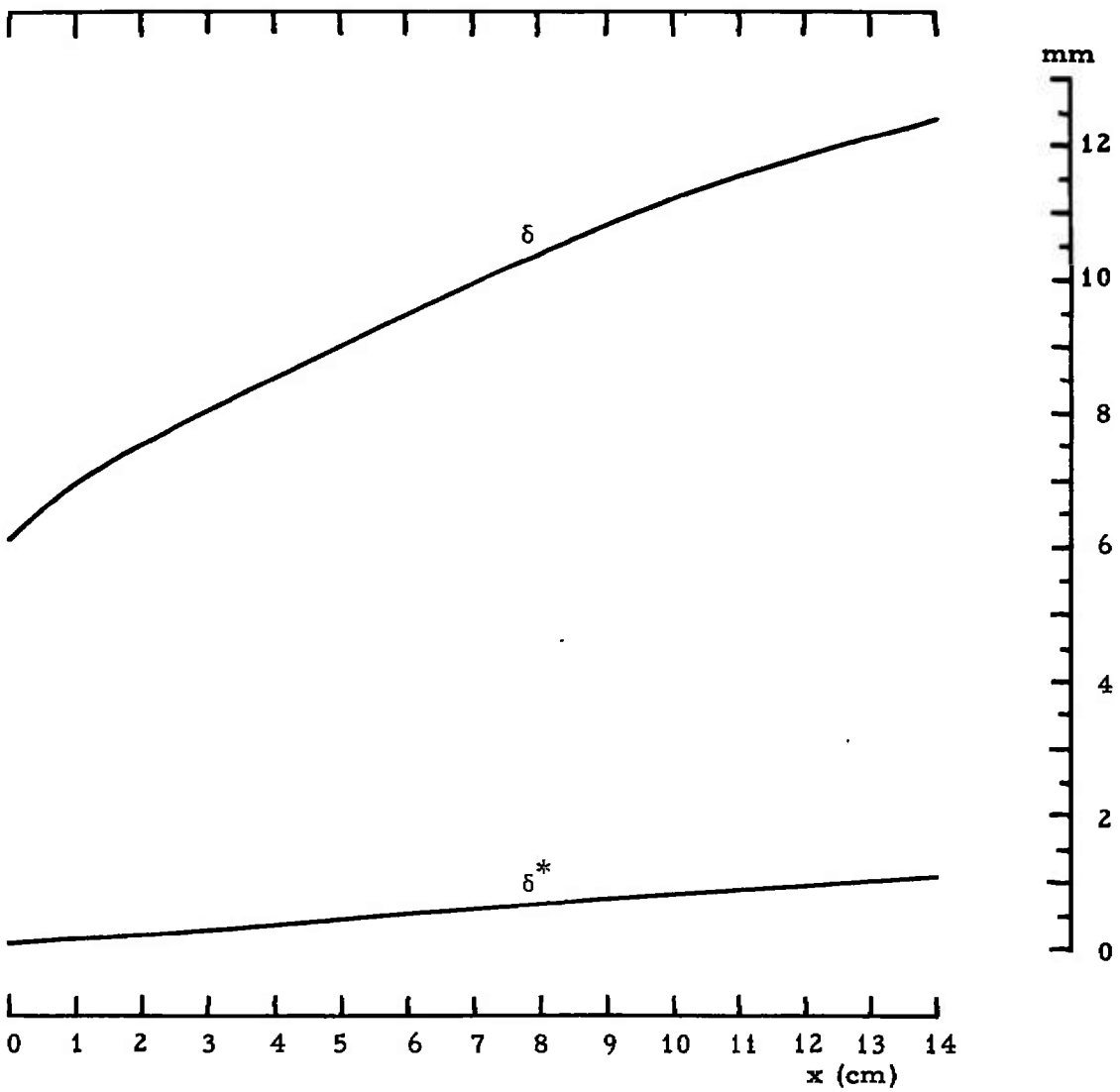

Fig. 25. Growth of boundary layer thickness $\delta = \delta_{995}$ and displacement thickness δ^*. [Operating conditions correspond to Hirho run 1412 (Ref. 8).]

REFERENCES

1. Argyropoulos, G. S., Demetriades, S. T. and Kendig, A. P., "Current Distribution in Crossed-Field Accelerators (Part I, Effects of Thermal Diffusion and Boundary Layers)," Arnold Engineering Development Center Technical Report AEDC-TR-67-135, Volumes I and II, July 1967.

2. Argyropoulos, G. S. and Demetriades, S. T., "Current Distribution in Crossed-Field Accelerators (Part II, Effects of Finite Reaction Rates and Electron Energy Convection)," Arnold Engineering Development Center Technical Report AEDC-TR-68-204, September 1968.

3. Argyropoulos, G. S., Demetriades, S. T., and Kendig, A. P., "Current Distribution in Nonequilibrium J × B Devices," J. Appl. Phys. 38, 5233-5239 (1967).

4. Argyropoulos, G. S., Casteel, M. A., and Demetriades, S. T., "Two-Dimensional Distribution of Current Along Magnetohydrodynamic Channels," Tenth Symposium on Engineering Aspects of Magnetohydrodynamics, Massachusetts Inst. Tech., Proceedings, pp. 29-32 (1969).

5. Argyropoulos, G. S. and Demetriades, S. T., "Influence of Relaxation Effects in Nonequilibrium J × B Devices," J. Appl. Phys. 40, 4500-4509 (1969).

6. Demetriades, S. T. and Argyropoulos, G. S., "Ohm's Law in Multicomponent Nonisothermal Plasmas with Temperature and Pressure Gradients," Phys. Fluids 9, 2136-2149 (1966).

7. Argyropoulos, G. S., Demetriades, S. T. and Lackner, K., "Compressible Turbulent Magnetohydrodynamic Boundary Layers," Phys. Fluids 11, 2559-2566 (1968).

8. Norman, W., and Siler, L. G., "Experiments on a Shock Tunnel Augmented by a Magnetohydrodynamic Nozzle Accelerator," Von Karman Gas Dynamics Facility, Arnold Engineering Development Center Technical Report AEDC-TR-68-232, December 1968.

9. Demetriades, S. T., "Determination of Energy-Loss Factors for Slow Electrons in Hot Gases," Phys. Rev. 158, 215-217 (1967).

10. Demetriades, S. T. and Maxwell, C. D., "Determination of Energy-Loss Factors for Slow Electrons in Hot Gases," Final Report on Contract NAS2-3580, NASA/Ames Research Center (15 August 1969).

11. Ring, L. E., personal communication concerning experiences with a 2 MW constant area accelerator at AEDC, and a 1 MW generator channel (Chrysler Corp. Tech. Rep. HMD-R23-69).

12. Teno, J., Lin, C., and Brogan, T. R., "Boundary Layers in MHD Generators," Tenth Symposium on Engineering Aspects of Magnetohydrodynamics, Massachusetts Inst. Tech., Proceedings, pp. 15-22 (1969).

13. High, M. D. and Felderman, E. J., personal communication.

14. Van Driest, E. R., "On Turbulent Flow Near a Wall," J. Aero. Sci. 23, 1007 (1956).

15. Johnson, D. S., "Velocity and Temperature Fluctuation Measurements in a Turbulent Boundary Layer Downstream of a Stepwise Discontinuity in Wall Temperature," J. Appl. Mech. 26, 325 (1959).

16. Bradshaw, P., Ferriss, D. H. and Atwell, N. P., "Calculation of Boundary-Layer Development Using the Turbulent Energy Equation," J. Fluid Mech. 28, 593-616 (1967).

17. Patankar, S. V., "Heat and Mass Transfer in Turbulent Boundary Layers," Ph.D. Thesis, Imperial College of Mech. Eng., Univ. of London (1967).

18. Smith, A. M. O., Jaffe, N. A. and Lind, R. C., "Study of a General Method of Solution of the Incompressible Turbulent Boundary Layer Equations," Report No. LB 52949, Douglas Aircraft Division (Navy Contract NOw 64-0352c), November 1965.

19. Von Mises, R., "Bemerkungen zur Hydrodynamik," ZAMM 7, 425 (1927).

20. Fox, P., "The Solution of Hyperbolic Partial Differential Equations by Difference Methods," in "Mathematical Methods for Digital Computers," John Wiley and Sons, New York (1967).

21. Cebeci, T., Smith, A. M. O., and Wang, L. C., "A Finite-Difference Method for Calculating Compressible Laminar and Turbulent Boundary Layers," Report No. DAC-67131, McDonnell Douglas Aircraft Company, Inc., March 1969.

22. Bradshaw, P., "The Turbulence Structure of Equilibrium Boundary Layers," J. Fluid Mech. 29, Part 4, 625-645 (1967).

23. Preliminary Proceedings of AFOSR-IFP-Stanford 1968 Conference on Turbulent Boundary Layers (Stanford, 1968), Volume I: Prediction Methods and Physical Structure.

24. Preliminary Proceedings of AFOSR-IFP-Stanford 1968 Conference on Turbulent Boundary Layers (Stanford, 1968), Volume II: Compiled Data.

25. Johnson, P. W., "Two-dimensional flow calculations for linear MHD Channels," Tenth Symposium on Engineering Aspects of Magnetohydrodynamics, Massachusetts Institute of Technology, Proceeding, pp. 33-34 (1969).

APPENDIX A

DESCRIPTION OF COMPUTER PROGRAM "INLET"

A. 1. GENERAL DESCRIPTION

Program INLET has been written to solve the coupled electrical + gasdynamic problem over the whole inlet or exit regions (see main text). The user may, at his option, specify solution of the electrical part of the problem alone, or of the coupled problem; in the latter case, the gas velocity and temperature variations are calculated along the streamlines, without viscosity or heat conduction effects. The solution may be performed over any specified geometry incorporating up to twenty electrode pairs (powered and unpowered) bounded by insulating walls or insulator segments at the upstream and downstream ends. INLET can treat any working fluid, distinguishing as many as 25 separate components, formed from up to 10 distinct elements and taking part in up to 22 reactions. Channel geometry (including dimensions of all conductor and insulator segments), axial distribution of magnetic field strength, electric current passed through each electrode pair, distribution of streamfunction across the channel at upstream and downstream ends (when required), and initial profiles of gasdynamic unknowns must all be provided. INLET will then proceed for a specified number of iterations between gasdynamic and electrical solutions, whereupon a restart deck may be generated in order to continue the calculation from this point at a later time.

INLET has been coded in FORTRAN for Control Data Corporation 6000 series computers, requiring approximately 100, 000 memory locations and capacity to retain 28 significant digits (double precision). Typical calculations require approximately 40 seconds of central processor time on the CDC 6600 for each complete (electrical-gasdynamic) iteration cycle.

The following sections provide a more detailed description of program INLET. Section A. 2 describes input data and formats, A. 3 lists available output, A. 4 lists the routines included in the program,

and Section A. 5 defines important variable names used in these routines.

A. 2. INPUT DATA AND FORMATS

Columns	Format	
1-80	10A8	The first card contains the HEADING to be printed at the top of each new page. Leaving columns 1-8 blank terminates the program.
1-24	8I3	The second card controls the OPTIONAL METHODS OF SOLUTION. Each field on this card controls one of the options listed below, and a non-zero punch in any field selects the corresponding option.

OPTION	INDEX
Compute electric field and potential	1
Solve for gasdynamic variables U, T	2
Use of implicit algebraic equation for T_e	3
Include effects of thermal and concentration diffusion	4
Impose periodicity over one electrode period as boundary condition on Ψ:	5
If field contains 1, at upstream end	
If 2, at downstream end	
Assume instantaneous Saha equilibrium	6
Assume instantaneous electron energy relaxation	7
Assume (6) and (7) during first cycle	8

Columns	Format	
1-3	I3	Number of current density iteration cycles to be performed (up to 25)
1-30	10I3	The fourth card is the INPUT CONTROL card. The remaining input is separated into nine categories, corresponding to the first nine fields on this card. To select input of these categories a non-zero punch is placed in the appropriate fields. A non-zero punch in the tenth field indicates that a computation in process has been interrupted for input and is to be continued.

INPUT CATEGORY	INDEX
Output control deck	1
Specification of working fluid	2
Specification of reactions	3
Specification of geometry and grid	4
Specification of problem parameters	5
Specification of initial velocity, temperature and number density profiles	6
Specification of axial distribution of velocity and temperature	7
Specification of initial electron temperature distribution	8
Restart deck	9

Category 1 OUTPUT CONTROL

The first 8 cards in this category control printout of the current values of quantities of interest at the end of each iteration cycle. Each card corresponds to one of the following output categories, and to select output of any category at the ends of any given cycles, punch the numbers of those cycles (1 through 25) in successive fields on the appropriate card. A non-zero, negative number punched in the first field on any card will select that output at the end of every cycle.

OUTPUT CATEGORY	INDEX
Stream function field	1
Current density field	2
Electron number density field	3
Plasma property fields $\frac{\epsilon}{\sigma}$, $\frac{\beta}{\sigma}$	4
T_e field	5
T_e increment (from previous cycle) field	6
T, U fields	7
Electric field and potential	8

Columns	Format	
1-75	25I3	Format of each OUTPUT CONTROL card

The next 2 cards in this category control punched output (described in Section B. 3), suitable for computer-generated contour plots of electron temperature or number density, current streamfunction, or electric potential, or for continuing the computation at a later date.

PUNCH CATEGORY	INDEX
Plot deck	9
Restart deck	10

1-75	25I3	Format of PUNCH CONTROL cards

The last card in this category indicates plot decks desired.

1-12	4I3	Quantities for which plot decks are desired are selected by a non-zero punch in the appropriate field on this card

Quantity	Format		
		QUANTITY	INDEX
		Electron temperature	1
		Electron number density	2
		Current streamfunction	3
		Electric potential	4

Category 2 WORKING FLUID

1-10	E10.3	Ratio of specific heats (c_p/c_v)	
1-5	I5	Number of elements (up to 10)	
6-10	I5	Number of components (up to 25)	

Each element is described on a card of the following format

1-10	A10	Name of element	
11-20	E10.3	Atomic weight of element	(amu)

Each component is then described on a card of the following format

1-4	A4	Name of component	
11-60	10A5	The composition of this component in terms of the specified elements is defined by punching, in the appropriate fields, the number of particles of the corresponding elements contained in each particle of this component.	
1-10	E10.3	Excitation energy of each component above its neutral ground state	(eV)

Integrated electron-neutral collision cross sections, energy loss factors, and weighting factors are given for each neutral component in tabular form as functions of electron temperature.

1-10	E10.3	Minimum value of T_e for tables	(^oK)
11-20	E10.3	Tabular interval in T_e for tables	(^oK)
21-30	E10.3	Maximum value of T_e for tables	(^oK)

Each table is input in the following format, where more than one card will generally be required.

Columns	Format	
1-18	18x	May be used for identification
19-28	E10.3	Electron-neutral collision cross section Q (m^2)
29-38	E10.3	Weighting factor $A^{(2)}$
39-48	E10.3	Weighting factor $A^{(5)}$
49-58	E10.3	Electron-neutral energy-loss factor δ_{eff}

Category 3 CHEMICAL REACTIONS

1-5	I5	Number of reactions (up to 22)

Each reaction, which may be written symbolically as

$$\sum_{j=1}^{4} \nu_j a_j \underset{k_r}{\overset{k'_r}{\rightleftharpoons}} \sum_{j=1}^{4} \nu'_j a'_j$$

is characterized by specifying the components a_j, a_j' taking part, their stoichiometric coefficients ν_j and ν'_j, the reverse reaction rate constant k_r, and the equilibrium constant $K \equiv k'_r/k_r$. The rate constant k_r is specified as a function of temperature by the expression $k_r = AT^B \exp(C/T)$, and the equilibrium constant K by the expression $K = A'T^{B'}R(T) \exp(C'/T)$. $R(T)$ is the ratio of partition functions of the components on the right-hand side to those on the left-hand side, given in tabular form as a function of temperature (see Category 2 for table parameters). The forward reaction constant may then be written: $k'_r = AA'T^{(B+B')}R(T) \exp[(C+C')/T]$. Specifications of each reaction will require the following group of cards.

1-40	8I5	Stoichiometric coefficients ν_j and indexes of components a_j, in the order: $\nu_1\ a_1\ \nu_2\ a_2\ \nu_3\ a_3\ \nu_4\ a_4$
41-80	8I5	Stoichiometric coefficients ν'_j and indexes of components a'_j, as above
1-5	I5	Temperature flag for K and k'_r. If blank or zero, use gas temperature; if 1 use electron temperature

Columns	Format	
6-10	5x	May be used for identification
11-20	E10.3	Constant factor A'
21-30	E10.3	Temperature exponent B'
31-40	E10.3	Energy exponent C'
41-45	I5	Temperature flag for k_r
46-50	5x	May be used for identification
51-60	E10.3	Constant factor A
61-70	E10.3	Temperature exponent B
71-80	E10.3	Energy exponent C
1-80	8E10.3	Table of partition function ratio R(T); may require more than one card

Category 4 GEOMETRY AND GRID

1-3	I3	Number of rows	(max. 31)
4-6	I3	Number of columns	(max. 81)
7-9	I3	Number of electrodes	(max. 20)

x- and y-spacings of the grid may vary in x and y respectively. In that case, the number of cards read will equal either the number of x-spacings or the number of y-spacings, whichever is greater. A uniform grid may be specified by providing a single card with the negative of the desired x-spacing in the first field and the desired y-spacing in the second.

1-10	E10.3	Desired x-spacing	(m)
11-20	E10.3	Desired y-spacing	(m)
1-80	26I3, I2	Electrode geometry for the wall y = 0, specified by giving the number of grid spaces covered by the leading insulator, first conductor segment, next insulator segment, etc. More than one card may be required.	
1-80	26I3, I2	Electrode geometry for the wall y = D, as above.	

Columns	Format	
1-30	3E10.3	Quadratic polynomial coefficients A, B, C for z-dimension of channel $W = A + Bx + Cx^2$ (m) (Needed for solution of gasdynamic problem.)

Category 5 PROBLEM PARAMETERS

1-10	D10.3	Total current in x-direction (A/m)
1-80	8E10.3	Array of values of B, one value per grid column (Wb/m^2)
1-80	8D10.3	Total current flowing through each electrode pair (A/m)
1-80	8D10.3	Given values of streamfunction on each grid row at column 1 (if required) (A/m)
1-80	8D10.3	Given values of streamfunction on last column (if required) (A/m)
1-10	E10.3	Allowable relative variation in U
11-20	E10.3	Allowable relative variation in T
21-30	E10.3	Allowable relative variation in T_e
1-80	8E10.3	Allowable relative variations in component number densities
1-10	E10.3	Initial gas pressure (atm)
11-20	E10.3	Value of T for initial current density calculation (^oK)
21-30	E10.3	Value of T_e for initial current density calculation (^oK)
31-40	E10.3	Seed fraction by weight
1-10	E10.3	Allowable relative error in T_e for algebraic solution
11-13	I3	Maximum number of iterations allowed in algebraic solution for T_e

Columns	Format	
		Category 6 INITIAL PROFILES
1-80	8E10.3	Initial values of all component number densities on rows (by row) (m^{-3}) For uniform profile, make the first field of row 1 specifications negative.
1-80	8E10.3	Initial profile of T_e (^oK) For uniform profile place ($-T_e$) in the first field.
1-80	8E10.3	Values of T/T_{CL} for all rows For uniform profile place ($-T/T_{CL}$) in the first field.
1-80	8E10.3	Values of U/U_{CL} for all rows For uniform profile place ($-U/U_{CL}$) in the first field.
		Category 7 AXIAL VARIATION OF U, T
1-80	8E10.3	Values of T_{CL} for all columns (^oK) For uniform distribution place ($-T_{CL}$) in the first field.
1-80	8E10.3	Values of U_{CL} for all columns (m/s) For uniform distribution place ($-U_{CL}$) in the first field.
		Category 8 ELECTRON TEMPERATURE DISTRIBUTION
1-80	8E10.3	Values of electron temperature for all grid points (^oK) First row-first column, first row-second column, etc.

Columns	Format	

Category 9 RESTART DECK

As suitable for each field	Read restart deck as punched by INLET	

A. 3. AVAILABLE OUTPUT

Both printed and punched output are available from INLET, the latter to provide for continuing a calculation after interruption or to facilitate computer plotting of important quantities.

Printed output, besides giving the values at all points of any quantities described in Category 1 of input, always collects and prints values of:

Root-mean-square variation of electron temperature between present and previous distributions

Minimum electron temperature

Maximum electron temperature

Number of points where T_e is approaching a steady value from cycle to cycle ("converging")

J_y at trailing edge of the middle electrode at $y = 0$

J_y at leading edge of the middle electrode at $y = D$

Maximum J_y on center line, and the angle between the current vector and the y-axis at this point

Minimum J_y on centerline, and the angle between the current vector and the y-axis at this point

Hall potential between first and last columns

Each available plot deck contains one card for every grid point, in the following format:

4-13	F10. 5	x-coordinate of this grid point (relative to first column)	(m)
14-23	F10. 5	y-coordinate of this grid point (relative to first row)	(m)
24-33	F10. 1	Value of chosen quantity at this grid point	

The restart deck contains values of all the unknown quantities required to continue a calculation. It should be placed as a unit at the end of the input deck. Care should be taken that the input deck specifies the same working fluid, geometry and grid as the original computation.

A. 4. ROUTINES USED IN PROGRAM INLET

Program INLET is composed of a main program, which performs control functions, and 26 subroutines which perform input, output and the tasks involved in the solution procedure. The list below includes a short description of the function of each routine, where M = main program, S = subroutine, F = function subroutine.

ROUTINE		FUNCTION
INLET	M	Controls solution
OP	S	Performs all printing output
IP	S	Performs all input
SETUP	S	Performs tasks associated with initializing or continuing a problem
PRPGTE	S	Principal routine in solution of finite-difference equations for streamfunction
SPREAD	S	Subordinate to PRPGTE
PSF	S	Calculates values of streamfunction after PRPGTE has achieved solution
CDCF	S	Calculates current density field by differentiation of streamfunction
ANODE	S	Calculates elements of finite-difference coefficient array along wall at y = 0
CORE	S	Calculates elements of finite-difference coefficient array away from walls
CATHODE	S	Calculates elements of finite-difference coefficient array along wall at y = D
HALL	S	Calculates plasma properties for a given set of conditions
TAND	S	Performs solution for gasdynamic variables (U, T, T_e, n_a) along streamlines

TTEST	S	Compiles and evaluates general characteristics
POTENT	S	Calculates electric field and potential
COMPOS	S	Calculates plasma composition at Saha equilibrium
RK	F	Calculates reaction rate constants
DIFTE	F	Evaluates dT_e/dx for use in TAND
E	F	Iterative solution of implicit algebraic equation for T_e
F	F	Iterative solution of implicit algebraic equation for T_e
ANEWTE	F	Subordinate to E, F
PVAL	F	Table lookup function
MATINV	S	Matrix inverter
PDECK	S	Performs all punched output
PROP	S	Calculates plasma properties all along a grid row
RELAX	S	Evaluates relaxation lengths and stabilities
DZ	F	Evaluates z-dimension of channel

A. 5. IMPORTANT VARIABLE NAMES

This list defines the important variable names used internally by the FORTRAN program. Dimensions assigned to arrays are given in parenthesis. * = Double precision.

VARIABLE NAME		DEFINITION	
A(2449, 5)	*	Array of finite-difference coefficients	
AARRAY (81, 80)	*	Recursion array 1	
AIXA	*	Total current in x-direction	(A/m)
AIA(20)	*	Total current through each electrode	(A/m)
AJX(31, 81)		J_x field	(A/m^2)
AJY(31, 81)		J_y field	(A/m^2)
ALC(20)		Lengths of conductor segments on wall at $y = 0$	(m)

VARIABLE NAME		DEFINITION	
ALCC(20)		Lengths of conductor segments on wall at y = D	(m)
ALI(20)		Lengths of insulator segments on wall at y = 0	(m)
ALIC(20)		Lengths of insulator segments on wall at y = D	(m)
ALO		Length of leading insulator on wall at y = 0	(m)
ALOC		Length of leading insulator on wall at y = D	(m)
AN(25)		Values of number densities at the current grid point	(m^{-3})
ANEF(31, 81)		Electron number density field	(m^{-3})
ANIC(25, 31)		Initial values of number densities	(m^{-3})
BARRAY(81, 80)	*	Recursion array 2	
BF		Magnetic induction	(Wb/m^2)
BETOSIG(31, 81)		Ohm's Law coefficient ratio β/σ	
CP		Specific heat c_p	$(J/(kg \cdot {}^{o}K))$
CRIT		Critical value of β/ϵ	
D		y-dimension of channel	(m)
EL		Electron energy relaxation length	(m)
EPSOSIG(31, 81)		Ohm's Law coefficient ratio ϵ/σ	
EX(31, 81)		E_x field	(v/m)
EY(31, 81)		E_y field	(v/m)
HX(81)		x-spacing of grid	(m)
HY(31)		y-spacing of grid	(m)
ICYCLE		Iteration cycle count	
KELECT		Number of electrodes in region	
M2		Number of grid rows	
N		Number of grid columns	
NCYCLE		Number of iteration cycles to be performed	
S(2449)	*	Streamfunction field	(A/m)

VARIABLE NAME	DEFINITION	
TA(31, 81)	Gas temperature field	(^{o}K)
TE(31, 81)	Electron temperature field	(^{o}K)
U(31, 81)	Gas velocity field	(m/s)

APPENDIX B

DESCRIPTION OF COMPUTER PROGRAM "CHANNEL"

B. 1. GENERAL DESCRIPTION

Program CHANNEL has been written to solve the gasdynamic part of the problem in the core region, and to derive overall performance data for a J × B device. Solution accuracy is automatically held to user's specifications. CHANNEL can treat the flow of any specified fluid, distinguishing as many as 25 separate components, formed from up to 10 distinct elements and taking part in up to 22 reactions. Channel geometry and magnetic field and current density distributions are required input. Friction and heat losses to the channel walls, boundary layer and electrode sheath voltage drops may be included at the option of the user. Printout of the values of the dependent variables and other important parameters may be requested at specified intervals along the channel. Upon reaching the specified terminal value of x, the program, without disturbing the status of the completed calculation, attempts to read another input deck.

CHANNEL has been coded in FORTRAN for the Control Data Corporation 6000 series computers. On a CDC 6600 computer the program occupies 22500 storage locations, typically requiring 40 seconds of central processor time for a computation over one meter of length of a J × B accelerator, with detailed output (at 6 mm intervals). Central processor time is strongly affected by the frequency of output required, and by the specified allowable rates of change of the dependent variables.

More detailed information relating to the use of program CHANNEL is supplied in Sections B. 2 to B. 5 below. Section B. 2 contains a description of input data and formats, Section B. 3 a list of quantities available for output, Section B. 4 contains a list of the routines which make up program CHANNEL, and Section B. 5 lists important variable names used in these routines.

B. 2. INPUT DATA AND FORMATS

Columns	Format	
1-80	8A10	The first card contains the HEADING to be printed at the top of each new page. Leaving columns 1-10 blank terminates the program.
1-33	11I3	The second card is the INPUT CONTROL card. The remaining input is separated into eleven categories, input of which are selected by punching the indexes of those desired in successive fields on this card, beginning with the first field.

CATEGORY	INDEX
Solution methods control	1
Iteration controls	2
Specifications of geometry, current and magnetic field	3
Fluid model	4
Cross sections and weighting factors used in Ohm's Law	5
Specification of component number densities to be found using differential equations	6
Specification of chemical reactions	7
Initial conditions	8
Electrode voltage drops	9
Required accuracy in integration	10
Gas parameters	11

Category 1 METHOD CONTROL

1-15	5I3	Solution methods to be used are selected by punching their indexes in successive fields of this card.

Columns	Format		
		METHOD	INDEX
		Differential equation for electron temperature	1
		Continue calculation interrupted by input	2
		Use as initial values for all variables those supplied in the input deck	3
		Assume T_e and all number densities to remain frozen at initial values	4
		Include momentum and heat losses to the channel walls	5

Category 2 ITERATION CONTROL

1-5	I5	Maximum number of iterations at any point for algebraic solution of electron temperature equation.
6-15	E10.3	Required accuracy in algebraic solution for electron temperature.

Category 3 GEOMETRY, CURRENT AND MAGNETIC FIELD

1-10	E10.3	Initial value of independent variable, x	(m)
11-20	E10.3	Tabular interval (in x) for specification of J_x and J_y	
21-30	E10.3	Terminal value of x	(m)
31-40	E10.3	Output interval	(m)
		The y- and z-dimensions of the channel and the magnetic field strength are specified as quadratic functions of x: $A + Bx + Cx^2$	

Columns	Format		
1-30	3E10.3	A, B and C for y-dimension	(m)
31-60	3E10.3	A, B and C for z-dimension	(m)
1-30	3E10.3	A, B and C for magnetic field strength	(Wb/m^2)
		Values of J_x and J_y are specified for the initial value of x and at intervals in x specified on the first card in this category, up to the terminal value of x.	
1-80	8E10.3	Table of values of J_y (one or more cards)	(A/m^2)
1-80	8E10.3	Table of values of J_x (one or more cards)	(A/m^2)

Category 4 FLUID MODEL

1-5	I5	Number of elements (up to 10)	
6-10	I5	Number of components (up to 25)	
Each element is described on a card of the following format			
1-10	A10	Name of element	
11-20	E10.3	Fractional content of element in the fluid (by number density; required only if initial composition of fluid is not specified in Category 8)	
21-30	E10.3	Atomic weight of element	(amu)
Each component is then described on a card of the following format			
1-4	A4	Name of component	
11-60	10I5	The composition of this component in terms of the specified elements is defined by punching, in the appropriate fields, the number of particles of the corresponding elements in each particle of this component	

Columns	Format		
1-10	E10.3	Excitation energy of each component above its neutral ground state.	(eV)

Category 5 CROSS SECTIONS

Cross sections, effective energy-loss factors and weighting factors for each neutral component are given in tabular form as a function of temperature. All tables are specified by the parameters on the first card in this category. The maximum table length is 51 entries.

1-10	E10.3	Minimum temperature for tables	(^{o}K)
11-20	E10.3	Tabular interval in temperature	(^{o}K)
21-30	E10.3	Maximum temperature for tables	(^{o}K)

Following this card are the tables of cross sections, energy-loss factors and weighting factors for all neutral components, in the order the components were described in Category 4. The values appear in order of increasing temperature.

1-18	18x	May be used for identification or sequencing	
19-28	E10.3	Electron-neutral collision cross section Q	(m^2)
29-38	E10.3	Weighting factor $A^{(2)}$	
39-48	E10.3	Weighting factor $A^{(5)}$	

For each neutral component there will be up to 51 cards in the above format, followed by the same number in the following format.

1-10	E10.3	Effective energy-loss factor for electron-neutral collisions δ_{eff}	

Columns	Format	
		Category 6 INDEPENDENT COMPONENTS
1-80	16I5	Since one may express an algebraic conservation relation for each element, it is not necessary to solve a differential equation for every component. Those components for which differential equations are to be used are selected by punching the index of each in successive fields, recalling the order in which they were described in Category 4. This may require two cards.

Category 7 CHEMICAL REACTIONS

1-5	I5	Number of reactions (up to 22)

Each reaction, which may be written symbolically as

$$\sum_{j=1}^{4} \nu_j a_j \underset{k_r}{\overset{k'_r}{\rightleftharpoons}} \sum_{j=1}^{4} \nu'_j a'_j$$

is characterized by specifying the components a_j, a'_j taking part, their stoichiometric coefficients ν_j and ν'_j, the reverse reaction rate constant k_r, and the equilibrium constant $K \equiv k'_r/k_r$. The rate constant k_r is specified as a function of temperature by the expression $k_r = AT^B \exp(C/T)$, and the equilibrium constant K by the expression $K = A'T^{B'} R(T) \exp(C'/T)$. $R(T)$ is the ratio of partition functions of the components on the right-hand side tc those on the left-hand side, given in tabular form as a function of temperature (see Category 5 for table parameters). The forward reaction constant may then be written: $k'_r = AA'T^{(B+B')} R(T) \exp[(C+C')/T]$. Specifications of each reaction will require the following group of cards.

Columns	Format	
1-40	8I5	Stoichiometric coefficients ν_j and indexes of components a_j, in the order: $\nu_1\ a_1\ \nu_2\ a_2\ \nu_3\ a_3\ \nu_4\ a_4$
41-80	8I5	Stoichiometric coefficients ν_j' and indexes of components a_j, as above
1-5	I5	Temperature flag for K and k_r'. If blank or zero, use gas temperature; if 1 use electron temperature
6-10	5x	May be used for identification
11-20	E10.3	Constant factor A'
21-30	E10.3	Temperature exponent B'
31-40	E10.3	Energy exponent C'
41-45	I5	Temperature flag for k_r
46-50	5x	May be used for identification
51-60	E10.3	Constant factor A
61-70	E10.3	Temperature exponent B
71-80	E10.3	Energy exponent C
1-80	8E10.3	Table of partition function ratio R(T); may require more than one card

Category 8 INITIAL CONDITIONS

If Method 3 is not selected, initial conditions are computed from given stagnation conditions and entrance Mach number. Electron temperature is set to a value between T_{stag} and T depending on a specified parameter f: $T_e = T + f \cdot (T_{stag} - T)$.

1-10	E10.3	Stagnation temperature T_{stag}	(^oK)
11-20	E10.3	Stagnation pressure	(atm)
21-30	E10.3	Entrance Mach number	
31-40	E10.3	Parameter f	

If Method 3 is selected, initial values of all dependent variables must be specified.

1-10	E10.3	Initial value of velocity	(m/s)
11-20	E10.3	Initial value of gas temperature	(^oK)

Columns	Format	
21-30	E10.3	Initial value of electron temperature (^{o}K)
1-80	8E10.3	Initial values of component number densities (m^{-3}) May require more than one card

Category 9 ELECTRODE VOLTAGE DROP

The boundary layer voltage drop is specified as a quadratic polynomial in x, $V = A + Bx + Cx^2$, in volts

1-30	3E10.3	Coefficients A, B and C for boundary layer voltage drop.
31-40	E10.3	Constant value of electrode sheath drop (v)

Category 10 INTEGRATION ACCURACY

Integration accuracy is controlled by restricting the fractional variation in every dependent variable over one integration step to some given value.

1-10	E10.3	Allowable relative variation of velocity
11-20	E10.3	Allowable relative variation of temperature
21-30	E10.3	Allowable relative variation of electron temperature
31-80	5E10.3	Allowable relative variation of first five component number densities
1-80	8E10.3	Allowable relative variation in remaining component number densities. May require more than one card.

Category 11 GAS PARAMETERS

1-10	E10.3	Ratio of specific heats (c_p/c_v)
1-10	E10.3	Recovery factor
11-20	E10.3	Wall temperature (^{o}K)
21-30	E10.3	Prandtl number

B.3. AVAILABLE OUTPUT

In addition to the current values of all dependent variables (u, T, T_e and n_a), printout at each station includes the values of the following parameters:

x-coordinate of current station — Cross-sectional area of channel
Magnetic field strength — Mach number
Current density components — Mass density
Angle current vector makes with y-direction
Gas pressure — Entropy relative to initial conditions
Electric field components
Boundary layer voltage drop — Ohm's Law coefficients σ, β, ϵ
Hall potential relative to initial point — Faraday potential $E_y \cdot D$
Energy flux through plane normal to flow direction
P-MHD $\equiv \int (\vec{E} \cdot \vec{J})\, dV$ = Total MHD power input
P-EL.DROPS $\equiv \int J_y V_{bl}\, dx$ = Total power dissipated over boundary layer voltage drop
P-INPUT $\equiv \int (\vec{E} \cdot \vec{J})\, dV$ + P-EL. DROPS = Total power input to flow
P-WALL $\equiv \int s_E\, dV$ = Total power loss to walls
Conversion efficiency $\equiv \int (\vec{E} \cdot \vec{J})\, dV / \int J_y Bu\, dV$
Total efficiency $\equiv \int J_y Bu\, dV /$ P-INPUT

B.4. ROUTINES USED IN PROGRAM CHANNEL

Program CHANNEL is composed of a main program, which performs control functions, and fourteen subroutines which perform input, output and the tasks associated with the numerical integration. The list below includes a short description of the function of each routine, where M = main program, S = subroutine, F = function subroutine.

ROUTINE		FUNCTION
CHANNEL	M	Controls integration and output
IP	S	Performs all input
OP	S	Performs all output

ROUTINE		FUNCTION
SETUP	S	Performs tasks associated with initializing or continuing a problem
STEP	S	Performs Runge-Kutta-Gill integration under control of main program
CANON	S	Evaluates components of derivative vector $\vec{f}$
COMPOS	S	Calculates plasma composition at Saha equilibrium at a given temperature
RKS	S	Calculates values of all reaction rate constants at current values of the characteristic temperatures
SOURCES	S	Evaluates the species source terms s_a
SE	F	Evaluates momentum and energy source terms s_M and s_E
REMAIN	S	Solves the system of algebraic equations expressing conservation of the elements
PROP	S	Calculates electrical properties of the plasma
FOX	S	Evaluates parameters specified as functions of x alone
EEE	S	Performs iterative solution of implicit algebraic equation for electron temperature
MATINV	S	Performs matrix inversion

B.5. IMPORTANT VARIABLE NAMES

This list defines the important variable names used internally by the FORTRAN program. Dimensions assigned to arrays are given in parenthesis.

VARIABLE NAME	DEFINITION
AMACH	Mach number
AN(25) ≡ Y(4-28)	Component number densities
BETAE	Ohm's law coefficient β_e

VARIABLE NAME	DEFINITION	
BETEPS	Ohm's law coefficient ratio β_e/ϵ_e	
BZ	Magnetic field strength	(Wb/m^2)
CP	Specific heat c_p	$(J/(kg \cdot {}^oK))$
DELOUT	Output interval	(m)
ENTHIN	Enthalpy flux at initial point	(J/s)
ENTROP	Entropy	$(J/(kg \cdot {}^oK))$
EPSE	Ohm's law coefficient ϵ_e	
EPSOS	Ohm's law coefficient ratio ϵ_e/σ	
GAMMA	Ratio of specific heats c_p/c_v	
HEIGHT	y-dimension of channel	(m)
MASFLO	ρuA	(kg/s)
NCOMP	Number of components	
NELEM	Number of elements	
NREAC	Number of reactions	
NTAB	Number of table entries for Q, $A^{(2)}$, $A^{(5)}$, δ_{eff}, R(T)	
PIN	Static pressure at initial point	(N/m^2)
PJSQ	$\lvert\vec{J}\rvert^2$	(A^2/m^4)
PJX	J_x	(A/m^2)
PJY	J_y	(A/m^2)
POTION (25)	Excitation energy of each component	(J)
POTONS	Electron energy source $\sum_i \epsilon_i s_i$	$(J/(m^3 \cdot s)$
PRANDTL	Prandtl number	
PRESS	Static pressure	(N/m^2)
PSTAG	Stagnation pressure	(N/m^2)
RHO	Mass density	(kg/m^3)
SDROP	Sheath drop	(v)
SIGMAE	Scalar conductivity	(mho/m)
SOURCE (25)	Species source terms s_a	
T ≡ Y(2)	Gas temperature	$({}^oK)$
TE≡ Y(3)	Electron temperature	$({}^oK)$
TOTDEL	Factor in collisional energy loss term: $\nu_t \delta_{eff}$	
TSTAG	Stagnation temperature	$({}^oK)$
TW	Wall temperature	$({}^oK)$

VARIABLE NAME	DEFINITION	
U ≡ Y(1)	Gas velocity	(m/s)
VDROP	Boundary layer voltage drop	(v)
WIDTH	z-dimension of channel	(m)
XCOOR	Value of x-coordinate	(m)
Y(28)	Array of dependent variables, $\vec{y}$	
Z(28)	Array of x-derivatives of dependent variables, $\vec{f}$	

APPENDIX C

DESCRIPTION OF COMPUTER PROGRAM "LAYER"

C. 1. GENERAL DESCRIPTION

Program LAYER has been written to solve the two-dimensional gasdynamic part of the problem in the compressible, turbulent boundary layer, including magnetohydrodynamic effects. LAYER treats the flow of potassium-seeded air and requires input only of initial conditions, freestream velocity distribution, wall conditions, and electric current and magnetic field distributions. Upon reaching the specified terminal value of x the program, without disturbing the status of the completed calculation, attempts to read another input deck.

LAYER has been coded in FORTRAN for Control Data Corporation 6000 series computers. On a CDC 6600 computer the program occupies 16500 storage locations. Because step size in the x-direction is limited to half the boundary layer thickness, typical execution time requirements are difficult to state; however, each step requires about 0. 6 second of central processor time with 20 grid points in the y-direction, or 1. 2 seconds with 40 points.

More detailed information relating to the use of program LAYER is supplied in sections C. 2 to C. 5 below. Section C. 2 contains a description of input data and formats, Section C. 3 a list of quantities included in the output, Section C. 4 lists the routines which make up program LAYER, and Section C. 5 the important variable names used in these routines.

C. 2. INPUT DATA AND FORMATS

Columns	Format	
1-80	8A10	The first card contains the HEADING to be printed at the top of each new page. Leaving columns 1-10 blank terminates the program.

Columns	Format		
1-5	I5	If blank or zero, the rest of this card is ignored. Otherwise the contents of the four remaining fields replace the current values of the corresponding quantities, and no more cards are read.	
6-15	E10.3	New terminal value for x	(m)
16-25	E10.3	New constant term in polynomial for U_∞	(m/s)
26-35	E10.3	New linear coefficient in polynomial for U_∞	
36-45	E10.3	New quadratic coefficient in polynomial for U_∞	
1-10	E10.3	Initial value of x	(m)
11-20	E10.3	Terminal value of x	(m)
21-30	E10.3	Output interval	(m)
31-40	E10.3	Initial boundary layer thickness	(m)
41-45	I5	Desired number of intervals across the boundary layer	
1-10	E10.3	Initial value of free-stream temperature	(^oK)
11-20	E10.3	Initial value of static pressure	(atm)
21-30	E10.3	Wall temperature	(^oK)
31-40	E10.3	Seed fraction (by weight)	
41-50	E10.3	Effective energy-loss factor in electron-neutral collisions for this mixture	
1-10	E10.3	Constant term in polynomial expression for U_∞	(m/s)
11-20	E10.3	Linear coefficient in expression for U_∞	

Columns	Format		
21-30	E10.3	Quadratic coefficient in expression for U_∞	
1-10	E10.3	Constant term in polynomial expression for B	(Wb/m^2)
11-20	E10.3	Linear coefficient in expression for B	
21-30	E10.3	Quadratic coefficient in expression for B	
1-10	E10.3	Constant term in polynomial expression for J_x	(A/m^2)
11-20	E10.3	Linear coefficient in expression for J_x	
21-30	E10.3	Quadratic coefficient in expression for J_x	
31-40	E10.3	Constant term in polynomial expression for J_y	(A/m^2)
41-50	E10.3	Linear coefficient in expression for J_y	
51-60	E10.3	Quadratic coefficient in expression for J_y	
1-10	E10.3	Exponent γ in expression for initial profile of y: $y_i = \delta(i/N)^\gamma$ $i = 0...N$ for N+1 grid points in the y direction	
11-20	E10.3	Exponent β in expression for initial profile of gas velocity: $U_i = U_\infty(y_i/\delta)^\beta$ $i = 0...N$	
21-30	E10.3	Exponent γ in expression for initial profile of gas temperature: $T_i = T_w + (T_\infty - T_w)\cdot(y_i/\delta)^\gamma$, $i = 0...N$	

Columns	Format	
1-10	E10.3	Maximum allowable relative error in electron temperature calculation

If the exponent γ for the profile of y is zero, the following group of cards is input

1-80	8E10.3	Table of values of y_i/δ $i = 0...N$

If the exponent β for the velocity profile is zero, the following group of cards is input

1-80	8E10.3	Table of values of U_i/U_∞ $i = 0...N$

If the exponent γ for the temperature profile is zero, the following group of cards is input

1-80	8E10.3	Table of values of T_i/T_∞ $i = 0...N$

C.3. AVAILABLE OUTPUT

The values of the normalized cross-coordinate ω, as calculated from the initial profiles, are printed on the first page of output. At the initial station and wherever output is requested, profiles of quantities dependent on y and values of quantities independent of y are printed.

Quantities independent of cross-coordinate

Value of x-coordinate
Static pressure, p
Current density components, J_x and J_y
Displacement thickness, δ^*
Shape factor, δ^*/θ
Displacement thickness Reynolds number, Re_{δ^*}
Momentum thickness Reynolds number, Re_θ
Wall heat flux, $J_{H,w}$
Wall shear stress, τ_w
Mass flow through boundary layer
Magnetic field, B
Wall temperature, T_w
Momentum thickness, θ
x-Reynolds number, Re_∞

Skin friction coefficient, $c_f \equiv \tau_w / \frac{1}{2} \rho_\infty U_\infty^2$

Heat transfer coefficient, $c_H = J_{H,w} / \rho_\infty U_\infty (H_\infty - H_w)$

Quantities dependent on cross-coordinate

Distance from wall, y
Gas temperature T
Mass density, ρ
Mach number, M
Scalar conductivity, σ
Electric field components, E_x and E_y
Turbulent shear stress, τ
Ohm's Law coefficients, β and ϵ
Electron energy relaxation length, L_E
Static enthalpy, h
Gas velocity, u
Electron temperature, T_e
Electron concentration, c_e
Ionization relaxation length, L_R
Total enthalpy, H
Electron number density, n_e

C. 4. ROUTINES USED IN PROGRAM LAYER

Program LAYER is composed of a main program, which controls the solution and output, and subroutines which perform input, output and various tasks associated with the solution. The list below includes a short description of the function of each routine, where M = main program, S = subroutine, and F = function subroutine.

ROUTINE		FUNCTION
LAYER	M	Controls solution and output
EEE	S	Controls iterative solution of implicit algebraic equation for T_e
E	F	Performs iterative solution for T_e
F	F	Performs iterative solution for T_e
ANEWTE	F	Subordinate to E and F
BEGIN	S	Performs all input and tasks associated with initiating or continuing computations
COEFF	S	Calculates finite-difference coefficients away from the wall and freestream boundaries
COMPOS	S	Calculates plasma composition at Saha equilibrium

COND	S	Evaluates viscosity, conductivity and diffusivity factors
ENTRN	S	Evaluates mass entrainment term $\dot{m}_E$
LENGTH	S	Calculates boundary layer thickness, δ_{995}, and turbulence correlation functions a_2 and a_3
OHM	S	Calculates Ohm's Law coefficients σ, β, ϵ, and electric field components E_x and E_y
OUTPUT	S	Performs all output
PAIR	S	Calculates static enthalpy as a function of pressure and temperature for air
PAPH	S	Calculates temperature as a function of pressure and static enthalpy for air
READY	S	Calculates distance from wall for each grid point
SLIP	S	Calculates finite-difference coefficients for points at wall and freestream boundaries
SOLVE	S	Performs solution of finite-difference equations
SOLVE 2	S	Performs solution of coupled finite-difference equations for u, τ
SOURCE	S	Evaluates source terms for all equations
VEFF	S	Evaluates "eddy viscosity"
VISCO	F	Calculates molecular viscosity
WALL	S	Controls Couette-flow solutions
WF1	S	Performs Couette-flow solution for velocity
WF3	S	Performs Couette-flow solutions for other unknowns

C.5. IMPORTANT VARIABLE NAMES

This list defines the important variable names used internally by the FORTRAN program. Dimensions assigned to arrays are given in parenthesis.

VARIABLE NAME	DEFINITION
AMACH(43)	Mach number at each grid point
BETAE(43)	Ohm's Law coefficient β_e
BF	Magnetic field strength (Wb/m^2)
CF	Friction coefficient c_f

CH	Heat transfer coefficient c_H	
DDIS	Displacement thickness δ^*	(m)
DMOM	Momentum thickness θ	(m)
DX	Current interval in x for calculation	(m)
EPSE(43)	Ohm's Law coefficient ϵ_e	
EX(43)	Electric field component E_x	(v/m)
EY(43)	Electric field component E_y	(v/m)
F(4, 43)	Array of unknowns. F(i, j) j = 1, 43 are values of: i = 1 H; i = 2 h_e; i = 3 c_e; i = 4 τ/ρ	
FLUX (3)	Wall flux of H, h_e, c_e	
HSTAT(43)	Static enthalpy	(J/kg)
N	Number of intervals across boundary layer	
OM(43)	Values of normalized coordinate ω	
PEI	Mass flow through boundary layer	(kg/(m· s))
PINF	Static pressure	(N/m^2)
RHO(43)	Mass density	(kg/m^3)
SF	Seed fraction	
SIGMA(43)	Scalar conductivity	(mho/m)
TAU(43)	Turbulent shear stress τ	($kg/(m\cdot s^2)$)
TEMP(43)	Gas temperature	(^oK)
TEMPE(43)	Electron temperature	(^oK)
TW	Wall temperature	(^oK)
U(43)	Gas velocity	(m/s)
XNE(43)	Electron number density	(m^{-3})
Y(43)	Distance from wall	(m)
YL	Boundary layer thickness δ_{995}	(m)

UNCLASSIFIED

Security Classification

DOCUMENT CONTROL DATA - R & D

(Security classification of title, body of abstract and indexing annotation must be entered when the overall report is classified)

1. ORIGINATING ACTIVITY (Corporate author)	2a. REPORT SECURITY CLASSIFICATION
STD Research Corporation Box 4127, Catalina Station Pasadena, California 91106	UNCLASSIFIED
	2b. GROUP N/A

3. REPORT TITLE

CURRENT DISTRIBUTION IN CROSSED-FIELD ACCELERATORS (PART III, ELECTRICAL AND GASDYNAMIC PERFORMANCE OF J X B ACCELERATORS)

4. DESCRIPTIVE NOTES (Type of report and inclusive dates)

Final Report - January 1, 1968 to June 30, 1969

5. AUTHOR(S) (First name, middle initial, last name)

G. S. Argyropoulos, M. A. Casteel, and S. T. Demetriades

6. REPORT DATE	7a. TOTAL NO. OF PAGES	7b. NO. OF REFS
March 1970	112	25

8a. CONTRACT OR GRANT NO.	9a. ORIGINATOR'S REPORT NUMBER(S)
AF 40(600)-1166 b. PROJECT NO. 8950	AEDC-TR-70-86
c. Program Element 62405334 d. Task 895001	9b. OTHER REPORT NO(S) (Any other numbers that may be assigned this report) Research Report STD

10. DISTRIBUTION STATEMENT This document is subject to special export controls and each transmittal to foreign governments or foreign nationals may be made only with prior approval of Arnold Engineering Development Center (AETS), Arnold Air Force Station, Tennessee 37389.

11. SUPPLEMENTARY NOTES	12. SPONSORING MILITARY ACTIVITY
Available in DDC	Arnold Engineering Development Center, Air Force Systems Command, Arnold AF Station, Tenn. 37389

13. ABSTRACT

Realistic analytical description of local behavior and of overall performance of crossed-field accelerators is obtained by computing coupled two-dimensional distributions of current density, plasma properties, and fluid velocity, temperature and pressure, over the whole length of the channel. The analysis includes consideration of electron non-equilibrium, thermal and concentration diffusion, compressible turbulent boundary layers, finite reaction rates, and electron energy relaxation, and the effect of each is investigated. The development of compressible, turbulent, magnetohydrodynamic boundary layers on the electrode walls is obtained through a novel formulation that includes a transport equation for the Reynolds' stress, and a fast numerical method of solution. Analytical results obtained in this study gave consistently good agreement with experimental measurements. Applications to seeded-nitrogen and seeded-air accelerators indicate limited current fringing in the entrance and exit regions and rapid approach to periodical current density, electric field, and plasma property distributions in the main part of the channel.

This document is subject to special export controls and each transmittal to foreign governments or foreign nationals may be made only with prior approval of Arnold Engineering Development Center (AETS), Arnold Air Force Station, Tennessee 37389.

DD FORM 1 NOV 65 1473

UNCLASSIFIED

Security Classification

14. KEY WORDS	LINK A ROLE	LINK A WT	LINK B ROLE	LINK B WT	LINK C ROLE	LINK C WT
current distribution						
potential distribution						
velocity distribution						
temperature distribution						
1. J X B accelerators						
nonequilibrium flow						
nonuniformities						
turbulent boundary layers						
multielectrode geometries						
entrance effects						
current fringing						
relaxation effects						
2. Crossed field accelerators						
3 MHD accelerator						
15-20						

AFSC
Arnold AFS Tenn